Surface-Modified Magnetite Nanoparticles for Advanced Separation and Purification

by

Xuyang Liu

A thesis submitted in partial fulfillment of the requirements for the degree of

Doctor of Philosophy

in

Chemical Engineering

Department of Chemical and Materials Engineering

University of Alberta

Abstract

When used as selective sorbents, surface-modified magnetic nanoparticles possess numerous advantages, including cost-effectiveness, high adsorption capacities, tunable surface properties, and convenient solid-liquid separation, making them a promising solution for challenging separation problems. In this thesis research, the author studied the potential and significance of utilizing surface-modified magnetite nanoparticles in two specific areas: (1) removal of fine mineral solids from non-aqueous extracted (NAE) bitumen, and (2) extraction and purification of nucleic acids from biomatrix.

In the oil sands industry, relatively high fine mineral solids content in produced bitumen (greater than 300 ppm or 0.03 wt%) is one of the hurdles preventing non-aqueous extraction from being used in commercial operations. In this work, surface-modified magnetite nanoparticles were studied to capture fine solids in cyclohexane-diluted NAE bitumen at a low cyclohexane-to-bitumen ratio of 2. The magnetite nanoparticles, together with the captured fine solids, were removed from bitumen through a magnetic field-assisted sedimentation and filtration process. Stearylamine acetate-functionalized magnetite nanoparticles (SAA-MNPs) were prepared and characterized, and their performance in separating fine solids from NAE bitumen was quantitatively evaluated and compared with un-modified magnetite nanoparticles (MNPs). It was shown that surface modification by SAA significantly improved separation efficiency from 16% to 89%. The increased separation efficiency resulted from the formation of hetero-aggregates between the NAE fine solids and SAA-MNPs in cyclohexane.

Since asphaltenes in solvent-diluted-bitumen have a strong tendency to adsorb on any surfaces upon contact, asphaltene-modified magnetite nanoparticles (Asp-MNPs) were also used in this study. It was found that asphaltene coating of MNPs increased the fine solids separation efficiency

from 16% to 84%. Therefore, asphaltene adsorption on the MNPs was not a detriment but an advantage because it did not diminish the capture efficiency of the MNPs. Results illustrated that the re-generated and recycled SAA-MNPs and Asp-MNPs could lower fine solids content from 3600 ppm to 417 ppm (88% removal) and 587 ppm (84% removal), respectively, in a single pass.

The mechanisms of the developed magnetic sorbent separation process were studied using quartz crystal microbalance with dissipation monitoring (QCM-D) and atomic force microscopy (AFM) studies. Modification by SAA increased the adhesion interaction between the MNPs and NAE fine solids through a bridging effect, and the use of an external magnetic field helped form magnetic aggregates of SAA-MNPs and strengthened the hetero-aggregation between SAA-MNPs and the NAE fine solids. Interestingly, asphaltene-modified MNPs (Asp-MNPs) showed a repulsive force towards NAE fine solids due to steric effect because the latter was coated by asphaltene as well; however, the applied external magnetic field caused the formation of magnetic aggregation of Asp-MNPs, and the extended asphaltene polymer brushes of the Asp-MNP magnetic aggregates could capture the NAE fine solids through a sweeping effect by the networked Asp-MNPs. Therefore, this work demonstrated the unique advantage of magnetic sorbents, i.e., even without affinity to the target, the magnetic sorbents could still capture the target under an external magnetic field when coated with polymer "brushes". A non-magnetic sorbent would not be able to capture the target in this case.

For another advanced separation application, surface-modified SiO_2 encapsulated core-shell magnetic sorbents and associated buffers were developed aimed at SARS-CoV-2 viral RNA extraction. A wastewater sample containing SARS-CoV-2 virus collected from a wastewater plant in Alberta was used for the extraction studies. The human coronavirus strain 229E (hCoV-229E) was first spiked into the wastewater sample as a surrogate to study the RNA extraction abilities of

the core-shell magnetic beads and optimize the extraction process. Subsequently, the SARS-CoV-2 RNA extraction performances using the developed magnetic beads, buffer system, and protocol were investigated and compared with a commercial nucleic acid extraction kit (magnetic beads-based method) through reverse transcription polymerase chain reaction (RT-PCR) analysis. By using the developed protocol, both Fe_3O_4@SiO_2 and Fe_3O_4@SiO_2-COOH magnetic sorbents demonstrated high hCoV-229E extraction efficiency from hCoV-229E-spiked wastewater samples, with Fe_3O_4@SiO_2-COOH exhibiting superior extraction efficiency compared to the commercial kit. Additionally, following the developed protocol, Fe_3O_4@SiO_2 and Fe_3O_4@SiO_2-COOH showed comparable abilities as the commercial kit in extracting SARS-CoV-2 viral RNA from wastewater, providing a viable alternative to the commercial kit in case of severe shortage of supplies. The amino-functionalized Fe_3O_4@SiO_2-NH_2 showed significantly lower efficiency for hCoV-229E or SARS-CoV-2 viral RNA extraction from the same sample.

Preface

This thesis is compiled in the manuscript-based format, consisting of papers that have been published or are under preparation. The following is the statement of contributions to these co-authored papers presented in this thesis.

Chapter 3 presented a published work: Xuyang Liu, Kaipeng Wang, Xiaoli Tan, Hongbo Zeng, and Qi Liu. "Removal of fine solids from bitumen by hetero-aggregation and magnetic separation using surface-modified magnetite nanoparticles. Part 1: Proof of concept. *Separation and Purification Technology,* Volume 300, 2022, 121840." I contributed to experimental design and execution, data collection and analysis, and manuscript writing. Kaipeng Wang contributed to experimental design and data interpretation. Xiaoli Tan was involved in concept formation and experimental design. Hongbo Zeng was the supervisory author and contributed to experimental design and manuscript editing. Qi Liu was the supervisory author and contributed to concept formation, experimental design, data interpretation, and manuscript editing.

Chapter 4 presented a published work: Xuyang Liu, Jingqiao Li, Kaipeng Wang, Xiaoli Tan, Anthony Yeung, Hongbo Zeng, and Qi Liu. "Removal of fine solids from bitumen by hetero-aggregation and magnetic separation using surface-modified magnetite nanoparticles. Part 2: Role of surface modification. *Separation and Purification Technology,* Volume 333, 2024, 125928." I contributed to concept formation, experimental design and execution, data collection and analysis, and manuscript writing. Jingqiao Li was involved in experimental design and execution. Kaipeng Wang contributed to experimental design. Xiaoli Tan was involved in concept formation and experimental design. Anthony Yeung contributed to experimental design and data interpretation. Hongbo Zeng was the supervisory author and contributed to experimental design and manuscript

editing. Qi Liu was the supervisory author and contributed to concept formation, experimental design, data interpretation, and manuscript editing.

Chapter 5 presented a paper in preparation: Xuyang Liu, Kaipeng Wang, Jiaao Yu, Hongbo Zeng and Qi Liu. "Surface-modified Fe_3O_4@SiO_2 core-shell magnetic beads for RNA extraction and detection of SARS-CoV-2 virus." I contributed to experimental design and execution, data collection and analysis, and manuscript writing. Kaipeng Wang contributed to experimental design and was involved in magnetic beads preparation. Jiaao Yu contributed to experimental design and execution of RT-PCR tests. Hongbo Zeng and Qi Liu were the supervisory authors and contributed to concept formation, experimental design, and data interpretation.

Acknowledgments

This thesis has been realized thanks to the generous support and substantial contributions of many individuals and institutions. I would like to extend my deep and sincere gratitude to the following :

My supervisor, Dr. Qi Liu, for his patient guidance, expertise, invaluable advice, encouragement, and continuous support throughout my PhD program; also, for his considerate and wise suggestions when I was facing dilemmas.

My supervisor, Dr. Hongbo Zeng, for his patience, insightful feedback and suggestions, and unconditional support during my PhD study.

Dr. Xiaoli Tan, for his exceptional suggestions and feedback on my research work, particularly concerning experimental designs related to asphaltene, oil sands processing, and fine solids removal in non-aqueous oil sands extraction.

Dr. Kaipeng Wang, for his guidance and help in the fabrication of nanoparticles and operation of magnetic separation, and experienced suggestions to my research work.

Dr. Anthony Yeung, for his constructive comments and suggestions on my research work regarding the surface modification of magnetite nanoparticles and fine solids removal from non-aqueous extracted bitumen.

Dr. Lilly Pang, for generously allowing RT-PCR tests to be conducted in her labs.

Dr. Joseph Thomas at the WATLab, University of Waterloo, for his assistance with the magnetic susceptibility measurements.

Jingqiao Li, for his invaluable input and helpful advice on the AFM measurements.

Jiaao Yu, for her invaluable assistance and advice on the RT-PCR tests and data analysis.

Lisa Brandt and Brittany Mackinnon, for the equipment training and technical support.

My group members (current and previous), Hanyu Zhang, Daowei Wang, Dong Wang, Menatalla Ahmed, Hao Li, and Haoran Sun, for their encouragement and help in my PhD study; for their support which brought me strength in my PhD life.

Institute for Oil Sands Innovation (IOSI) at the University of Alberta, for granting me access to their research labs.

Natural Sciences and Engineering Research Council of Canada (NSERC) and Future Energy System under the Canada First Research Excellence Fund (CFREF) for financial support.

All my friends, for the joyful moments and unforgettable memories we've shared together.

My boyfriend, for his companionship, care, and love.

And my family, to whom I dedicate this thesis work, for their endless love and support.

Table of contents

List of Tables

List of Figures

List of Abbreviations

AEAPTMS	3-(2-aminoethylamino) propyl trimethoxysilane
AFM	Atomic force microscopy
Asp-MNPs	Asphaltene-modified magnetite nanoparticles
ATR	Attenuated total reflectance
CHWE	Clark hot water extraction
DLS	Dynamic light scattering
DTGS	Deuterated triglycine sulfate
EDS	Energy dispersive spectroscopy
EtBr	Ethidium bromide
FTIR	Fourier transform infrared spectroscopy
hCoV-229E	Human coronavirus strain 229E
IL	Ionic liquid
ILASE	Ionic liquid assisted solvent extraction
MNPs	Magnetite nanoparticles
NAE	Non-aqueous extraction
NMR	Nuclear magnetic resonance
PBS	Phosphate-buffered saline
PCIA	Phenol, chloroform, and isoamyl alcohol mixture
PCR	Polymerase chain reaction
PEG	Polyethylene glycol
QCM-D	Quartz crystal microbalance with dissipation

RT	Room temperature
RT-PCR	Reverse transcription-polymerase chain reaction
SAA	Stearylamine acetate
SAA-MNPs	Stearylamine acetate-modified magnetite nanoparticles
SARS	Severe acute respiratory syndrome
SARS-CoV-2	Severe acute respiratory syndrome coronavirus 2
SC-MNPs	Sodium citrate-modified magnetite nanoparticles
SDS	Sodium dodecylsulfate
SEM	Scanning electron microscopy
SEM-FIB	Scanning electron microscopy-focused ion beam
SESA	Solvent extraction spherical agglomeration
SHS	Switchable hydrophilicity solvent
SHSE	Switchable hydrophilicity solvent extraction
SHTAs	Switchable-hydrophilicity tertiary amines
SQUID	Superconducting quantum interference device
TEM	Transmission electron microscope
TEOS	Tetraethyl orthosilicate
TMS-EDTA	N-[(3-Trimethoxysilyl) propyl] ethylenediamine triacetic acid
WHIMS	Wet high-intensity magnetic separator
XPS	X-ray photoelectron spectroscopy
XRD	X-ray diffraction

CHAPTER 1 Introduction

1.1 Research background

1.1.1 Surface-modified magnetic nanoparticles for advanced separation and purification

Solid-liquid separation plays a dominant role in various industrial sectors such as wastewater treatment, mineral processing, and biomedical diagnostics. The low efficiency of traditional solid-liquid separation techniques has increasingly become a significant issue, affecting product quality and overall process economy. In the last decades, advanced techniques of solid-liquid separation based on membrane filtration, electrophoresis, adsorption/desorption and so on, have been developed to improve separation efficiency. As a new-generation adsorbent, surface-modified magnetic nanoparticles exhibit great promise in solid-liquid separation applications owing to their low cost, strong adsorption capabilities, adjustable surface characteristics, and the convenience of magnetic-field-induced separation. Not surprisingly, magnetic sorbents have been widely used in environmental engineering and biomedical technology applications [1-2].

1.1.2 Surface-modified magnetic nanoparticles for fine solids removal from non-aqueous extracted bitumen

1.1.2.1 Background

Non-aqueous oil sands extraction is an alternative to the traditional Clark hot water bitumen extraction (CHWE) from Alberta oil sands. Using organic solvent to recover bitumen, NAE process potentially eliminates water use and can be operated at ambient temperature, hence the problems associated with the CHWE process, i.e., high consumption of fresh water and energy, high greenhouse gases emission, and the requirement to impound large volumes of unconsolidated fluid fine tailings, can be solved.

"Fine solids" in Alberta oil sands industry generally refer to mineral solids with diameters less than 45 μm. However, the fine solids in non-aqueous extracted (NAE) bitumen that are difficult to remove are usually much smaller than 45 μm, and are composed of quartz, kaolinite and illite, with trace amount of siderite, pyrite, feldspar, and chlorite. The majority of these mineral solids have particle sizes ranging from 10 nm to 10 μm [3-4]. Due to Brownian motion, the individual fine particles can remain suspended indefinitely, or settle at undetectable low velocity in organic solvents. Most of the clay minerals are hydrophilic, however, fine solids have been proven to be closely associated with organic matters from bitumen, especially asphaltene, which is the most polar fraction in bitumen [5]. The coating of the organic matters on the fine solids makes them bi-wettable or hydrophobic, thus increasing the possibility for them to stay in bitumen product when the solvent is evaporated.

The NAE bitumen should contain less than 0.03 wt% (300 ppm) of fine solids (on the basis of solvent-free bitumen) so that it can be fed directly to high conversion refineries without needing an upgrader [6]. However, at present NAE bitumen product cannot meet the quality requirement by using any of the available solid-liquid separation techniques. Conventional solid-liquid separation methods such as gravitational sedimentation, centrifugation and filtration can only remove relatively large solid particles. Newly developed methods such as adding wetting agents or polymers in NAE process would decrease fine solids content [7], but it is still much higher than the required solid content of less than 0.03 wt%. Using poor solvents in the NAE process could decrease fine solids content in NAE bitumen dramatically due to the capture of fine solids by precipitated asphaltene aggregates, but these solvents also lower bitumen recovery because of the loss of asphaltene. The inability to remove fine solids from bitumen product is one of the two most

significant issues that impede the industrial application of NAE process, while the other is the high cost and environmental pollution due to solvent loss to extraction gangue.

Recently, surface-modified magnetic nanoparticles have shown extraordinary advantages when being used as an adsorbent for impurities removal from crude oil or bitumen. For example, ethyl-cellulose-grafted Fe_3O_4 nanoparticles exhibited a strong affinity to water droplets in bitumen emulsion and could remove more than 80% of water from an industrial bitumen froth through magnetic separation [8-9]. Amine-functionalized Fe_3O_4 nanoparticles, reported by Ko et al., showed strong attachment with crude oil droplets in an oil-in-water emulsion, and played a critical role in the efficient and accelerated oil droplets removal in a magnetic field [10]. In the work of Setoodeh et al., it was observed that surface coating of Fe_3O_4 nanoparticles with polythiophene could increase the nanoparticles' adsorption capacity of asphaltene and thus could be potentially used in asphaltene removal from crude oil [11]. Inspired by those previous studies, a research program was initiated to separate fine solids from NAE bitumen by magnetic separation using surface-modified Fe_3O_4 nanoparticles.

1.1.2.2 Separation of the hetero-aggregates from fluid system

Hetero-aggregates would be formed if the target particles would be captured by magnetic nanoparticles. The formed magnetic aggregates can be efficiently separated from the fluid system if the magnetic force dominates the fluid drag, gravitational, lift forces, and Brownian force acting on the magnetic aggregates [12]. The forces affect the motion of magnetic aggregates in fluid system, and corresponding equations are summarized in Table 1.1. The motion of magnetic aggregates in a fluid under the influence of an applied magnetic field is affected by several factors, including the magnitude and the gradient of the applied magnetic field, the properties of the particles (size, density, velocity, magnetic susceptibility), the properties of the fluids (viscosity,

velocity), etc. [13]. All these factors, which in turn depend on the operation conditions and the particle parameters, should be taken into account for the design of magnetic separation process.

Table 1.1 Summary of forces in magnetic separation process [14].

Type of force	Classic equation
Magnetic force	$F_m = \frac{V_p \cdot \Delta\chi}{\mu_0}(B \cdot \nabla)B$ F_m: magnetic force (N); V_P: volume of particle (m^3); B: Magnetic induction; μ_0: permeability of vacuum, equals $4\pi \times 10^{-7}$ (T mA^{-1}); ∇ : mathematical operator that shows the gradient of the magnetic field; $\Delta\chi$: difference between magnetic susceptibilities of particles and base fluid.
Gravitational force	$F_g = V_p(\rho_P - \rho_f)g$ F_g: gravitational force; V_P: volume of the particle; ρ_P: density of particle; ρ_f: density of fluid; g: acceleration of gravity.
Fluid drag force	$F_f = 3\pi d_c(\mu_f - \mu_p)$ d_c: apparent diameter of the composite particles; μ_f: velocities of fluid; μ_p: velocities of particles.
Lift force	$F_{L,S} = \frac{\pi}{8}\rho_f \omega u d_p^{\,3}$ $F_{L,b} = 9.22(\frac{9}{4}\frac{\cup^2}{h^2})\rho_f d_p^{\,4}$ $F_{L,S}$: shear gradient induced lift forces; $F_{L,b}$: boundary layer lift force; d_p: diameter of the particle; ρ_f: density of the fluid; h: channel height; ω: vorticity of the flow; $\cup$: average velocity of the particle.
Brownian force	$F_B = \xi\sqrt{\frac{6\pi\kappa_B T d_p}{\Delta t}}$ k_B: Boltzmann constant; T: absolute temperate; d_p: diameter of the particle; Δt: magnitude of the time step; ξ: a Gaussian random number with zero mean and unit variance.

1.1.3 Magnetic beads for separation and purification of nucleic acids

Another important application of surface-modified magnetic nanoparticles for advanced separation is biomedical purification, which includes separation and purification of cells, proteins (antibodies and biomarkers), pathogens (bacteria and viruses), peptides, and nucleic acids [15]. Nucleic acid extraction, the initial step in genomic workflows, aims to obtain high purity nucleic acids, which is crucial for subsequent analytical or preparative procedures. Traditional nucleic acid extraction methods such as phenol–chloroform extraction, centrifugation, or spin column extraction are time-consuming, highly toxic, and expensive. Nucleic acid extraction using magnetic beads (surface-modified magnetic nanoparticles) is a revolution in this area and has several advantages. With tunable surface properties and magnetic susceptibility of the magnetic beads, the separation and purification of nucleic acids can be realized with exceptional efficiency and specificity. There are hardly any sample volume limitations in nucleic acids extraction process using this method. Besides, magnetic separation is easy to operate and highly efficient thus the method is suitable for large scale purification of nucleic acids [16-17].

Since the appearance of the SARS-CoV-2 (COVID-19) coronavirus in 2019, it rapidly spread worldwide, evolving into a pandemic that has infected over 770 million individuals and led to approximately 6.9 million deaths [18]. Testing for SARS-CoV-2 virus in hospitals and diagnostic labs has overwhelmed the workflow throughout the pandemic in Canada, and a major cause remains to be the access to reagents and buffers required for rapid viral RNA extraction from patient samples. This is a necessary pre-requisite for downstream reverse transcription polymerase chain reaction (RT-PCR), which is recommended as the gold standard for in vitro diagnostics of COVID-19. Most commercial nucleic acid extraction kits are based on magnetic bead technology due to the advantages mentioned above, and in the beginning of the pandemic, the market and

supply of COVID-19 viral RNA extraction kits were dominated by biotech companies such as Thermo Fisher Scientific Inc. (USA), Perkin Elmer Chemagen Technologie GmbH. (Germany), and Promega Corp. (USA). The supply shortages in reagents were directly caused by Canada's dependence on these foreign suppliers which adversely affected the supply chain due to the high global demand. Thus, Canada is in urgent need of access to locally sourced magnetic-based reagents for sample preparation and viral RNA extraction.

1.2 Research objectives

Magnetic nano-adsorbents represent a new generation of materials for advanced separation processes [19]. The objective of this study is to investigate the capabilities and significance of surface-modified magnetic nanoparticles in (1) the capture and removal of fine solids from NAE bitumen and (2) the extraction of nucleic acids from biomatrix. The concept is to explore appropriate surface modifications to magnetite nanoparticles, enhancing their affinity to the targets, i.e., NAE fine solids or viral RNA, and facilitating the formation of magnetic hetero-aggregates between the surface-modified magnetite nanoparticles and the targets. The subsequent removal or isolation of the targets can be achieved via magnetic separation. The specific objectives are:

(1) Design and synthesize suitable surface-modified magnetite nanoparticles that have high affinity to the targets, i.e., NAE fine solids or viral RNA.

(2) Design the process for removing fine solids from NAE bitumen by hetero-aggregation and magnetic separation using surface-modified magnetite nanoparticles; study the NAE fine solids separation performance by using this process.

(3) Investigate the interactions of surface modified magnetite nanoparticles with NAE fine solids to illustrate the fine solids removal mechanism.

(4) Develop an RNA extraction kit based on surface-modified magnetic nanoparticles (magnetic beads) and demonstrate the feasibility of viral RNA isolation and purification by using this kit.

1.3 Thesis organization

Chapter 1 includes a brief introduction to the background of the application of surface-modified magnetic nanoparticles for advanced separation, particularly in impurities removal from crude oil or bitumen and nucleic acids extraction.

Chapter 2 reviews the relevant literature about the current NAE fine solids removal techniques and the development and application of magnetic bead technology in nucleic acid extraction.

Chapter 3 proposes a novel method for fine solids removal from NAE bitumen by hetero-aggregation with surface-modified magnetite nanoparticles followed by magnetic separation. Stearylamine acetate-functionalized magnetite nanoparticles (SAA-MNPs) were prepared and characterized, and the separation performance of fine solids from NAE bitumen by the proposed approach using SAA-MNPs was quantitatively evaluated and compared with un-modified magnetite nanoparticles (MNPs). The regeneration and reuse of SAA-MNPs and MNPs were also investigated.

Chapter 4 is based on the research work presented in Chapter 3 and focuses on the influence of the surface modification of MNPs in their interactions with NAE fine solids. Asphaltene-modified magnetite nanoparticles (Asp-MNPs) were prepared, and their ability to remove fine solids from NAE bitumen was evaluated and compared with SAA-MNPs. The influence of the surface modification with SAA or asphaltene on MNPs in their interactions with NAE fine solids was investigated through quartz crystal microbalance with dissipation monitoring (QCM-D) and atomic force microscopy (AFM) studies. In addition, the influence of the external magnetic field

on the formation of hetero-aggregates was studied. The schematics of magnetic field-assisted hetero-aggregation between surface-modified MNPs and the NAE fine solids were proposed.

Chapter 5 investigates the extraction of viral RNA from wastewater sample using the developed core-shell magnetic bead extraction kit.

Chapter 6 summarises the major conclusions and original contribution of this work. The recommendations for future work are also presented.

1.4 References

1. Qu, X.; Alvarez, P.J.; Li, Q., Applications of nanotechnology in water and wastewater treatment. *Water Research* **2013,** *47* (12), 3931-3946.

2. Wang, T.; Ai, S.; Zhou, Y.; Luo, Z.; Dai, C.; Yang, Y.; Zhang, J.; Huang, H.; Luo, S.; Luo, L., Adsorption of agricultural wastewater contaminated with antibiotics, pesticides and toxic metals by functionalized magnetic nanoparticles. *Journal of Environmental Chemical Engineering* **2018,** *6* (5), 6468-6478.

3. Meadus, F.W.; Bassaw, B.P.; Sparks, B.D., Solvent extraction of Athabasca oil-sand in a rotating mill Part 2. Solids—liquid separation and bitumen quality. *Fuel Processing Technology* **1982,** *6* (3), 289-300.

4. Nikakhtari, H.; Wolf, S.; Choi, P.; Liu, Q.; Gray, M.R., Migration of fine solids into product bitumen from solvent extraction of Alberta oilsands. *Energy & Fuels* **2014,** *28* (5), 2925-2932.

5. Wang, S.; Liu, Q.; Tan, X.; Xu, C.; Gray, M.R., Study of asphaltene adsorption on kaolinite by X-ray photoelectron spectroscopy and time-of-flight secondary ion mass spectroscopy. *Energy & Fuels* **2013,** *27* (5), 2465-2473.

6. Pal, K.; Nogueira Branco, L. d. P.; Heintz, A.; Choi, P.; Liu, Q.; Seidl, P. R.; Gray, M. R., Performance of solvent mixtures for non-aqueous extraction of Alberta oil sands. *Energy & Fuels* **2015,** *29* (4), 2261-2267.

7. Lin, F.; Stoyanov, S.R.; Xu, Y., Recent advances in nonaqueous extraction of bitumen from mineable oil sands: a review. *Organic Process Research & Development* **2017,** *21* (4), 492-510.

8. Peng, J.; Liu, Q.; Xu, Z.; Masliyah, J., Novel Magnetic demulsifier for water removal from diluted bitumen emulsion. *Energy & Fuels* **2012,** *26* (5), 2705-2710.

9. He, X.; Liu, Q.; Xu, Z., Cellulose-coated magnetic Janus nanoparticles for dewatering of crude oil emulsions. *Chemical Engineering Science* **2021,** *230*, 116215.

10. Ko, S.; Kim, E. S.; Park, S.; Daigle, H.; Milner, T. E.; Huh, C.; Bennetzen, M. V.; Geremia, G. A. In oil droplet removal from produced water using nanoparticles and their magnetic separation, *SPE Annual Technical Conference and Exhibition* **2016.**

11. Setoodeh, N.; Darvishi, P.; Esmaeilzadeh, F., Adsorption of asphaltene from crude oil by applying polythiophene coating on Fe_3O_4 nanoparticles. *Journal of Dispersion Science and Technology* **2018,** *39* (4), 578-588.

12. Moeser, G.D.; Roach, K.A.; Green, W.H.; Alan Hatton, T.; Laibinis, P.E., High-gradient magnetic separation of coated magnetic nanoparticles. *AIChE Journal* **2004,** *50* (11), 2835-2848.

13. Gómez-Pastora, J.; Bringas, E.; Ortiz, I., Recent progress and future challenges on the use of high performance magnetic nano-adsorbents in environmental applications. *Chemical Engineering Journal* **2014,** *256*, 187-204.

14. Hejazian, M.; Li, W.; Nguyen, N.T., Lab on a chip for continuous-flow magnetic cell separation. *Lab on a Chip* **2015,** *15* (4), 959-970.

15. Yildiz, I., Applications of magnetic nanoparticles in biomedical separation and purification. *Nanotechnology Reviews* **2016,** *5* (3), 331-340.

16. Tang, C.; He, Z.; Liu, H.; Xu, Y.; Huang, H.; Yang, G.; Xiao, Z.; Li, S.; Liu, H.; Deng, Y; Chen, Z., Application of magnetic nanoparticles in nucleic acid detection. *Journal of Nanobiotechnology* **2020,** *18* (1), 1-19.

17. Berensmeier, S., Magnetic particles for the separation and purification of nucleic acids. *Applied Microbiology and Biotechnology* **2006,** *73*, 495-504.

18. World Health Organization Report. https://covid19.who.int/ Accessed on 20th September 2023.

19. Peralta, M.E.; Ocampo, S.; Funes, I.G.; Onaga Medina, F.; Parolo, M.E.; Carlos, L., Nanomaterials with tailored magnetic properties as adsorbents of organic pollutants from wastewaters. *Inorganics* **2020,** *8* (4), 24.

CHAPTER 2 Literature Review

2.1 Fine solids removal from non-aqueous extracted bitumen

2.1.1 Properties of NAE fine solids

The NAE fine solids consist primarily of clay minerals like kaolinite and illite as well as non-clay minerals such as quartz, feldspar, calcite, siderite [1]. Mixed layer clay minerals such as illite–smectite or kaolinite–smectite may be also present in low concentrations. The fine solids that are difficult to remove normally have particle sizes ranging from 10 nm to 10 μm. The separation of these fine and ultrafine solids is inefficient using conventional solid-liquid separation techniques due to the dominant effects of fine solids properties and interfacial interactions [2]. For particles in the micron size range or smaller, colloidal and interfacial forces are more significant. In NAE bitumen extraction process, the surface properties of fine solids, such as hydrophobicity or surface composition are readily altered due to their interactions with bitumen components, which influences their interfacial interactions and separation efficiency.

It has been shown that the fine solids are closely associated with organic matters from bitumen. SEM-FIB analysis of fine solids in cyclohexane extracted bitumen illustrated that the minerals and the organic matters were in intimate contact, according to the study of Nikakhtari et al [1]. Czarnecka et al. showed that both maltenes and asphaltenes extracted from Athabasca oil sands could be adsorbed by the four common clay minerals in Athabasca oil sands (illite, kaolinite, montmorillonite, and chlorite) [3]. Clays, with large specific surface areas, were found to retain more residual organic matter after non-aqueous solvent bitumen extraction on per unit mass basis, and the adsorbed organic matters on the external surfaces of clay mineral particles was shown to be in patches rather than as a continuous coating. This conclusion was drawn from the observation that Al, Si, Fe could still be detected in bitumen-coated clays in XPS analysis [1,4-6]. The

adsorption of these organic matters on the clay mineral surfaces makes them hydrophobic or bi-wettable. Contact angles of organic-matter-coated fines in the solvent-extracted bitumen supernatant were found to be about 90° [1]. Also, it was reported that when treated with bitumen or asphaltene, the hydrophilic clay minerals became hydrophobic with contact angles larger than 90° [7-8]. These bi-wettable or hydrophobic characteristics increase the possibility of fine solids to migrate to bitumen product, lowering bitumen product grade.

It is worth mentioning that asphaltenes were found to interact with iron minerals in oil sands, and the presence of iron minerals could enhance asphaltene aggregate formation. Hematite and iron-containing chlorite mineral were shown to adsorb more than twice as much asphaltenes than non-iron-bearing clays [9-10]. The polarity of asphaltene was dramatically affected with the addition of iron compounds [11]. Evidence suggested that Fe_2O_3 affected the hydrogen bonding tendency of asphaltene and resin hydrocarbon group types, and Fe_2O_3 had a specific attractive interaction for the aromatic moieties of asphaltenes [12-13]. Impregnating Fe_2O_3 on kaolinite, montmorillonite, and SiO_2 surfaces greatly enhanced crude oil polar hydrocarbons adsorption relative to the unmodified sorbent substrates [12].

2.1.2 NAE fine solids removal strategies

Different strategies have been developed for the fine solids removal from NAE bitumen, as summarized in Table 2.1.

Table 2.1 Summary of fine solids removal strategies

Fine solids removal strategies	Principle	Reference
Aggregation by poor solvents	Fine solids trapped by asphaltene aggregates during precipitation	[17]
Polymer flocculation	Bridging flocculation between polymer and fine solids	[19]
Agglomeration by water/surfactant	Fine solids trapped at water/oil interface	[20, 21]
Electric field assisted separation	Retained by dielectric medium under external electric field	[23]

2.1.2.1 Aggregation of fine solids by poor solvents

Using poor solvents for asphaltenes such as alkanes in NAE process is beneficial to a lower fine solids content. Asphaltenes are stabilized in crude oil by the attachment of smaller hydrocarbon resin units. Paraffin molecules in poor solvents act to isolate resins, preventing their bonding with asphaltene molecules, ultimately leading to the destabilization of the asphaltene emulsion [14-15]. During the asphaltene precipitation, the fine solids can be trapped and collected in the "network" structure of asphaltene aggregates. Besides, the fine solids can function as nuclei for asphaltene precipitation. The asphaltene coating on fine solid surfaces provides bonding bridge between fine solids, resulting in the formation of larger aggregates [16].

The disadvantage of using poor solvents in NAE process is that it leads to a lower bitumen recovery because of the loss of asphaltene. Using alkanes alone as the sole solvents in NAE would cause the loss of up to 20% hydrocarbon upfront in the form of precipitated asphaltenes. To reduce the loss of asphaltenes, good solvent could be used in extraction followed by blending a poor solvent to precipitate part of the asphaltenes to remove fine solids [17]. However, the solvent blending and

separation would significantly complicate the industrial application of the process, and would still lead to losses of hydrocarbons*.

2.1.2.2 Destabilization of fine solids suspension by additives

Different additives have been investigated in NAE process to destabilize the suspension of fine solids, which include polymers, (emulsified) water, aqueous alkaline solution, surfactants, or ionic liquids. Flocculation or agglomeration of fine solids may be induced by the addition of additives, which are common strategies to facilitate particle aggregation in solid-liquid separation, albeit more so in aqueous suspensions.

When adsorbed onto the surface of colloidal particles, high molecular weight polymers can act as a bridge between particles, resulting in flocculation and destabilization of the suspension. It is believed that effective polymer flocculants for NAE fine solids aggregation must be oil-soluble or be capable of dispersion in non-aqueous media [16,18]. Additionally, it should incorporate some polar end groups or blocks of hydrophilic polymers to facilitate adsorption onto fine solids [18]. Dixon et al. [18] selected and screened different kinds of polymers, including hydrophobic polymers with hydrophilic branches, block copolymers containing a main hydrophobic chain with hydrophilic chain ends, and random copolymers containing hydrophilic and hydrophobic monomers, for flocculation study using kaolinite suspended in diluted bitumen and toluene as a model system. However, the observations revealed that the tested polymers did not display significant flocculation effects on kaolinite in toluene, highlighting the difficulties associated with the selection of suitable polymers as flocculants in the NAE system. Ngnie et al. studied the sedimentation behaviors of organic-coated kaolinite particles (< 1 μm) and dry mature fine tailings

* The commercial paraffinic froth treatment (PFT) processes use pentane or hexane to dilute bitumen froths generated from the CHWE process. It generates a clean bitumen product that can be sent to a high conversion refinery but loses about 8% of the hydrocarbon as precipitated asphaltenes.

in cyclohexane in the presence of polyethylene glycol (PEG_{1000}). The results demonstrated that the introduction of PEG_{1000} led to an increased settling rate for both types of particles, suggesting the potential effectiveness of the tested polymer in NAE fine solids removal [19].

Water or surfactant dissolved in water can also be used to assist fine solids removal in NAE process. With the addition of water, as in the Solvent Extraction Spherical Agglomeration (SESA) process (discussed in Section 2.1.3.1), the hydrophilic fine particles can be bound by water and form large aggregates. For hydrophobic fine particles, i.e., particles coated by bitumen components, appropriate surfactant can act as a bridge to promote their aggregation with water droplets. With surfactant dissolved in water droplets, the hydrophobic tail of the surfactant can attach to the hydrophobic fine solids, thereby trapping them at the water/oil interface. Alquist et al. [20] proposed an NAE bitumen extraction process employing aqueous solutions of surfactant to capture suspended fine solids, with coarse particles separated initially through settling, followed by the removal of fine particles through mixing diluted bitumen with water containing a cationic surfactant. The solids content in the final bitumen product was lowered to approximately 0.2 wt% under optimized conditions. Liu et al. [21] utilized water droplets to destabilize bitumen-coated silica particles in a cyclohexane suspension. Initially, the amphiphilic polymer poly(ethylene glycol)-block-poly(propylene glycol)-block-poly(ethylene glycol), i.e., PEG-PPG-PEG, was added to modify the particle surfaces, followed by the addition of a small amount of water to collect the modified particles to form large aggregates. The two-step method significantly enhanced the settling rate of the particles and reduced the content of residual solids in the supernatant simultaneously.

2.1.2.3 Electric field assisted separation

Electric field assisted separation is a novel technique for NAE fine solids removal. Typically, colloidal particles in organic solvents are unable to retain a net charge because of the low dielectric permittivity of such solvents. However, Zhang et al. [22] have demonstrated that kaolinite coated with bitumen or bitumen fractions (i.e., maltene or asphaltene) could be electrodeposited on electrodes from cyclohexane media. This was attributed to the functional groups present in the surface coating. Cullinane et al. [23] patented a physical separation and electrostatic filtration method to remove fine solids from NAE bitumen. Filtration was first performed to separate large particles from NAE bitumen. Afterwards, the filtrate was passed through an electrostatic separator which housed a bed of dielectric particles such as glass beads. The removal of fine solids was realized by applying a voltage across the electrodes that were separated by the dielectric medium creating a voltage gradient between the electrodes. As the filtrate passed through, fine solids with charges would be attracted and retained by the dielectric medium and removed from the oil stream. Fine solids content in the NAE bitumen product could be reduced to 1200 ppm (0.12 wt%) by using this method.

2.1.3 Fine solids removal in modified NAE processes

2.1.3.1 Solvent extraction spherical agglomeration

Solvent Extraction Spherical Agglomeration (SESA) is an approach that combines the introduction of solvent and a small amount of another liquid that is immiscible with the solvent, typically water, to effectively separate bitumen from oil sands. Figure 2.1 illustrates the flow diagram of a typical SESA process. The crushed oil sands ore is mixed with an organic solvent and a small amount of water in a tumbler. Water is added as an immiscible bridging agent that triggers the agglomeration of the fine solids. The oil–water interface network can trap fine particles, and the water droplets

can establish liquid bridge between the suspended fine particles. The agglomerated solids are removed by a series of liquid−solid separation steps including tumbler, thickener, agglomerate washing on a belt filter. The recovered solvent is reused in the extraction process. In Sparks et al.'s work, after extraction with SESA process, the fine solids content (based on the extracted bitumen in solution) was less than 2 wt% [24].

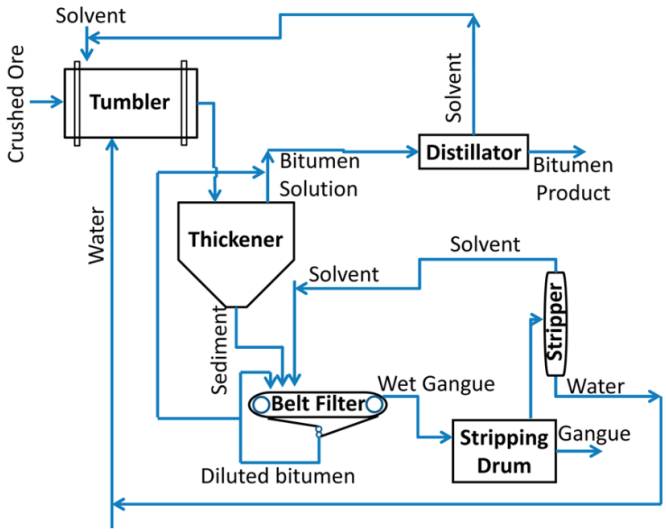

Figure 2.1 Schematic of a solvent extraction spherical agglomeration (SESA) process [16].

2.1.3.2 Switchable hydrophilicity solvent extraction

Switchable hydrophilicity solvent extraction (SHSE) is a modified NAE process first tested in 2010. The solvent used in the process, also called switchable hydrophilicity solvent (SHS), could reversibly switch between being hydrophobic and being hydrophilic. The trigger for the switch is the addition or removal of the switch agent (usually CO_2). Figure 2.2 illustrates a typical SHSE process using $CyNMe_2$ as the SHS. Briefly, the process starts with bitumen extraction using $CyNMe_2$ in its hydrophobic form. Afterward, the solids are separated by filtration or decantation, while the liquid phase (bitumen in $CyNMe_2$ mixture) is treated with carbonated water to expel $CyNMe_2$ from bitumen by converting it into a water-soluble bicarbonate salt $[CyNMe_2H][HCO_3]$.

The bitumen is then collected by decantation, and the $CyNMe_2$ is separated from water by removing the CO_2 through heating or blowing nitrogen gas/air into the mixture. Sui et al. [25] developed another SHS, switchable-hydrophilicity tertiary amines (SHTAs, such as triethylamine, N, N-dimethylcyclohexylamine, N,N-dimethylbenzylamine), and studied its roles in heavy hydrocarbons recovery from oil sands ores by solvent extraction. The results showed that it was efficient to liberate bitumen from fine solids by introducing SHTAs due to an increase in the hydrophilicity of the solid surface leading to a reduction in bitumen−solid interaction, and the generated bitumen product contained 0.12 wt% fine solids.

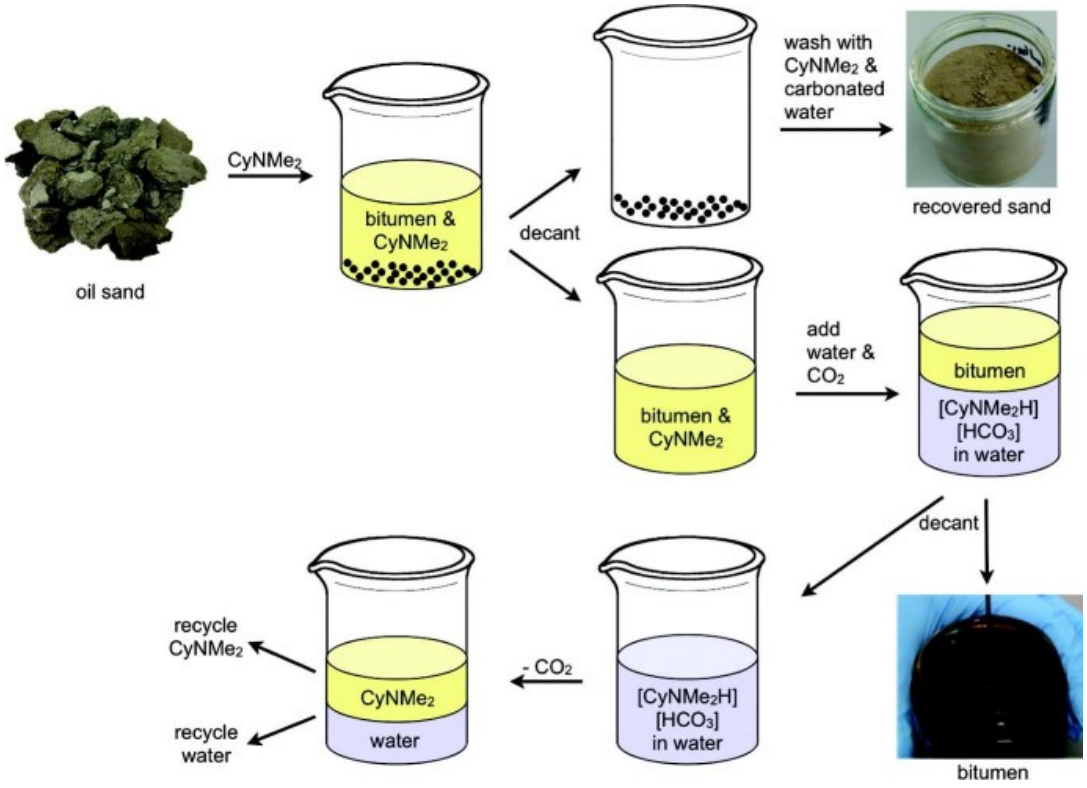

Figure 2.2 Schematic of a switchable hydrophilicity solvent extraction (SHSE) process [26].

2.1.3.3 Ionic liquid assisted solvent extraction

Ionic liquids (ILs) are compounds consisting of cations and anions with a melting point equal to or below 100ºC [27]. Recent studies have shown that ionic liquids can successfully extract bitumen from oil-wet as well as water-wet oil sand easily [28]. This technology was initially developed by Painter et al. and published in 2010 [29]. Figure 2.3 illustrates a schematic diagram of IL assisted solvent extraction (ILASE) of bitumen. When ionic liquid and organic solvent are introduced as co-solvents to oil sands, they give rise to three distinct layers: an upper organic layer containing bitumen, a middle layer of ionic liquid, and a bottom layer of clay/sands. After the formation of the three layers, the bitumen at the top is separated and extracted by evaporating the organic solvent. The mixture of IL and sand is separated through water washing; subsequently, water is evaporated to recover the IL. So far, the effect of ionic liquids on the oil–solid interaction force is still not clear. Hou et al. [30] suggested in their study that the IL could modify the oil–solid interface, making the sand surface more hydrophilic and decreasing heavy oil–solid interaction forces. Liu et al. [31] indicated that IL had strong electrostatic interactions with the surface of mineral particles in oil sands, resulting in the detachment of bitumen from these particles and thereby facilitating the recovery of bitumen. The ILASE technology has excellent performance in fine solids removal and bitumen recovery and can be performed in ambient conditions. Pulati et al. used ionic liquid, a deep eutectic mixture of choline chloride and urea, together with diluent naphtha to extract bitumen from oil sands and found that the obtained bitumen had only trace amounts of mineral fines, below 0.5 wt% [32].

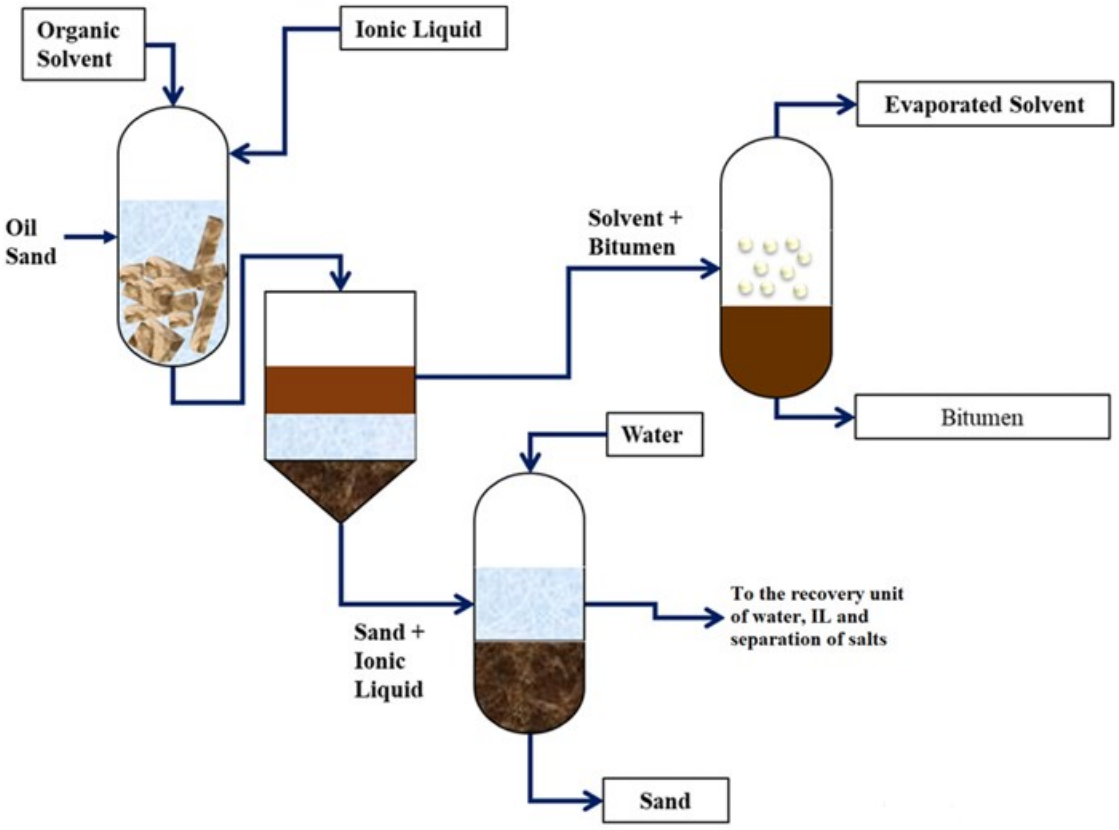

Figure 2.3 Schematic of an ionic liquid assisted solvent extraction (ILASE) process [28].

2.1.4 Summary

In summary, while various strategies have been developed over the past decades for the removal of fine solids from NAE bitumen, none of them have proven suitable for practical commercial implementation. Firstly, the efficacy of current developed strategies in NAE fine solids removal is insufficient, resulting in the products failing to meet the refinery's requirement (fine solids content below 0.03 wt%). Conventional solid-liquid separation techniques, including gravitational sedimentation, centrifugation, and membrane filtration following an NAE extraction, are time-consuming, and only manage to remove relatively large solid particles. Laboratory studies using additives (polymers, water droplets, or wetting surfactants) during the NAE process, or ionic liquid-assisted solvent extraction could obtain cleaner NAE bitumen products, but the fine solids

contents were typically still much higher than 0.03 wt%. Secondly, the solvent systems utilized in current methods were not compatible with the requirements of commercial operations. Some methods such as switchable hydrophilicity solvent extraction used high-cost and toxic solvents, rendering them impractical for commercial use. Furthermore, all current studies use high solvent/bitumen ratios, typically higher than 10, which presents a challenge for aligning with commercial practices that typically demand a solvent/bitumen ratio of 2:1 or lower.

2.2 Magnetic beads for the extraction and purification of nucleic acids

2.2.1 Traditional nucleic acid purification methods

2.2.1.1 Phenol-chloroform extraction

Phenol–chloroform extraction is a widely used nucleic acid extraction process that involves the thorough mixing of a phenol-chloroform solution with the sample, followed by centrifugation [34]. A typical process for using this method for DNA extraction from cells is shown in Figure 2.4. First, sodium dodecylsulfate (SDS) and proteinase K are introduced to disrupt the cell membranes and degrade proteins and non nucleic acid cellular components. After incubation, a mixture of phenol, chloroform, and isoamyl alcohol is added to facilitate the separation of lipids and cellular debris, directing them into the organic phase, while the DNA remains dispersed in the aqueous phase [33-34]. Upon centrifugation, undesirable proteins and cellular debris are effectively separated from the aqueous phase, allowing the clean transfer of double-stranded DNA molecules for subsequent analysis. DNA from the aqueous phase can also be concentrated using ethanol precipitation or a centrifugal filter unit, enabling further purification and concentration of the DNA within the samples [35-36]. This method can also be employed for RNA extraction by concomitant use of guanidinium isothiocyanate, and the process is known as guanidinium thiocyanate-phenol-chloroform extraction as described by Chomczynski and Sacchi [37]. The process works because

in the acidic conditions, total RNA will remain in the upper aqueous phase of the whole mixture, while DNA and proteins remain in the interphase or lower organic phase [38]. While this method is relatively easy and useful for the extraction of nucleic acids, it is time-consuming and requires great hands-on effort and skills. Besides, phenol has limitations in being used in clinical microbiology laboratory because it is toxic, caustic, and flammable [39-40].

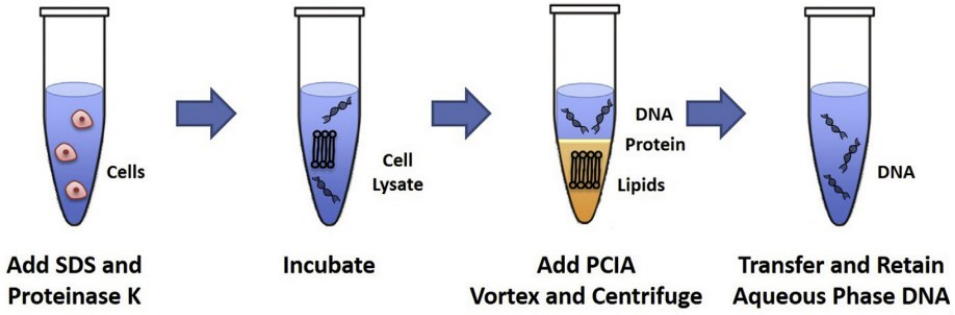

Figure 2.4 Schematic of phenol-chloroform DNA extraction method. The extraction utilizing phenol, chloroform, and isoamyl alcohol mixture (PCIA) results in DNA being separated to the aqueous phase, while lipids and proteins are partitioned to either the organic phase or the aqueous-organic interface [34].

2.2.1.2 Cesium chloride (CsCl) / ethidium bromide (EtBr) density gradient centrifugation

Since the 1950s, density gradient centrifugation utilizing CsCl and EtBr has been employed as a DNA extraction method, establishing itself as a standard procedure in research laboratories [41]. CsCl is a heavy salt with a high density, and EtBr is an intercalating agent that can intercalate between the base pairs of DNA. This method is based on the phenomenon of buoyancy and specific density. Through the intercalation of EtBr, DNA molecules can be distinctly separated into bands based on variations in their densities within the gradient [33,41-42]. Since EtBr becomes fluorescent under UV light, the DNA bands can be easily located and subsequently extracted. The hydrophobic EtBr is then removed with appropriate hydrophobic solvents and the purified nucleic

acid is reprecipitated with alcohol [43]. There are limitations to this method, including the necessity for an expensive ultracentrifuge and considerable time, complicated process, and toxicity of EtBr [33,35].

2.2.1.3 Spin-column extraction

In the 1980s, the recognition of spin columns' potential and effectiveness for nucleic acid extraction and purification was underscored, exemplified by Marko et al.'s successful binding of plasmid DNA from cell lysate using glass powder in the presence of a sodium perchlorate solution [44-45]. The spin column method has evolved and is now incorporated into commercial kits for nucleic acid extraction. The method relies on the use of specialized spin columns that contain a silica-based membrane or other materials with affinity to nucleic acids [45]. Figure 2.5 shows a schematic of the spin column extraction process. Firstly, the sample is lysed with a lysis buffer to break down the cell membrane. Then the sample is transferred into the spin column in which the nucleic acids bind to the membrane inside the column. By applying a vacuum or centrifugal force, the solution containing unwanted materials is pulled through the membrane. To wash away unbound components, a wash buffer is passed through the spin column, using vacuum or centrifuge, to maintain binding conditions but remove binding salts and any other remaining contaminants. Lastly, elution buffer is added to the spin column to liberate the nucleic acids from the membrane and collect them in the tube. The advantages of spin column extraction are that it is efficient, economical, and provides high yield and high purity nucleic acids. The primary limitations of this method include the potential for membrane clogging, and that large volumes of elution buffer are required, which leads to low nucleic acid concentrations [46-47].

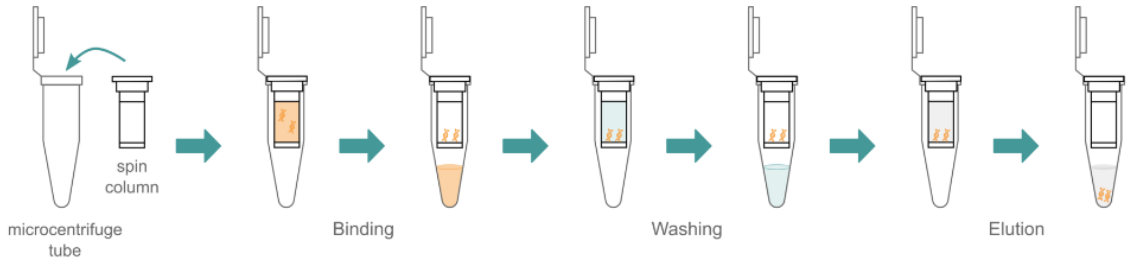

Figure 2.5 Schematic of spin column extraction process [48].

2.2.2 Magnetic bead extraction technology

2.2.2.1 Principle

Magnetic beads have been proven to be suitable for extraction of nucleic acids due to their efficiency, ease of use, and adaptability to automated workflows [49-51]. With surface modification and magnetic field-responsive property, they can effectively bind nucleic acids and facilitate comprehensive nucleic acid assays without the need for pipetting driven by pumps and centrifuges. A comparison of magnetic bead extraction method with traditional extraction methods is shown in Table 2.2.

Table 2.2 Comparison of magnetic bead extraction method with traditional nucleic acid extraction methods.

Nucleic acid extraction methods	Advantages	Disadvantages
Phenol-chloroform extraction	Easy; useful	Time-consuming; hands-on skills required; toxic solvent
Cesium chloride (CsCl) / ethidium bromide (EtBr) density gradient centrifugation	Efficient; visual separation	Expensive; time-consuming; complicated process; toxic
Spin-column extraction	Efficient; economical; provides high yield / high purity nucleic acids	Potential for membrane clogging; low nucleic acid concentrations
Magnetic bead extraction	Simple and convenient; high efficiency and specificity; high sample-processing ability	Viscous samples may impede migration of magnetic beads

As a bridge, magnetic beads are connected to the integrated steps of separation, purification, amplification, and detection [52]. Numerous kits for magnetic bead extraction are now available as commercial products, compatible with manual or automatic operations. Figure 2.6 shows the nucleic acids extraction processes using magnetic beads. As illustrated, either the liquids or the magnetic beads are required to be transferred [53-54], but the principles are the same. Initially, a lysis buffer is added to the sample to disrupt the cell membrane. Then the magnetic beads are introduced to capture the desired nucleic acids. This interaction relies on the specific affinity of the ligand on the surface of the beads. Afterward, a magnetic field is introduced, thus the magnetic beads with the bound nucleic acids are rapidly and efficiently separated from the remaining sample components. In the final stage, the bead-bound target is released in a suitable volume of elution buffer for use in downstream analysis.

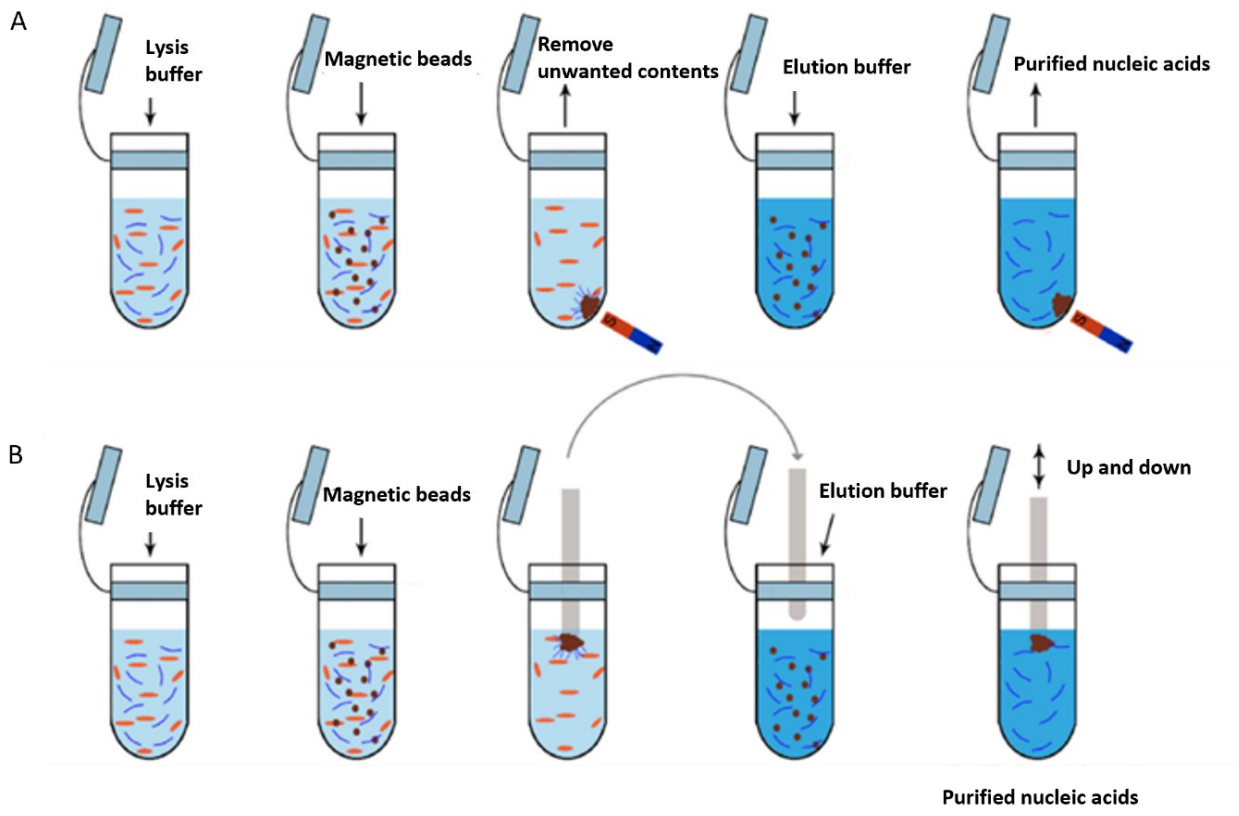

Figure 2.6 Schematic of magnetic beads nucleic acid purification process [52]. (A) The magnetic beads nucleic acid extraction assay requiring liquid transfer. (B) The magnetic beads nucleic acid extraction assay requiring magnetic beads transfer.

2.2.2.2 Surface modification of magnetic beads

Surface modification is a crucial step in the preparation of magnetic beads to enhance their bio-compatibility and affinity for target molecules. The most prevalent surface modifications include silica coating, carboxyl group grafting, and amino group grafting on beads surface. Recently, magnetic beads have been developed with modifications involving diverse ligands such as oligonucleotides, antibodies, streptavidin, or aptamers, making them versatile for a range of downstream applications.

Silica coating is a basic and popular modification strategy in magnetic beads preparation due to its high flexibility and bio-compatibility. Various ligands can be grafted on magnetic beads through the engineering of silica-coated magnetic bead surfaces to enable a broad range of additional functionalities to the magnetic beads. The binding of nucleic acids to the surface of silica-coated magnetic beads probably relies on hydrogen-bonding interaction under chaotropic conditions, or interaction of silica with nucleic acids in a condensed state under high polymer and salt concentrations [55]. The use of chaotropic salts to induce nucleic acids adsorption onto silica surfaces is a commonly employed method in nucleic acid isolation procedures. The nucleic acids binding has been carried out in the presence of chaotropic agents such as NaI, $NaClO_4$, guanidinium hydrochloride (GuHCl) and Gu thiocyanate (GuSCN) [56-58]. The chaotropic agents strongly capture water molecules which induces dehydration effects on the nucleic acid and silica surfaces [56]. Under acidic conditions, numerous phosphorus and silanol groups, especially the geminal silanol groups, undergo protonation which facilitates the formation of intermolecular hydrogen bonds between the DNA–silica contact layer [59-61]. Besides chaotropic agents, polymer-salt aqueous system is also used in nucleic acid extraction using silica-coated magnetic beads [62-63]. The mechanism is discussed in more detail in the next paragraph. It was reported that core-shell structured silica-coated iron oxide ($Fe_3O_4@SiO_2$) nanobeads were able to separate nucleic acids from various biological samples such as cancer cells, viruses, and bacteria [64]. Wang et al. [65] demonstrated that silica-coated magnetic particles could extract both DNA and RNA simultaneously from Hepatocellular Carcinoma, and the high quality and quantity of DNA and RNA could be used in PCR and RT-PCR that were essential for molecular oncologic studies.

Carboxyl-coated magnetic nanoparticles are also capable of extracting nucleic acids. Typically, the introduction of carboxyl groups onto the surface is achieved through polymer coating, which

provides stability as well as a surface with a weak negative charge. Unmodified single-stranded oligonucleotide can adsorb efficiently on negatively charged carboxyl-coated magnetic nanoparticles through hydrogen-bonding interaction [66], whereas double-stranded DNA does not possess this adsorbing property [55,67]. Yet carboxyl-coated magnetic beads have been effectively employed for isolating PCR products, plasmid DNA, and bacterial DNAs from various complex samples [55,67-71]. This is because counterion-mediated coupling facilitated by multivalent counterions can occur between the carboxyl-modified magnetic beads and DNA [72]. The counterions act as bridges between the negatively charged DNA and magnetic beads, effectively neutralizing the charges and facilitating their binding. This mechanism relies on the electrostatic interactions between the charged species and the multivalent ions. Also, a polymer- and salt-induced condensation mechanism is well-accepted for the like-charge sorbent/DNA complexation [55,73-74]. This mechanism involves the addition of polymers and salts to induce the condensation of nucleic acids onto the like-charge sorbents. Polymers, such as polyethylene glycol (PEG), and salts, such as sodium chloride (NaCl), can alter the ionic strength and solution properties, leading to the compaction of nucleic acid molecules [75-76]. This compaction reduces the electrostatic repulsion between the negatively charged nucleic acids and negatively charged magnetic beads (carboxyl-modified magnetic beads, or silica-coated magnetic beads mentioned in the previous paragraph), promoting DNA adsorption on the surface of magnetic beads. It has been demonstrated that carboxyl-modified magnetic beads are rapid and efficient in PCR-ready DNA extraction from Staphylococcus aureus bacteriophages using the PEG 6000 and NaCl system [77]. Sarkar et al. showed that in addition to the specific extraction of plasmid DNA, carboxyl-modified magnetic beads also exhibited the capability to extract mRNA from mammalian cells [78].

The phosphate backbone imparts a negative charge to DNA and RNA molecules [79]. Thus, modifying the surfaces of magnetic beads with positively charged molecules represents a straightforward strategy to improve their affinity with nucleic acids by increasing the electrostatic attraction. The use of amino groups ($–NH_2$), which provide cationic surface charge, to modify silica-coated magnetic beads is a commonly employed approach for preparation of positively charged magnetic beads. In the work of He et al. [80], amino-silica coated magnetic nanoparticles were synthesized and applied for the pEGFP-N3 plasmid DNA concentration and isolation from crude bacteria. The extraction procedure was efficient, and the obtained pEGFP-N3 plasmid retained biological activity that could be suitable for downstream applications. In the work of Bai et al. [81], a type of amino-rich silica-coated magnetic nanoparticles was also prepared and the synthesized beads showed great potential for bacterial genomic DNA capture.

2.2.3 Magnetic beads in COVID-19 pandemic

Since the appearance of the SARS-CoV-2 (COVID-19) coronavirus in 2019, it rapidly spread and evolved into a global pandemic. Reverse transcription-polymerase chain reaction (RT-PCR) is widely recognized as the gold standard for establishing a microbiological diagnosis of SARS-CoV-2 due to its high specificity of almost 100% [82]. The principle is that in conventional PCR, multiple cycles of heating and cooling are performed, facilitating the amplification of the target DNA segment through denaturation, annealing, and extension of DNA sequences in each cycle. And in RT-PCR, RNA is first converted into its complementary DNA sequence by reverse transcriptase, to synthesise a second strand with DNA polymerase, and finally to generate a double stranded complementary DNA molecule which can be amplified by PCR in the normal way [83]. The amplified DNA products are detected using fluorescent dyes for quantification of the initial amount of RNA present in the sample.

The SARS-CoV-2 viral RNA extraction from patient samples is a necessary pre-requisite for the RT-PCR tests. Magnetic bead-based RNA extraction presents numerous advantages, such as high efficiency and specificity, ease of operation, and compatibility with high-throughput automated platforms. These attributes have played a crucial role in facilitating widespread testing for SARS-CoV-2, contributing significantly to early detection, surveillance, and management of the pandemic. However, the pandemic has led to shortages of various materials and supplies, particularly in diagnostic and treatment resources for SARS-CoV-2 due to disruptions in manufacturing, transportation, and supply chains caused by lockdown measures, and increased demand. As a result, laboratories and research facilities have faced challenges in acquiring essential materials required for rapid SARS-CoV-2 diagnosis, impacting the assessment and control of the pandemic. A similar issue occurred in Alberta, Canada, where hospitals and diagnostic labs faced overwhelming demands for SARS-CoV-2 testing, affecting their workflow. In March 2020, in the middle of the author's dissertation research of using magnetite sorbents to clean NAE bitumen, we were approached by Alberta Health Services to help develop the RNA extraction kit based on magnetic bead technique, targeting for the extraction of SARS-CoV-2 viral RNA. Different commercial nucleic acid extraction kits based on magnetic beads coupled with suitable buffer systems have been developed for SARS-CoV-2 viral RNA extraction and purification, however, details regarding surface modification of the magnetic beads, particle sizes, and the recipes of the buffers (including binding buffer, washing buffer, and elution buffer), remain undisclosed. Given the urgent and substantial demand, it was crucial to develop domestic SARS-CoV-2 viral RNA extraction kits using surface-modified magnetic beads and compatible buffers to relieve the diagnostic burdens during the pandemic.

2.3 References

1. Nikakhtari, H.; Wolf, S.; Choi, P.; Liu, Q.; Gray, M.R., Migration of fine solids into product bitumen from solvent extraction of Alberta oilsands. *Energy & Fuels* **2014,** *28* (5), 2925-2932.

2. Tarleton, E., The role of field-assisted techniques in solid/liquid separation. *Filtration & Separation* **1992**, *29* (3), 246-238.

3. Czarnecka, E.; Gillott, J.E., Formation and characterization of clay complexes with bitumen from Athabasca oil sand. *Clays and Clay Minerals* **1980,** *28*, 197-203.

4. Wang, S.; Liu, Q.; Tan, X.; Xu, C.; Gray, M.R., Study of asphaltene adsorption on kaolinite by X-ray photoelectron spectroscopy and time-of-flight secondary ion mass spectroscopy. *Energy & Fuels* **2013,** *27* (5), 2465-2473.

5. Osacky, M.; Geramian, M.; Ivey, D.G.; Liu, Q.; Etsell, T.H., Influence of nonswelling clay minerals (illite, kaolinite, and chlorite) on nonaqueous solvent extraction of bitumen. *Energy & Fuels* **2015,** *29* (7), 4150-4159.

6. Bensebaa, F.; Kotlyar, L.S.; Sparks, B.D.; Chung, K.H., Organic coated solids in Athabasca bitumen: Characterization and process implications. *The Canadian Journal of Chemical Engineering* **2000,** *78* (4), 610-616.

7. Lin, F.; He, L.; Primkulov, B.; Xu, Z., Dewetting dynamics of a solid microsphere by emulsion drops. *The Journal of Physical Chemistry C* **2014,** *118* (25), 13552-13562.

8. Hannisdal, A.; Ese, M.H.; Hemmingsen, P.V.; Sjöblom, J., Particle-stabilized emulsions: Effect of heavy crude oil components pre-adsorbed onto stabilizing solids. *Colloids and Surfaces A: Physicochemical and Engineering Aspects* **2006,** *276* (1-3), 45-58.

9. Dubey, S.T.; Waxman, M.L., Asphaltene adsorption and desorption from mineral surfaces. *SPE Reservoir Engineering* **1991,** *6* (03), 389-395.

10. González, G.; Moreira, M.B., The wettability of mineral surfaces containing adsorbed asphaltene. *Colloids and Surfaces* **1991,** *58* (3), 293-302.

11. Nalwaya, V.; Tantayakom, V.; Piumsomboon, P.; Fogler, S., Studies on asphaltenes through analysis of polar fractions. *Industrial & Engineering Chemistry Research* **1999,** *38* (3), 964-972.

12. Carbognani, L., Effects of iron compounds on the retention of oil polar hydrocarbons over solid sorbents. *Petroleum Science and Technology* **2000,** *18* (3-4), 335-360.

13. Alvarez-Ramirez, F.; Garcia-Cruz, I.; Tavizon, G.; Martinez-Magadan, J.M., Docking of an asphaltene molecular model on a Fe_2O_3 surface, an ab initio simulated annealing. *Petroleum Science and Technology* **2004,** *22* (7-8), 915-926.

14. Madge, D.N.; Garner, W.N., Theory of asphaltene precipitation in a hydrocarbon cyclone. *Minerals Engineering* **2007,** *20* (4), 387-394.

15. Farnand, J.R.; Meadus, F.W.; Sparks, B.D., Removal of intractable fine solids from bitumen solutions obtained by solvent extraction of oil sands. *Fuel Processing Technology* **1985,** *10* (2), 131-144.

16. Lin, F.; Stoyanov, S.R.; Xu, Y., Recent advances in nonaqueous extraction of bitumen from mineable oil sands: a review. *Organic Process Research & Development* **2017,** *21* (4), 492-510.

17. Graham, R.J.; Helstrom, J.J.; Mehlberg, R.L., 1987. A solvent extraction process for tar sand. *Eastern Oil Shale Symposium* **1987**, 93–99.

18. Dixon, D.V.; Stoyanov, S.R.; Xu, Y.; Zeng, H.; Soares, J.B., Challenges in developing polymer flocculants to improve bitumen quality in non-aqueous extraction processes: an experimental study. *Petroleum Science* **2020,** *17*, 811-821.

19. Ngnie, G.; Baitan, D.; Dedzo, G.K.; Detellier, C., Sedimentation of fine particles of kaolinite and polymer-coated kaolinite in cyclohexane: Implications for fines removal from extracted bitumen in non-aqueous processes. *Fuel* **2018,** *234*, 218-224.

20. Alquist, H.E.; Ammerman, A.M., Phillips Petroleum Co, Process for extracting bitumen from tar sands. **1980,** *U.S. Patent 4,229,281.*

21. Liu, J.; Cui, X.; Santander, C.; Tan, X.; Liu, Q.; Zeng, H., Destabilization of fine solids suspended in oil media through wettability modification and water-assisted agglomeration. *Fuel* **2019,** *254,* 115623.

22. Zhang, H.; Tan, X.; Wang, K.; Liu, Q., Electrodeposition of bitumen-, asphaltene-, or maltene-coated kaolinite from cyclohexane suspensions. *Fuel* ***2022*****,** *311*, 122582.

23. Cullinane, J.T.; Minhas, B.S., ExxonMobil Upstream Research Co, Electrostatic filtration of fine solids from bitumen. **2017,** *U.S. Patent 9,752,079.*

24. Sparks, B.D.; Meadus, F.W.; Hoefele, E.O., Canadian Patents and Development Ltd, Solvent extraction spherical agglomeration of oil sands. **1988,** *U.S. Patent 4,719,008.*

25. Sui, H.; Xu, L.; Li, X.; He, L., Understanding the roles of switchable-hydrophilicity tertiary amines in recovering heavy hydrocarbons from oil sands. *Chemical Engineering Journal* **2016,** *290*, 312-318.

26. Holland, A.; Wechsler, D.; Patel, A.; Molloy, B.M.; Boyd, A.R.; Jessop, P.G., Separation of bitumen from oil sands using a switchable hydrophilicity solvent. *Canadian Journal of Chemistry* **2012,** *90* (10), 805-810.

27. Plechkova, N.V.; Seddon, K.R., Applications of ionic liquids in the chemical industry. *Chemical Society Reviews* **2008,** *37* (1), 123-150.

28. Joshi, V.A. and Kundu, D., 2021. Ionic liquid promoted extraction of bitumen from oil sand: A review. *Journal of Petroleum Science and Engineering*, *199*, p.108232.

29. Painter, P.; Williams, P.; Mannebach, E., Recovery of bitumen from oil or tar sands using ionic liquids. *Energy & Fuels* **2010,** *24* (2), 1094-1098.

30. Hou, J.; Lin, S.; Zhang, M., Ionic-liquid-enhanced solvent extraction mechanism: A novel concept. *Journal of Environmental Chemical Engineering* **2022,** *10* (3), 107899.

31. Liu, J.; Xu, Z.; Masliyah, J., Studies on bitumen− silica interaction in aqueous solutions by atomic force microscopy. *Langmuir* **2003,** *19* (9), 3911-3920.

32. Pulati, N.; Lupinsky, A.; Miller, B.; Painter, P., Extraction of bitumen from oil sands using deep eutectic ionic liquid analogues. *Energy & Fuels* **2015,** *29* (8), 4927-4935.

33. Price, C.W.; Leslie, D.C.; Landers, J.P., Nucleic acid extraction techniques and application to the microchip. *Lab on a Chip* **2009,** *9* (17), 2484-2494.

34. McKiernan, H.E.; Danielson, P.B., Molecular diagnostic applications in forensic science. *Molecular Diagnostics* **2017,** 371-394. Academic Press.

35. Tan, S.C.; Yiap, B.C., DNA, RNA, and protein extraction: the past and the present. *BioMed Research International* **2009.**

36. Sobieralski, C.A.; Stanley, D.M., DNA Extraction Strategies for amplified fragment length polymorphism analysis. *Journal of Forensic Science* ***1994.*** 1254-1269.

37. Chomczynski, P.; Sacchi, N., Single-step method of RNA isolation by acid guanidinium thiocyanate-phenol-chloroform extraction. *Analytical Biochemistry*, **1987,** *162* (1), 156-159.

38. Chomczynski, P.; Sacchi, N., The single-step method of RNA isolation by acid guanidinium thiocyanate–phenol–chloroform extraction: twenty-something years on. *Nature Protocols* **2006,** *1* (2), 581-585.

39. Köchl, S.; Niederstätter, H.; Parson, W., DNA extraction and quantitation of forensic samples using the phenol-chloroform method and real-time PCR. *Forensic DNA Typing Protocols* **2005,** 13-29.

40. Maaroufi, Y.; Ahariz, N., Husson, M.; Crokaert, F., Comparison of different methods of isolation of DNA of commonly encountered Candida species and its quantitation by using a real-time PCR-based assay. *Journal of Clinical Microbiology* **2004,** *42* (7), 3159-3163.

41. Shin, J.H., Nucleic acid extraction techniques. *Advanced Techniques in Diagnostic Microbiology* **2013,** 209-225.

42. Ali, N.; Rampazzo, R.D.C.P.; Costa, A.D.T.; Krieger, M.A., Current nucleic acid extraction methods and their implications to point-of-care diagnostics. *BioMed Research International* **2017.**

43. Wink, M. ed., An introduction to molecular biotechnology: fundamentals, methods and applications. *John Wiley & Sons* **2020.**

44. Marko, M.A.; Chipperfield, R.; Birnboim, H.C., A procedure for the large-scale isolation of highly purified plasmid DNA using alkaline extraction and binding to glass powder. *Analytical Biochemistry* **1982,** *121* (2), 382-387.

45. Shi, R.; Lewis, R.S.; Panthee, D.R., Filter paper-based spin column method for cost-efficient DNA or RNA purification. *PLOS One* **2018,** *13* (12), e0203011.

46. Mirna Lorena, S.; Cynthia, P.C.; Maria Isabela, A.R.; Pamela, V.M.; Gabriela, R.H.; Jorge, B.; Mariano, G., Nucleic Acids Isolation for Molecular Diagnostics: Present and Future of the Silica-based DNA/RNA Purification Technologies. *Separation & Purification Reviews* **2023,** *52* (3), 193-204.

47. Gautam, A., Spin Column-Based Isolation of Nucleic Acid. *DNA and RNA Isolation Techniques for Non-Experts* **2022,** 47-53 Cham: Springer International Publishing.

48. Éva Mészáros, Spin column extraction, May 27, 2021. https://www.integra-biosciences.com/france/en/blog/article/comparison-rna-and-dna-extraction-methods Accessed on 14th November 2023.

49. Olsvik, O.; Popovic, T.; Skjerve, E.; Cudjoe, K.S.; Hornes, E.; Ugelstad, J.; Uhlén, M., Magnetic separation techniques in diagnostic microbiology. *Clinical microbiology reviews* **1994,** *7* (1), 43-54.

50. Stormer, M.; Kleesiek, K.; Dreier, J., High-volume extraction of nucleic acids by magnetic bead technology for ultrasensitive detection of bacteria in blood components. *Clinical chemistry* **2007,** *53* (1), 104-110.

51. Tang, C.; He, Z.; Liu, H.; Xu, Y.; Huang, H.; Yang, G.; Xiao, Z.; Li, S.; Liu, H.; Deng, Y.; Chen, Z., Application of magnetic nanoparticles in nucleic acid detection. *Journal of Nanobiotechnology* **2020,** *18* (1), 1-19.

52. Chen, Y.; Liu, Y.; Shi, Y.; Ping, J.; Wu, J.; Chen, H., Magnetic particles for integrated nucleic acid purification, amplification and detection without pipetting. *TrAC Trends in Analytical Chemistry* **2020,** *127*, 115912.

53. Berensmeier, S., Magnetic particles for the separation and purification of nucleic acids. *Applied Microbiology and Biotechnology* **2006,** *73*, 495-504.

54. Fang, X.; Willis, R.C.; Burrell, A.; Evans, K.; Hoang, Q.; Xu, W.; Bounpheng, M., Automation of nucleic acid isolation on KingFisher magnetic particle processors. *JALA: Journal of the Association for Laboratory Automation* **2007,** *12* (4), 195-201.

55. Rittich, B.; Španová, A., SPE and purification of DNA using magnetic particles. *Journal of Separation Science* **2013,** *36* (15), 2472-2485.

56. Melzak, K.A.; Sherwood, C.S.; Turner, R.F.; Haynes, C.A., Driving forces for DNA adsorption to silica in perchlorate solutions. *Journal of Colloid and Interface Science* **1996,** *181* (2), 635-644.

57. Lakshmi, R.; Baskar, V.; Ranga, U., Extraction of superior-quality plasmid DNA by a combination of modified alkaline lysis and silica matrix. *Analytical Biochemistry* **1999,** *272* (1), 109-112.

58. Li, X.; Zhang, J.; Gu, H., Adsorption and desorption behaviors of DNA with magnetic mesoporous silica nanoparticles. *Langmuir* **2011,** *27* (10), 6099-6106.

59. Luhmer, M.; d'Espinose, J.B.; Hommel, H.; Legrand, A.P., High-resolution ^{29}Si solid-state NMR study of silicon functionality distribution on the surface of silicas. *Magnetic Resonance Imaging* **1996,** *14* (7-8), 911-913.

60. Braga, P.R.; Costa, A.A.; de Macedo, J.L.; Ghesti, G.F.; de Souza, M.P.; Dias, J.A.; Dias, S.C., Liquid phase calorimetric-adsorption analysis of Si-MCM-41: Evidence of strong hydrogen-bonding sites. *Microporous and Mesoporous Materials* **2011,** *139* (1-3), 74-80.

61. Rosenholm, J.M. and Lindén, M., Towards establishing structure–activity relationships for mesoporous silica in drug delivery applications. *Journal of Controlled Release* **2008,** *128* (2), 157-164.

62. Trachtová, Š.; Kaman, O.; Španová, A.; Veverka, P.; Pollert, E.; Rittich, B., Silica-coated $La_{0.75}Sr_{0.25}MnO_3$ nanoparticles for magnetically driven DNA isolation. *Journal of Separation Science* **2011,** *34* (21), 3077-3082.

63. Prodělalová, J.; Rittich, B.; Španová, A.; Petrová, K.; Beneš, M.J., Isolation of genomic DNA using magnetic cobalt ferrite and silica particles. *Journal of Chromatography a* **2004,** *1056* (1-2), 43-48.

64. Yue, H.; Shin, J.M.; Tegafaw, T.; Han, H.S.; Chae, K.S.; Chang, Y.; Lee, G.H., Magnetic separation of nucleic acids from various biological samples using silica-coated iron oxide nanobeads. *Journal of Nanoparticle Research* **2020,** *22*, 1-12.

65. Wang, J.; Ali, Z.; Si, J.; Wang, N.; He, N.; Li, Z., Simultaneous extraction of DNA and RNA from hepatocellular carcinoma (Hep G2) based on silica-coated magnetic nanoparticles. *Journal of Nanoscience and Nanotechnology* **2017,** *17* (1), 802-806.

66. Algar, W.R.; Krull, U.J., Adsorption and hybridization of oligonucleotides on mercaptoacetic acid-capped CdSe/ZnS quantum dots and quantum dot-oligonucleotide conjugates. *Langmuir* **2006,** *22* (26), 11346-11352.

67. Liang, G.; Zhang, P.; Li, H.; Zhang, Z.; Chen, H.; Zhang, S.; Kong, J., An efficient strategy for unmodified nucleotide-mediated dispersion of magnetic nanoparticles, leading to a highly sensitive MRI-based mercury ion assay. *Analytica Chimica Acta* **2012,** *726*, 73-78.

68. DeAngelis, M.M.; Wang, D.G.; Hawkins, T.L., Solid-phase reversible immobilization for the isolation of PCR products. *Nucleic Acids Research* **1995,** *23* (22), 4742.

69. Skowronski, E.W.; Armstrong, N.; Andersen, G.; Macht, M.; McCready, P.M., Magnetic, microplate-format plasmid isolation protocol for high-yield, sequencing-grade DNA. *Biotechniques* **2000,** *29* (4), 786-792.

70. Španová, A.; Rittich, B.; Štyriak, I.; Štyriaková, I.; Horák, D., Isolation of polymerase chain reaction-ready bacterial DNA from Lake Baikal sediments by carboxyl-functionalised magnetic polymer microspheres. *Journal of Chromatography A* **2006,** *1130* (1), 115-121.

71. Horák, D.; Rittich, B.; Španová, A., Carboxyl-functionalized magnetic microparticle carrier for isolation and identification of DNA in dairy products. *Journal of Magnetism and Magnetic Materials* **2007,** *311* (1), 249-254.

72. Messina, R., Holm, C.; Kremer, K., Like-charge colloid-polyelectrolyte complexation. *The Journal of Chemical Physics* **2002,** *117* (6), 2947-2960.

73. Jiang, H.; Han, X.; Li, Z.; Chen, X.; Hou, Y.; Gai, L.; Li, D.; Lu, X.; Fu, T., Superparamagnetic core–shell structured microspheres carrying carboxyl groups as

adsorbents for purification of genomic DNA. *Colloids and surfaces a: physicochemical and engineering aspects* **2012,** *401*, 74-80.

74. Chen, Y.; Liu, Y.; Shi, Y.; Ping, J.; Wu, J.; Chen, H., Magnetic particles for integrated nucleic acid purification, amplification and detection without pipetting. *TrAC Trends in Analytical Chemistry* **2020,** *127*, 115912.

75. Kleideiter, G.; Nordmeier, E., Poly (ethylene glycol)-induced DNA condensation in aqueous/methanol containing low-molecular-weight electrolyte solutions I. Theoretical considerations. *Polymer* **1999,** *40* (14), 4013-4023.

76. Vasilevskaya, V.V.; Khokhlov, A.R.; Matsuzawa, Y.; Yoshikawa, K., Collapse of single DNA molecule in poly (ethylene glycol) solutions. *The Journal of chemical physics* **1995,** *102* (16), 6595-6602.

77. Kahánková, J.; Španová, A.; Pantůček, R.; Horák, D.; Doškař, J.; Rittich, B., Extraction of PCR-ready DNA from Staphylococcus aureus bacteriophages using carboxyl functionalized magnetic nonporous microspheres. *Journal of Chromatography B* **2009,** *877* (7), 599-602.

78. Sarkar, T.R.; Irudayaraj, J., Carboxyl-coated magnetic nanoparticles for mRNA isolation and extraction of supercoiled plasmid DNA. *Analytical Biochemistry* **2008,** *379* (1), 130-132.

79. Lipfert, J.; Doniach, S.; Das, R.; Herschlag, D., Understanding nucleic acid–ion interactions. *Annual Review of Biochemistry* **2014,** *83*, 813-841.

80. He, X.; Huo, H.; Wang, K.; Tan, W.; Gong, P.; Ge, J., Plasmid DNA isolation using amino-silica coated magnetic nanoparticles (ASMNPs). *Talanta* **2007,** *73* (4), 764-769.

81. Bai, Y.; Cui, Y.; Paoli, G.C.; Shi, C.; Wang, D.; Zhou, M.; Zhang, L.; Shi, X., Synthesis of amino-rich silica-coated magnetic nanoparticles for the efficient capture of DNA for PCR. *Colloids and Surfaces B: Biointerfaces* **2016,** *145*, 257-266.

82. Teymouri, M.; Mollazadeh, S.; Mortazavi, H.; Ghale-Noie, Z.N.; Keyvani, V.; Aghababaei, F.; Hamblin, M.R.; Abbaszadeh-Goudarzi, G.; Pourghadamyari, H.; Hashemian, S.M.R.; Mirzaei, H., Recent advances and challenges of RT-PCR tests for the diagnosis of COVID-19. *Pathology-Research and Practice* **2021,** *221*, 153443.

83. Bachman, J., Reverse-transcription PCR (rt-PCR). *Methods in Enzymology* **2013,** *530*, 67-74.

CHAPTER 3 Removal of Fine Solids from Bitumen by Hetero-aggregation and Magnetic Separation Using Surface-modified Magnetite Nanoparticles: Proof of Concept*

3.1 Introduction

Separation of solid particles with very small particle sizes (i.e., fine and ultrafine solids) from liquid suspensions is a challenging problem in various industries, especially in systems where the solid and liquid phases consist of both organic and inorganic materials. This is because in such systems, the fine solid surface is prone to coating by hydrocarbon organic matters, which changes its properties (hydrophobicity, surface charge, surface chemical composition, etc.). Such issues exist in the bitumen extraction process from oil sands ore using non-aqueous extraction (NAE) method, which is a favored potential alternative to the commercial warm-water bitumen extraction process because of its lower energy consumption and the elimination of tailings ponds. Since the 1960s, research has been on and off to improve NAE technologies aiming at low environmental impact, low cost, and high product quality [1-2]. Two major requirements remain to be met, which prevent the NAE process from being commercially viable for Alberta oil sands. One is the high solvent recovery from extraction gangue at low energy consumption, and the other is the high NAE bitumen product quality. With regards to product quality, the NAE bitumen should contain less than 0.03 wt% (300 ppm) of fine solids (on the basis of solvent-free bitumen) such that it can be fed directly to high conversion refineries without needing an upgrader [3]. So far, it has not been possible to achieve such a target using any of the conventional solid–liquid separation techniques.

* The main part of this chapter was published as: Liu X, Wang K, Tan X, Zeng H, Liu Q, 2022. Removal of fine solids from bitumen by hetero-aggregation and magnetic separation using surface-modified magnetite nanoparticles. Part I: Proof of concept. Separation and Purification Technology, Vol. 300, 121840.

The main constituent mineral solids in Alberta oil sands are quartz, kaolinite, and illite. In the oil sands industry, particles smaller than 45 μm are considered "fine solids", but the ultrafine solids can range from 10 nm to 10 μm [4], although they are still collectively called "fine solids". The surfaces of the fine solids are usually coated by bitumen or bitumen components such as asphaltenes, which makes them partially hydrophobic. With enhanced hydrophobicity and loss of capillary forces from water in the NAE process [5], more fine solids may migrate to the solvent-diluted-bitumen product (i..e, dilbit).

Even though various techniques were investigated to separate the fine solids from NAE bitumen, they all suffer from severe handicaps, preventing the NAE process from advancing into commercial stage. Conventional mechanical solid–liquid separation techniques such as gravity sedimentation, centrifugation, and filtration can only remove relatively large solid particles, resulting in 0.5–15.0 wt% of solids content in NAE bitumen product [1,3,6-7]. Using poor solvents for asphaltenes such as alkanes in the extraction process is beneficial to a lower fine solids content since the solids can be trapped and removed together with the precipitated asphaltenes [1,8]. However, using alkanes alone as the sole solvents in NAE would cause the loss of up to 20% hydrocarbon upfront in the form of precipitated asphaltenes. To reduce the loss of asphaltenes, a strong solvent such as cyclohexane could be used in extraction, which could be followed by blending a poor solvent such as alkane to precipitate part of the asphaltenes. The solvent blending and switching would significantly complicate the industrial application of the process which is undesirable [2,9]. After introducing water, and/or wetting surfactants during the NAE process, the fine solids content could be lowered to 2.0 wt% on average. With the use of an ionic liquid, the fine solids content could be reduced to approximately 0.3 wt% [1,10-12]. Electric field assisted separation is a novel technique for NAE fine solids removal [13-14], and fine solids content in an

NAE bitumen product could be reduced to 0.1 wt% with electrostatic filtration [15]. A two-step agglomeration strategy was demonstrated to notably improve the gravity sedimentation of bitumen-coated fine solids suspended in cyclohexane with assistance from an amphiphilic polymer and water [16]. However, the achieved fine solids content was still higher than the target of 0.03 wt%, even in a laboratory test environment where operating parameters could be well controlled. Also, in most of the previous studies, the solvent/bitumen ratios were very high and not compatible with commercial practices which typically demand solvent/bitumen ratio of less than or equal to 2:1. Switchable hydrophilicity solvent extraction (SHSE) is a modified NAE process in which the solvent could reversibly switch between being hydrophobic and being hydrophilic [17]. The fine solids content in bitumen product from SHSE could be reduced to zero at high bitumen recovery [18]. However, the high costs and toxicity of the hydrophilicity-switchable solvents rule out the possibility of using them in commercial operations.

Magnetic separation techniques based on magnetic carriers has been used in a variety of separation processes such as impurity removal from mineral concentrates, toxicity mitigation of wastewater, and biomolecule isolation and purification from biometrics, and so on [19–22]. Iron oxide magnetic nanoparticles, as one of the most commonly used magnetic materials, can be made to possess superparamagnetic properties and large specific surface area, and their surfaces can also be modified and functionalized to prepare magnetic core/shell particles to target specific applications [20,23]. For example, maghemite (γ-Fe_2O_3) nanoparticles, functioning as magnetic crystal nuclei, have shown good performance in capturing solid impurities from sulfuric acid leaching solutions in the nonferrous metals hydrometallurgy industry [24,25]. Also, iron oxide core/shell nanoparticles encapsulated by chemical functional groups are commonly used for the extraction of conjugating biomolecules and ligands, thus successfully separating cells, proteins,

and nucleic acids from biofluids [26,27]. Recently, iron oxide nanoparticles also show applications in crude oil processing. For instance, ethyl-cellulose-grafted magnetite (Fe_3O_4) nanoparticles and a polymer/Fe_3O_4 nanocomposite have shown the ability to rapidly separate emulsified water from crude oil [28,29].

Inspired by previous studies, herein a novel method is reported to separate fine solids from NAE bitumen by magnetic separation using superparamagnetic magnetite (Fe_3O_4) nanoparticles. The Fe_3O_4 nanoparticles were synthesized and functionalized with stearylamine acetate (SAA), a chemical that we observed to interact strongly with fine solids in NAE bitumen in preliminary jar tests to screen different chemicals. The SAA-functionalized Fe_3O_4 nanoparticles were found to be able to aggregate with the fine solids in NAE bitumen. The subsequent removal of the hetero-aggregates was realized by a magnetic separator. The magnetic field assisted sedimentation and filtration ensured a low fine solids content in the final bitumen product. Bench-scale tests were conducted to evaluate the separation performance by the proposed process under a low solvent/bitumen ratio of 2:1 in line with commercial practices. In addition, the regeneration and reuse of the magnetite nanoparticles were tested. This work provides a new direction for the investigation of practical approaches for fine solids removal from NAE bitumen products. To the author's knowledge, this work is the first study of using magnetic nanoparticle hetero-aggregation and magnetic separation to remove fine solids and improve the quality of NAE bitumen product.

3.2 Materials and methods

3.2.1 Materials

All purchased chemicals were of analytical grade and were used without further purification. Ferrous chloride tetrahydrate ($FeCl_2 \cdot 4H_2O$), ferric chloride hexahydrate ($FeCl_3 \cdot 6H_2O$), and sodium citrate (tribasic dihydrate) were purchased from Sigma-Aldrich. Ammonium hydroxide

solution (29.47 wt% NH_3), ethanol, toluene, and cyclohexane were purchased from Fisher Scientific. Stearylamine acetate (SAA) was supplied by Tokyo Chemical Industry Co., Ltd. Distilled water was generated by a W4000 Merit water still system from Cole-Parmer. The non-aqueous extracted bitumen (NAE bitumen) sample was obtained by treating an Alberta oil sands ore sample using cyclohexane following the standard procedures developed by the Institute for Oil Sands Innovation [30]. NAE fine solids sample was prepared from cyclohexane-extracted gangue as follows: the gangue was mixed with cyclohexane at a volume ratio of 1:1 and allowed to settle for 7 days. Afterward, the supernatant was decanted and centrifuged to collect the fine solids. After repeated rinsing with cyclohexane, the collected fine solids were dried to remove cyclohexane to obtain the dry NAE fine solids. This NAE fine solids sample was used to measure its CHNS elemental composition, FTIR spectrum, and hetero-aggregation with magnetic nanoparticles.

3.2.2 Preparation of surface-modified magnetite nanoparticles

3.2.2.1 Synthesis of magnetite nanoparticles (MNPs)

The conventional chemical co-precipitation method [31] was followed with modification to synthesize the magnetite nanoparticles. An aqueous solution of ferrous chloride and ferric chloride with a Fe^{2+}/Fe^{3+} molar ratio of 0.5 was prepared by dissolving 2.13 g of $FeCl_2 \cdot 4H_2O$ and 5.79 g of $FeCl_3 \cdot 6H_2O$ in 50 mL distilled water under a high purity nitrogen gas flow at 75°C. Afterward, 25 mL of NH_4OH solution (excess base concentration) was added with vigorous stirring. Instant color change from orange to black was observed with precipitate formation. The formed black precipitates, which were magnetite nanoparticles (MNPs), were collected by sedimentation under a magnetic field, washed several times with distilled water and stored in slurry form.

3.2.2.2 Synthesis of SAA-functionalized magnetite nanoparticles (SAA- MNPs)

The surface functionalization of the magnetite nanoparticles with SAA was realized in two steps, shown in Figure 3.1. In a typical surface functionalization process, 2.5 g of MNPs were dispersed in 50 mL of distilled water, followed by the addition of 50 mL of aqueous sodium citrate solution (70 mg/mL). The mixture was slowly heated to 90ºC under reflux and allowed to react for 2.5 h with continuous stirring at this temperature. The resulting sodium citrate coated particles, designated as SC-MNPs, were collected, washed repeatedly with water, and re-dispersed in 50 mL of fresh distilled water. Afterward, 30 mL of an aqueous solution containing 0.35 g SAA, pre-prepared by stirring overnight at room temperature, was added dropwise into the suspension with vigorous stirring. The reaction mixture was stirred at 60ºC for 2 h to complete the surface functionalization. The obtained SAA- functionalized MNPs (SAA-MNPs) were rinsed several times with distilled water. To obtain SAA-MNPs suspension in cyclohexane, the SAA-MNPs particles suspended in water were washed sequentially with ethanol and cyclohexane, then re-dispersed in a certain volume of cyclohexane. During the preparation process, drying of the nanoparticles was avoided.

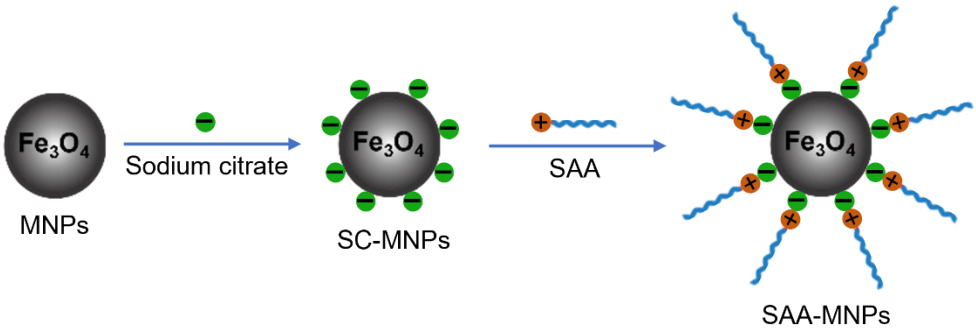

Figure 3.1 Schematic illustration of the surface functionalization process of magnetite nanoparticles (MNPs) with stearylamine acetate (SAA).

3.2.3 Characterization of prepared nanoparticles

X-ray diffraction (XRD) patterns were recorded on a Rigaku Ultima IV X-ray diffractometer with Cu K_α radiation (λ = 1.540 Å) at 40 kV and 44 mA to confirm the crystalline structures of the synthesized magnetite. Data were collected in the range of 20º to 70º (2θ) with a sampling width of 0.02º.

Fourier transform infrared (FTIR) spectroscopic measurements were performed using a Bruker ALPHA ATR-FTIR spectrometer to examine the surface compositions. Dried powder samples were used directly for the measurements in transmittance mode at room temperature. The measurements were carried out within the wavenumber range of 4000–500 cm^{-1} with a resolution of 4 cm^{-1}. Control of the instrument, and acquisition and analysis of data were accomplished using OPUS software.

Magnetic susceptibility of the synthesized magnetic particles was measured by a Quantum Design MPMS®3 SQUID magnetometer at the University of Waterloo. The measurements were taken at room temperature under different applied magnetic fields from -2 to +2 Tesla.

A transmission electron microscope (TEM, JEOL JEM-ARM200CF, 200 kV) was used to examine the size and morphology of the nanoparticles. To prepare TEM sample, the synthesized MNPs or SAA-MNPs were diluted in cyclohexane to a concentration of 0.05 mg/mL, then a droplet of the suspension was deposited on a copper grid and dried by evaporating the cyclohexane. The grid was carbon-coated before TEM measurement.

Particle size distribution of MNPs and SAA-MNPs dispersed in cyclohexane was determined using a Malvern Mastersizer 3000 particle size analyzer. MNPs-in-cyclohexane or SAA-MNPs-in cyclohexane suspension was added dropwise into the dispensing cell containing cyclohexane and

the obscuration was kept in the range of 5% to 12% during the measurements. Particle size at 10% (D_{10}), 50% (D_{50}), and 90% (D_{90}) of the number distribution were automatically calculated by the Mastersizer 3000 software. Five consecutive measurements were conducted automatically by the analyzer for each sample and the size distribution curve was plotted from the average values of the 5 measurements.

3.2.4 NAE fine solids removal process

Figure 3.2 shows the flow diagram used in the laboratory tests to remove fine solids from an NAE bitumen sample. Cyclohexane was used to dilute the NAE bitumen sample as well as to suspend the magnetite nanoparticles. The total amount of cyclohexane initially added was such that the S/B (solvent-to-bitumen) weight ratio was kept at about 2, and this included cyclohexane brought in by the magnetic nanoparticle suspension and cyclohexane used for NAE bitumen dilution. In a typical test, 6 mL of the prepared magnetic nanoparticle (MNP)-cyclohexane mixture, with a MNP concentration of 0.42 g per mL (i.e., 2.5 g MNPs), were added to a beaker containing a well-mixed solution of 10 g NAE bitumen and 20 mL cyclohexane. The mixture was stirred for 30 min to allow the magnetic nanoparticles to fully contact with fine solids. The beaker was then placed on top of the magnetic pole of an Outotec Laboratory WHIMS 3×4 L magnetic separator, with the generated magnetic field adjusted to ~1 Tesla. The magnetic field was used to accelerate the gravity sedimentation of the magnetic nanoparticles. The supernatant was decanted, and the sediment (i.e., magnetite nanoparticle-fine solids hetero-aggregate) was collected and washed twice with cyclohexane, then suspended in fresh cyclohexane for subsequent regeneration and re-use of the magnetic nanoparticles. The supernatants from the above decantation and washing were combined and passed through the separation chamber of the WHIMS packed with steel wools. The filtrate passing through the magnetic matrix was collected as the cleaned NAE bitumen product,

and its fine solid content was determined. The "filter cake" collected on the steel wools would be the fine solids waste stream. The settled magnetic particle – fine solids hetero-aggregates were regenerated by washing with cyclohexane and ultrasonic treatment. The cyclohexane supernatant from the regeneration may be combined with the magnetic filtration cakes as the final fine solids waste.

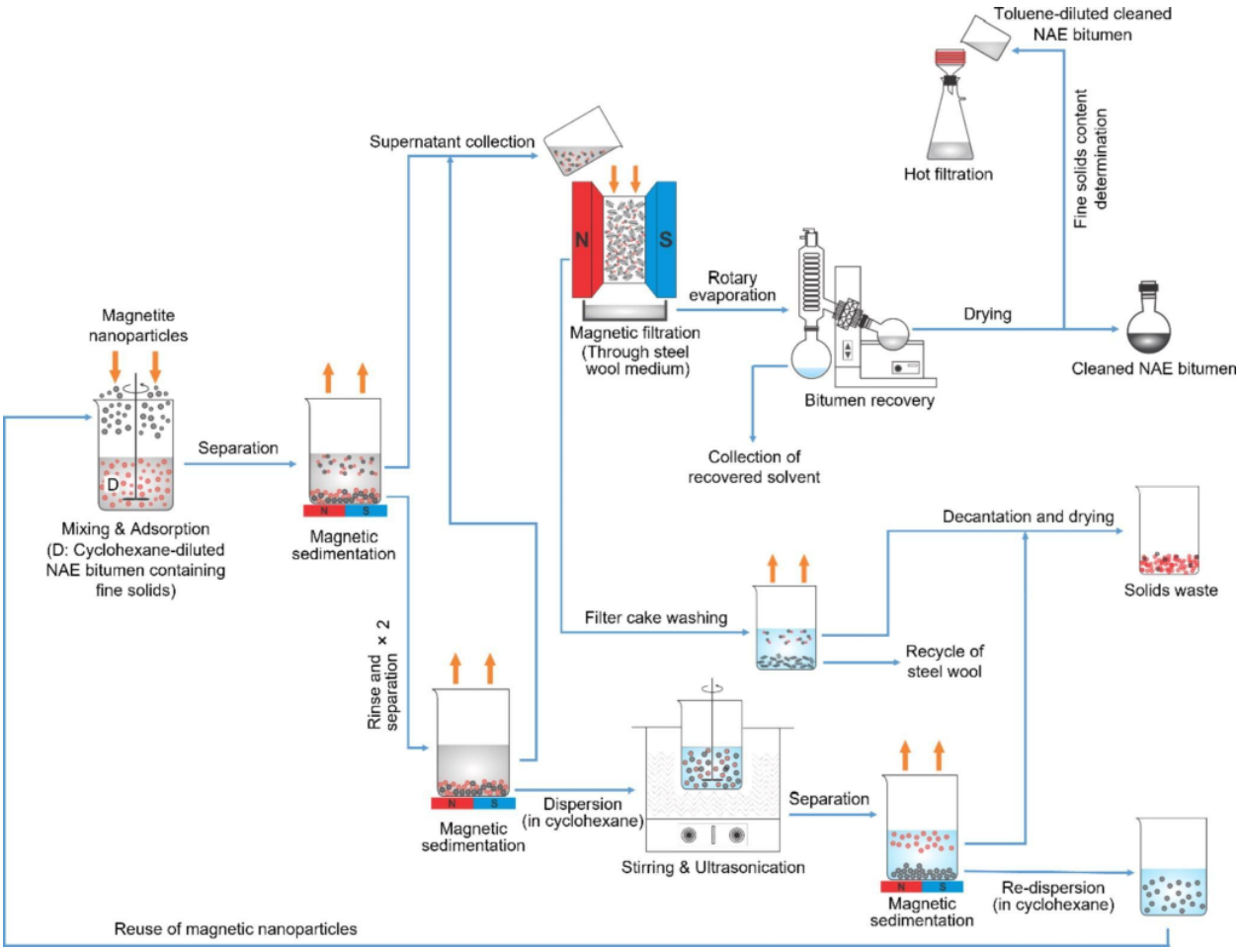

Figure 3.2 Laboratory test flow diagram for fine solids removal from NAE bitumen.

3.2.5 Fine solids content determination

The fine solids content of the bitumen product was determined following the methods of ASTM D4807-05 and ASTM D482-07 [32-33]. Firstly, 1 g of accurately weighed bitumen sample was

diluted in 100 mL toluene at 90°C. The hot bitumen-toluene solution was then carefully introduced into a stainless-steel vacuum filtration funnel, which was wrapped with copper coils with circulating 90°C hot water from a water bath. If the solution successfully passed through the 0.45 μm filter paper, then the filter paper with the retained solids was washed with hot toluene and placed in an oven at 105°C for 10 minutes to evaporate the solvent. The filter paper was then cooled in a desiccator for 10 minutes and weighed. The fine solids content was calculated by Equation 3.1 as follows:

$$S_{ppm} = \frac{m_{p+s} - m_p}{m_b} \times 10^6 \quad (3.1)$$

where S_{ppm} is the fine solids content of the bitumen sample expressed as ppm by weight, m_{p+s}, m_p, and m_b are the weights of filter paper with retained fine solids, filter paper, and bitumen sample, respectively. Repeated measurements were performed with a sample weight of 4 g for the filterable diluted bitumen product, and the repeatability of the measurements was presented as the variation about the mean, i.e., standard deviation divided by the mean of determined results then multiplied by 100. If the hot bitumen-toluene solution was not filterable by the above vacuum filtration apparatus, it would indicate that the fine solids content was high, and the ashing method was then used instead to find the solids content of the bitumen sample following the procedure in ASTM D482-07 [33].

3.3 Results and discussion

3.3.1 Properties of the synthesized magnetic nanoparticles

The XRD measurements were performed on dried samples of pristine and functionalized magnetite nanoparticles to confirm the crystalline phases present in the samples. Figure 3.3(a) shows the XRD patterns of the synthesized magnetic nanoparticles. The patterns of both MNPs and SAA-

MNPs samples show the characteristic diffraction peaks corresponding to magnetite (Fe_3O_4) with 2θ at 30.2º, 35.5º, 43.2º, 53.6º, 57.2º, and 62.8º, which were indexed to (220), (311), (400), (422), (511) and (440) planes, respectively [34-35]. The identical set of characteristic peaks of SAA-MNPs with that of MNPs demonstrates the stability of the crystalline phase of Fe_3O_4 nanoparticles during the subsequent surface functionalization of the magnetite nanoparticles.

Figure 3.3(b) displays the FTIR spectra of the prepared magnetite nanoparticles. The spectra of both MNPs and SAA-MNPs samples exhibit a strong band at 584 cm^{-1}, which corresponds to the characteristic stretching vibration of Fe–O bond from Fe_3O_4 [36]. In the spectrum of SAA-MNPs, two absorption peaks at 1623 cm^{-1} and 1387 cm^{-1} are respectively associated with the asymmetrical and symmetrical stretching vibration of C=O from carboxylate groups ($–COO^-$) [37], which indicates the presence of citrate on Fe_3O_4 surface (the acetate groups from SAA were not expected to be able to adsorb on citrate-modified magnetic particles). The presence of citrate could facilitate the subsequent adsorption of the stearylamine. Indeed, in addition to the peaks at 1623 cm^{-1} and 1387 cm^{-1}, the peak at 1458 cm^{-1} which refers to the asymmetrical deformation vibration of N–H from the primary amine salt ($–NH_3^+$) [38], and two peaks at 2925 cm^{-1} and 2855 cm^{-1} which could be assigned to asymmetrical and symmetrical stretching of C–H from alkane chain (–CH2-) [36], respectively, indicate the successful surface functionalization of magnetite nanoparticles by SAA.

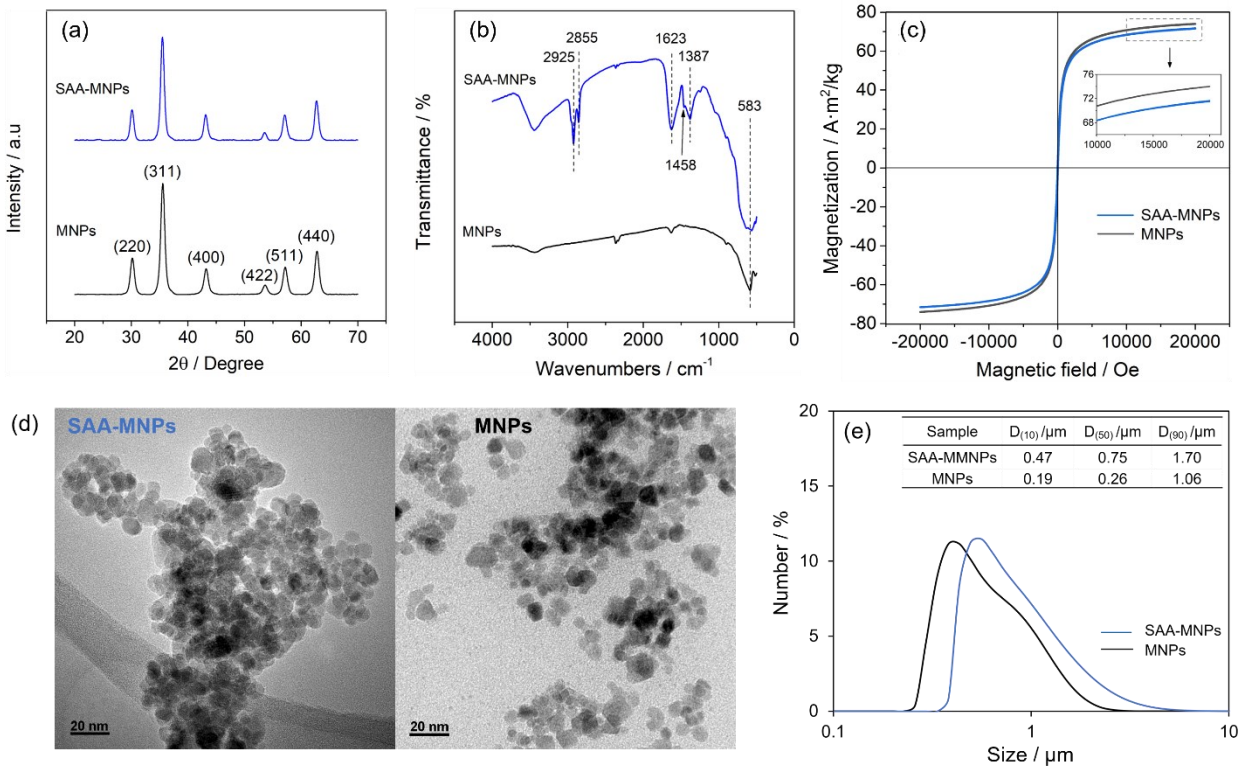

Figure 3.3 (a) XRD patterns, (b) FTIR spectra, (c) Magnetization curves, (d) TEM images and (e) Particle size distribution of synthesized magnetite nanoparticles suspended in cyclohexane.

Typical magnetization curves determined at room temperature for SAA-MNPs and MNPs samples are presented in Figure 3.3(c). The plots indicate that both MNPs and SAA-MNPs exhibit superparamagnetic behavior in which the remanence and coercivity are close to zero. The measured saturation magnetization for MNPs was 74.0 A·m^2/kg, compared with 92 A·m^2/kg for bulk magnetite [39]. This result was reasonable since the saturation magnetization for a magnetic particle in an external field is proportional to its particle size. The value was consistent with the reported values in literature when magnetite nanoparticles were synthesized under similar conditions, i.e., using coprecipitation method at a growth temperature of 75°C [40]. The saturation magnetization value of SAA-MNPs (71.6 A·m^2/kg) was slightly lower than the pristine magnetite

nanoparticles (MNPs). This result was possibly due to the decrease in surface moments of the SAA-MNPs by non-magnetic coatings (i.e., sodium citrate and SAA layers).

Figure 3.3(d) shows the typical TEM images of the primary magnetic nanoparticles before and after surface modification. The TEM image of MNPs shows that the primary magnetic nanoparticles have a narrow size distribution with an estimated primary particle size of 6.5–9 nm, which is consistent with reported values in literature [41-42]. After SAA functionalization, the particles showed a similar morphology and narrow size distribution, with an estimated primary particle size of 7.5-11 nm.

DLS particle size distribution of SAA-MNPs and MNPs suspended in cyclohexane is shown in Figure 3(e). Compared with the TEM imaging results, the measured DLS size in cyclohexane seemed to be the aggregates of the primary magnetic nanoparticles, with median sizes at 0.26 μm and 0.75 μm for MNPs and SAA-MNPs, respectively. It appeared that the polar groups on the surface of the MNPs and SAA-MNPs contributed to their aggregation in the non-polar solvent cyclohexane [43]. The curves show that most of SAA-MNPs or MNPs aggregates in cyclohexane lie in the <1 μm range, and the measured particle size shifts towards larger values after modification. One of the interim steps of SAA-MNPs preparation was sodium citrate modification of MNPs, which may be the main reason for the larger size of SAA-MNPs aggregates in cyclohexane. Excess amount of sodium citrate was added in the preparation process to ensure enough sites were provided for the subsequent SAA functionalization. However, the SAA amount added was not sufficient to bond each active functional group (i.e., $–COO^-$) from sodium citrate-modified nanoparticles. Due to the polarity of the sodium citrate-modified surfaces, the SAA-MNPs had the trend to aggregate in cyclohexane thus exhibited larger DLS particle size.

3.3.2. Removal of fine solids from NAE bitumen by the magnetic nanoparticles

The ability of SAA-MNPs to capture and separate fine solids from NAE bitumen via the proposed hetero-aggregation – magnetic separation process was investigated following the procedures shown in Figure 3.2, and the results were compared with un-modified magnetite nanoparticles (MNPs). The fine solids contents of the initial bitumen sample and final bitumen products were determined following the procedures described in Section 3.2.5. The initial fine solids content in the NAE bitumen was 3600 ppm (0.36 wt%). All the final bitumen products for fine solids content determination were taken after the series of process steps of magnetic separation, magnetic filtration, and solvent evaporation, i.e., from the "cleaned NAE bitumen" shown in Figure 3.2. As shown in Figure 3.4, the blue bars (Synthesized nanoparticles) indicate the initial cycle of fine solids removal from NAE bitumen by using fresh SAA-MNPs and MNPs. The red bars (Recycled nanoparticles) indicate the fine solids removal from NAE bitumen by reusing SAA-MNPs and MNPs recycled from the initial solid removal cycle. The grey bar shows control blank test in which no nanoparticles were added to NAE bitumen. At a solvent (cyclohexane) to bitumen (NAE bitumen) weight ratio of 2:1, magnetic nanoparticles to NAE bitumen weight ratio of 1:4, and magnetic field strength of 1 Tesla, SAA-MNPs could lower the fine solids content in the NAE bitumen from the initial 3600 ppm to 389 ppm (89% removal), while the same amount of MNPs could only lower the fine solids content to around 3000 ppm (16% removal). The NAE fine solids were non-magnetic. Consequently, they were not expected to respond to the external magnetic field. However, they could be removed if they aggregated with the introduced magnetic particles under a magnetic field. In fact, a control blank test, in which no magnetic particles were used, showed that the fine solids content in the NAE bitumen was reduced from the original 3600 ppm to 3150 ppm (12.5% removal). It was likely that the removed fine solids in the control blank test

were mostly trapped by the magnetic filtration medium and not retained by magnetic forces. The above results showed that SAA-MNPs were much more capable of capturing the fine and ultrafine solids than the un-modified MNPs.

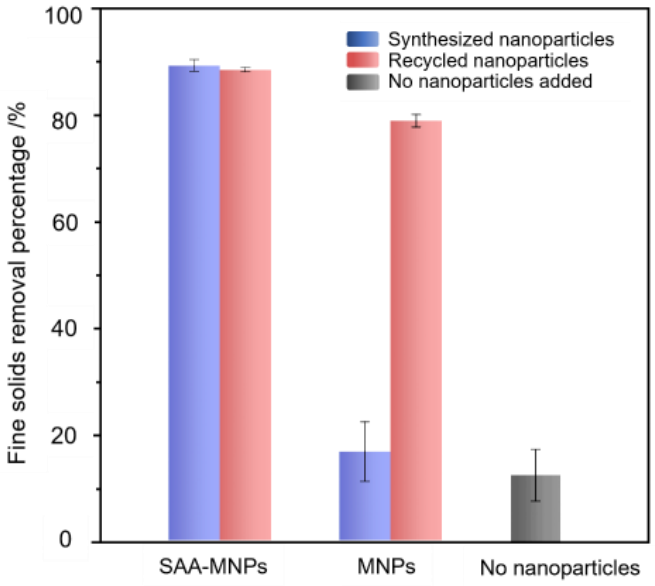

Figure 3.4 NAE fine solids removal efficiency by magnetic separation after the introduction of magnetic nanoparticles SAA-MNPs or MNPs. The repeatability (variation about the mean) between different measurements for fine solids content of the bitumen samples after solids removal by SAA-MNPs, MNPs, recycled SAA-MNPs, recycled MNPs was 7.5%, 6.7%, 3.6% and 5.7%. The repeatability for fine solids content measurements of bitumen samples collected after the magnetic separation with no nanoparticles addition was estimated to be 4.5%.

Since the magnetic nanoparticles could be easily recovered by the magnetic separator together with the captured fine solids, it was of interest to examine the possibility to regenerate and re-use the magnetic nanoparticles. As can be seen from the procedure shown in Figure 3.2, the collected magnetic nanoparticles – fine solids aggregates were redispersed in cyclohexane and subjected to ultrasonic treatment at room temperature for 45 min, followed by magnetic-field assisted

sedimentation and decantation. The regenerated magnetic particles were dispersed in 6 mL cyclohexane and re-used in the next cycle to remove fine solids from a new batch of NAE bitumen. The comparison of NAE fine solids removal efficiency using recycled SAA-MNPs and MNPs is shown in Figure 3.4 (red bars). As can be seen, after one cycle of use, the SAA-MNPs still maintained the same efficiency of fine solids removal from NAE bitumen, lowering the fine solids content to 417 ppm (88% removal). Interestingly, the fine-solids-removal ability of the unmodified magnetic nanoparticles (MNPs) improved significantly after being recycled: they lowered the fine solids content to 763 ppm (79% removal) when being used the second time. Apparently, the surfaces of MNPs were modified by cyclohexane-diluted bitumen in the first round, possibly coated by bitumen components, which enhanced their ability to form hetero-aggregates with the suspended fine solids in NAE bitumen. This result was a desirable outcome which indicates that the effectiveness of the magnetic nanoparticles did not degrade and may even improve with repeated use.

3.3.3. Formation of hetero-aggregates between NAE fine solids and SAA-MNPs

Fine solids have been proven to be closely associated with organic matters from bitumen through different characterization methods, such as elemental composition, FTIR, nuclear magnetic resonance (NMR) spectroscopy, and X-ray photoelectron spectroscopy (XPS). For example, in the work of Fu et al. [44], the relation between methanol-extracted materials and the total clay (<3 μm solids) or major clays (kaolinite and illite) present in the bitumen-free (toluene-extracted) solids from oil sands ore was investigated. The results showed that the weight ratio of methanol-extracted materials to total clay in bitumen-free solids was the same for different oil sands ore samples. Similar relation also existed between the methanol-extracted materials and kaolinite or illite. These good correlations suggested that the methanol-extracted organic matter was initially adsorbed on

the clay minerals in situ. Couillard et al. [45] tracked the carbon distribution in fine solids in solvent-diluted bitumen, and the carbon maps obtained demonstrated that organic matters were nonuniformly coated on the surface of clay mineral. Kotlyar et al. compared solid and metal contents in regular bitumen and solids-free bitumen, and the results revealed that solids in bitumen were closely associated with asphaltene component from bitumen. As the main components of NAE fine solids, kaolinite and illite were reported to have asphaltene adsorption capacities of 1.55–3.36 mg/m^2 and 0.3–2.7 mg/ m^2, respectively [46-50].

To better understand the formation of hetero-aggregates, the surface properties of NAE fine solids and their aggregation with SAA-MNPs were studied. Total C, H, N, and S contents were determined by a Thermo Scientific Flash 2000 CHNS Analyzers. The results indicated that the NAE fine solids contained 18.2 wt% C, 2.1 wt% H, 0.3 wt% N and 1.9 wt% S, signifying the presence of bitumen components in the fine solids sample [51]. Figure 3.5 shows the FTIR-ATR spectrum of the NAE fine solids, and both inorganic bonds (Al–O–H, Si–O, Si–O–Al, and Si–O–Si) and organic bonds (–CH_2- and C=C) were observed confirming that the NAE fine solids were coated by bitumen components.

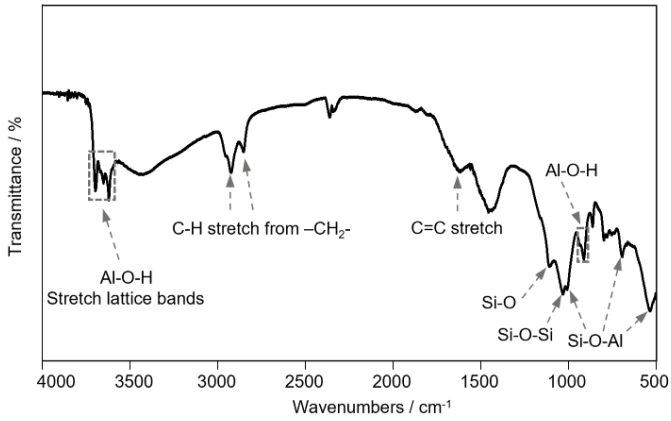

Figure 3.5 FTIR spectrum of NAE fine solids. The peaks were assigned according to literature [52-53].

To observe the hetero-aggregation between the magnetic nanoparticles and the NAE fine solids, about 0.01 g of SAA-MNPs or MNPs were added to 20 mL well-mixed cyclohexane suspension containing 1 mg/mL NAE fine solids (so the weight ratio between the magnetic particles and fine solids particles was about 1:2). The mixture was shaken for 10 min, then a hand magnet was placed next to the vial to recover the magnetic nanoparticles. As shown in Figure 3.6(a), in the vial where SAA-MNPs were added, the suspended particles were attracted by the magnet and gradually migrated towards the side of the vial. After 15 min, all the suspended particles, including both the SAA-MNPs and the NAE fine solids, were recovered by the magnet and the cyclohexane suspension became clear. It was also interesting to note that almost no particles settled to the bottom of the vial by gravity, which was clearly due to the ultrafine sizes of both the magnetic nanoparticles and the ultrafine NAE solids, and yet they could be completely recovered by the hand magnet. Figure 3.6(b) shows that when the un-modified magnetic nanoparticles MNPs were used, the suspension remained turbid throughout the 15 min test period. The observed phenomena revealed strong hetero-aggregation between the NAE fine solids and SAA-MNPs, while the un-modified MNPs could not aggregate with the NAE fine solids and therefore could not capture the NAE fine solids.

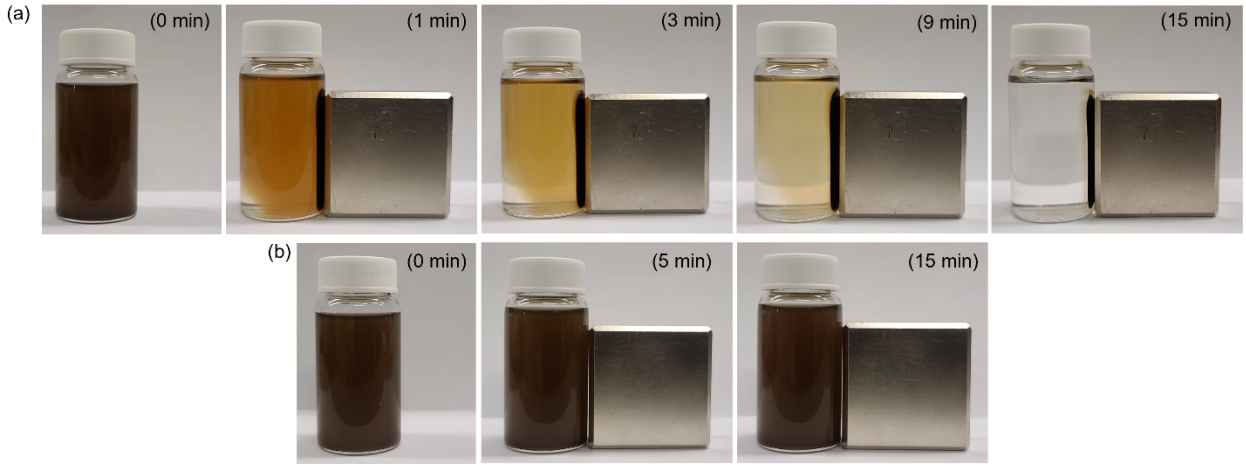

Figure 3.6 (a) NAE fine solids capture and removal by surface modified magnetic nanoparticles SAA-MNPs and a hand magnet. (b) Same test but with the un-modified MNPs used. About 0.01 g of magnetic nanoparticles were mixed in 20 mL cyclohexane suspension containing 1 mg/mL NAE fine solids.

Figure 3.7 shows the secondary electron image of the hetero-aggregates formed between SAA-MNPs and NAE fine solids. EDS spectra were acquired at 7 sample sites indicated in Figure 3.7, and the results are shown in Table 3.1. Figure 3.7 clearly shows that the particles were aggregated, and Table 3.1 shows that the bright and relatively large particles 1, 2 and 3 were likely the fine solids from NAE bitumen due to the high Al and low Fe contents, and the greyish particles 4, 5, 6 and 7 were SAA-MNPs due to the low Al and high Fe contents. In this field of view, it appears that the hetero-aggregates were formed by the coating of the fine magnetic nanoparticles on the larger NAE fine solids particles, and the fine magnetic particles seemed to have also aggregated themselves (as shown by the greyish aggregates in red circles). Such hetero-aggregates would be able to "sweep" through the NAE bitumen solution to capture and trap the non-magnetic fine solids, leading to their removal from solvent-diluted bitumen. Depending on the relative particle sizes of the magnetic particles and the NAE fine solids, other types of magnetic aggregates, namely

magnetic carrier (large magnetic particle and smaller fine solids) or magnetic seeding (comparable particle sizes) [54], may also exist due to the non-uniform particle size distribution of both the magnetic particles and the NAE fine solids. The outcome was that fine solids of various sizes in the NAE bitumen could be captured by the magnetic nanoparticles and removed by a magnetic separator.

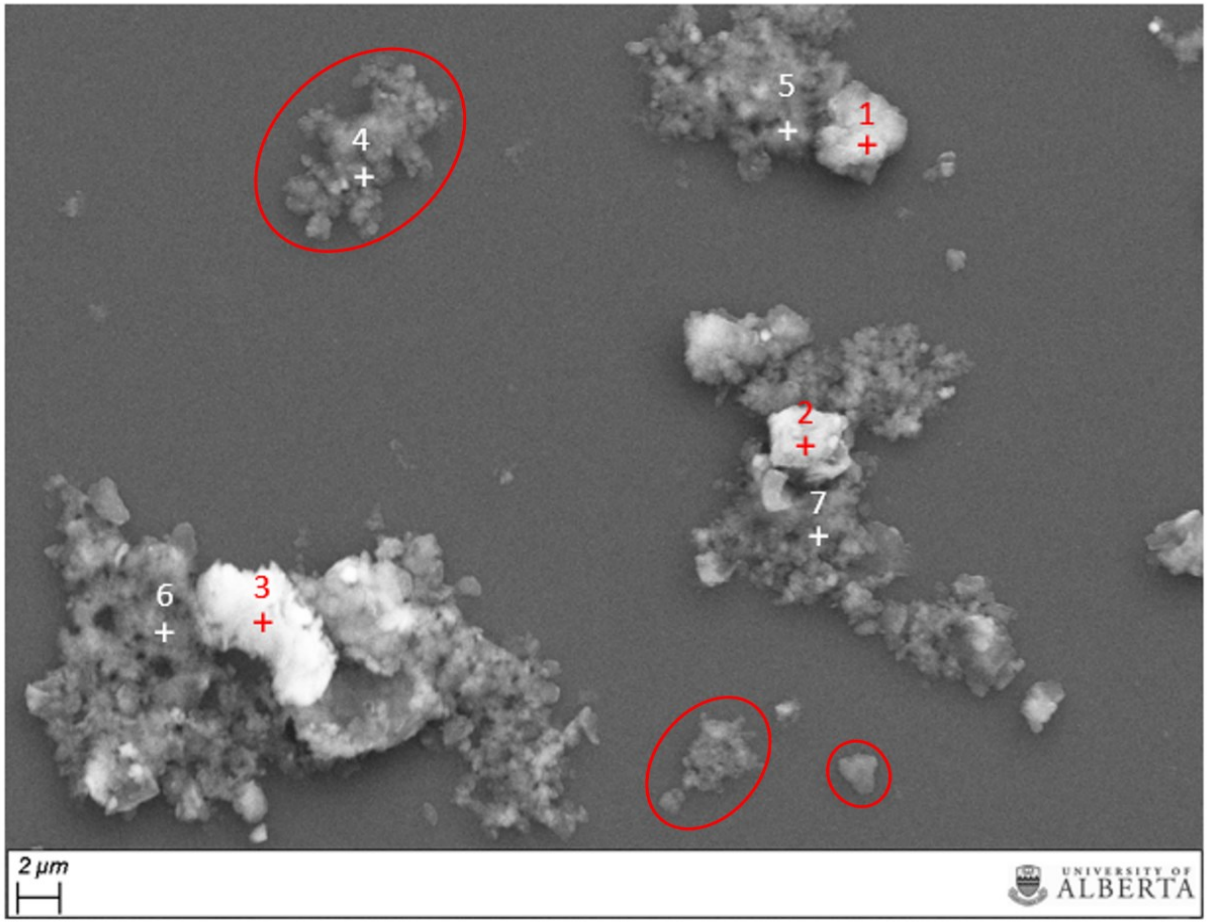

Figure 3.7 SEM secondary electron image of hetero-aggregates composed of SAA-MNPs and NAE fine solids. SAA-MNPs and NAE fine solids were mixed in cyclohexane. A drop of the suspension was cast on a glass holder, and the cyclohexane was then evaporated. The glass holder was then coated with carbon.

Table 3.1 Elemental composition of sample sites from SEM image (Figure 3.7) determined by EDS.

Site	Elemental content (wt%)							
	C	O	Na	Mg	Al	Si	Ca	Fe
1	39.8	36.4	2.4	0.8	5.2	12.8	0.8	0.7
2	46.9	28.6	2.4	0.7	2.3	10.7	1.1	5.3
3	36.7	39.2	2.3	0.7	5.8	12.9	0.7	0.9
4	35.2	31.2	4.5	1.2	0.4	16.3	2.2	8.6
5	37.0	27.9	3.7	1.0	0.4	14.5	2.1	13.0
6	33.1	23.1	3.6	1.2	0.4	19.8	2.9	15.5
7	32.8	31.3	3.9	1.1	0.4	17.3	2.6	10.2

3.4 Conclusions

In this chapter, a novel strategy was developed to remove fine solids from non-aqueous extracted (NAE) bitumen product through hetero-aggregation and magnetic separation. Stearylamine acetate (SAA) functionalized-magnetite nanoparticles (SAA-MNPs) were synthesized and mixed with cyclohexane diluted NAE bitumen, which led to their hetero-aggregation with the NAE fine solids. It was found that the fine solids could be effectively removed from the NAE bitumen product through a subsequent magnetic field-assisted sedimentation and filtration process. At a solvent (cyclohexane) to NAE bitumen weight ratio of 2:1, and magnetic nanoparticles to NAE bitumen weight ratio of 1:4, the fine solids content in the NAE bitumen could be lowered from 3600 ppm to 389 ppm in a single stage using the SAA-MNPs by applying the approach developed; while the un-modified MNPs could only lower the fine solids content to about 3000 ppm. The magnetic nanoparticles could also be regenerated and re-used without losing efficiency.

3.5 References

1. Lin, F.; Stoyanov, S. R.; Xu, Y., Recent Advances in Non-aqueous Extraction of Bitumen from Mineable Oil Sands: A Review. *Organic Process Research & Development* **2017,** *21* (4), 492-510.

2. Zhang, H.; Tan, X.; Liu, Q., Fine solids removal from non-aqueous extraction bitumen: A literature review. *Fuel* **2021,** *288*.

3. Pal, K.; Nogueira Branco, L. d. P.; Heintz, A.; Choi, P.; Liu, Q.; Seidl, P. R.; Gray, M. R., Performance of Solvent Mixtures for Non-aqueous Extraction of Alberta Oil Sands. *Energy & Fuels* **2015,** *29* (4), 2261-2267.

4. Hooshiar, A.; Uhlik, P.; Ivey, D. G.; Liu, Q.; Etsell, T. H., Clay minerals in non-aqueous extraction of bitumen from Alberta oil sands: Part 2. Characterization of clay minerals. *Fuel Processing Technology* **2012,** *96*, 183-194.

5. Nikakhtari, H.; Wolf, S.; Choi, P.; Liu, Q.; Gray, M. R., Migration of Fine Solids into Product Bitumen from Solvent Extraction of Alberta Oilsands. *Energy & Fuels* **2014,** *28* (5), 2925-2932.

6. Wu, J.; Dabros, T., Process for Solvent Extraction of Bitumen from Oil Sand. *Energy & Fuels* **2012,** *26* (2), 1002-1008.

7. Hooshiar, A.; Uhlik, P.; Liu, Q.; Etsell, T. H.; Ivey, D. G., Clay minerals in non-aqueous extraction of bitumen from Alberta oil sands. *Fuel Processing Technology* **2012,** *94* (1), 80-85.

8. Farnand, J. R.; F. W. Meadus;d B. D. Sparks., Removal of intractable fine solids from bitumen solutions obtained by solvent extraction of oil sands. *Fuel Processing Technology* **1985**, 10, 131-144.

9. Graham, R.; Helstrom, J.; Mehlberg, R., A Solvent Extraction Process for Tar Sand. *Eastern Oil Shale Symposium* **1987**, 93-99.

10. Painter, P.; Williams, P.; Lupinsky, A., Recovery of bitumen from Utah tar sands using ionic liquids. *Energy & Fuels* **2010,** *24* (9), 5081-5088.

11. Pulati, N.; Lupinsky, A.; Miller, B.; Painter, P., Extraction of bitumen from oil sands using deep eutectic ionic liquid analogues. *Energy & Fuels* **2015,** *29* (8), 4927-4935.

12. Sparks, B. D.; Meadus, F. W.; Hoefele, E. O., Canadian Patents and Development Ltd, Solvent extraction spherical agglomeration of oil sands. **1988,** *U.S. Patent 4,719,008.*

13. Zhang, H.; Tan, X.; Wang, K.; Liu, Q., Electrodeposition of bitumen-, asphaltene-, or maltene-coated kaolinite from cclohexane suspensions. *Fuel* **2022,** *311*, 122582.

14. Fritsche, G. R.; Bujas, R. S.; Caprioglio, G. C., General Atomics Corp, Electrostatic separator using a bead bed. **1994,** *U.S. Patent 5,308,586.*

15. Cullinane, J. T.; Minhas, B. S., ExxonMobil Upstream Research Co, Electrostatic filtration of fine solids from bitumen. **2017,** *U.S. Patent 9,752,079.*

16. Liu, J.; Cui, X.; Santander, C.; Tan, X.; Liu, Q.; Zeng, H., Destabilization of fine solids suspended in oil media through wettability modification and water-assisted agglomeration. *Fuel* **2019,** *254*.

17. HollandAmy; WechslerDominik; PatelAnjali; M., M.; R., B.; G., J., Separation of bitumen from oil sands using a switchable hydrophilicity solvent. *Canadian Journal of Chemistry* **2012,** *90* (10), 805-810.

18. Jessop, P. G.; Heldebrant, D. J.; Li, X.; Eckert, C. A.; Liotta, C. L., Reversible nonpolar-to-polar solvent. *Nature* **2005,** *436* (7054), 1102-1102.

19. Simonsen, G.; Strand, M.; Øye, G., Potential applications of magnetic nanoparticles within separation in the petroleum industry. *Journal of Petroleum Science and Engineering* **2018,** *165*, 488-495.

20. Xu, P.; Zeng, G. M.; Huang, D. L.; Feng, C. L.; Hu, S.; Zhao, M. H.; Lai, C.; Wei, Z.; Huang, C.; Xie, G. X.; Liu, Z. F., Use of iron oxide nanomaterials in wastewater treatment: a review. *Science of the Total Environment* **2012,** *424*, 1-10.

21. Pan, Y.; Du, X.; Zhao, F.; Xu, B., Magnetic nanoparticles for the manipulation of proteins and cells. *Chemical Society Reviews* **2012,** *41* (7), 2912-42.

22. Wierucka, M.; Biziuk, M., Application of magnetic nanoparticles for magnetic solid-phase extraction in preparing biological, environmental and food samples. *TrAC Trends in Analytical Chemistry* **2014,** *59*, 50-58.

23. You, N.; Wang, X.-F.; Li, J.-Y.; Fan, H.-T.; Shen, H.; Zhang, Q., Synergistic removal of arsanilic acid using adsorption and magnetic separation technique based on Fe_3O_4@ graphene nanocomposite. *Journal of Industrial and Engineering Chemistry* **2019,** *70*, 346-354.

24. Yue, T.; Niu, Z.; Tao, H.; He, X.; Sun, W.; Hu, Y.; Xu, Z., Green Recycling of Goethite and Gypsum Residues in Hydrometallurgy with α-Fe_3O_4 and γ-Fe_2O_3 Nanoparticles:

Application, Characterization, and DFT Calculation. *ACS Sustainable Chemistry & Engineering* **2019**, 7 (7), 6821-6829.

25. Yue, T.; Xu, Z.; Hu, Y.; Han, H.; Sun, W., Magnetic Separation and Recycling of Goethite and Calcium Sulfate in Zinc Hydrometallurgy in the Presence of Maghemite Fine Particles. *ACS Sustainable Chemistry & Engineering* **2018**, 6 (2), 1532-1538.

26. Yildiz, I., Applications of magnetic nanoparticles in biomedical separation and purification. *Nanotechnology Reviews* **2016,** *5* (3), 331-340.

27. Gupta, A. K.; Gupta, M., Synthesis and surface engineering of iron oxide nanoparticles for biomedical applications. *Biomaterials* **2005,** *26* (18), 3995-4021.

28. Peng, J.; Liu, Q.; Xu, Z.; Masliyah, J., Novel Magnetic Demulsifier for Water Removal from Diluted Bitumen Emulsion. *Energy & Fuels* **2012,** *26* (5), 2705-2710.

29. Ali, N.; Zhang, B.; Zhang, H.; Zaman, W.; Li, X.; Li, W.; Zhang, Q., Interfacially active and magnetically responsive composite nanoparticles with raspberry like structure; synthesis and its applications for heavy crude oil/water separation. *Colloids and Surfaces A: Physicochemical and Engineering Aspects* **2015,** *472*, 38-49.

30. Nikakhtari, H.; Vagi, L.; Choi, P.; Liu, Q.; Gray. MR., Solvent screening for a non-aqueous extraction of Alberta oil sands process. *Canadian Journal of Chemical Engineering* **2012,** *91* (6), 1153-1160.

31. Wu, W.; He, Q.; Jiang, C., Magnetic iron oxide nanoparticles: synthesis and surface functionalization strategies. *Nanoscale Research Letters* **2008,** *3* (11), 397-415.

32. ASTM, ASTM D4807-05, Standard Test Method for Sediment in Crude Oil by Membrane Filtration. **2017**.

33. ASTM, ASTM D482-07, Standard Test Method for Ash from Petroleum Products. **2013**.

34. Adhikari, M.; Echeverria, E.; Risica, G.; McIlroy, D. N.; Nippe, M.; Vasquez, Y., Synthesis of Magnetite Nanorods from the Reduction of Iron Oxy-Hydroxide with Hydrazine. *ACS Omega* **2020,** *5* (35), 22440-22448.

35. Singh, D.; Gautam, R. K.; Kumar, R.; Shukla, B. K.; Shankar, V.; Krishna, V., Citric acid coated magnetic nanoparticles: Synthesis, characterization and application in removal of Cd(II) ions from aqueous solution. *Journal of Water Process Engineering* **2014,** *4*, 233-241.

36. Ruparelia, N.; Soni, U.; Desai, R. P.; Ray, A., Silica anchored colloidal suspension of magnetite nanorods. *Journal of Solid State Chemistry* **2020,** *290*, 121574.

37. Hong, R.; Zhang, S.; Di, G.; Li, H.; Zheng, Y.; Ding, J.; Wei, D., Preparation, characterization, and application of Fe3O4/ZnO core/shell magnetic nanoparticles. *Materials Research Bulletin* **2008,** *43* (8-9), 2457-2468.

38. Lawrie, G.; Keen, I.; Drew, B.; Chandler-Temple, A.; Rintoul, L.; Fredericks, P.; Grøndahl, L., Interactions between alginate and chitosan biopolymers characterized using FTIR and XPS. *Biomacromolecules* **2007,** *8* (8), 2533-2541.

39. Zaitsev, V. S.; Filimonov, D. S.; Presnyakov, I. A.; Gambino, R. J.; Chu, B., Physical and chemical properties of magnetite and magnetite-polymer nanoparticles and their colloidal dispersions. *Journal of Colloid and Interface Science* **1999,** *212* (1), 49-57.

40. Fang, M.; Ström, V.; Olsson, R. T.; Belova, L.; Rao, K. V., Particle size and magnetic properties dependence on growth temperature for rapid mixed co-precipitated magnetite nanoparticles. *Nanotechnology* **2012,** *23* (14), 145601.

41. Radoń, A.; Drygała, A.; Hawełek, Ł.; Łukowiec, D., Structure and optical properties of Fe3O4 nanoparticles synthesized by co-precipitation method with different organic modifiers. *Materials Characterization* **2017,** *131*, 148-156.

42. Ma, M.; Zhang, Y.; Yu, W.; Shen, H.-y.; Zhang, H.-q.; Gu, N., Preparation and characterization of magnetite nanoparticles coated by amino silane. *Colloids and Surfaces A: Physicochemical and Engineering Aspects* **2003,** *212* (2), 219-226.

43. Jin, Y.; Liu, W.; Liu, Q.; Yeung, A., Aggregation of silica particles in non-aqueous media. *Fuel* **2011,** *90* (8), 2592-2597.

44. Dongbao, F.; Woods, J. R.; Kung, J.; Kingston, D. M.; Kotlyar, L. S.; Sparks, B. D.; Mercier, P. H. J.; McCracken, T.; Ng, S., Residual Organic Matter Associated with Toluene-Extracted Oil Sands Solids and Its Potential Role in Bitumen Recovery via Adsorption onto Clay Minerals. *Energy & Fuels* **2010,** *24* (4), 2249-2256.

45. Couillard, M.; Mercier, P. H. J., Analytical Electron Microscopy of Carbon-Rich Mineral Aggregates in Solvent-Diluted Bitumen Products from Mined Alberta Oil Sands. *Energy & Fuels* **2016,** *30* (7), 5513-5524.

46. Collins, S.; Melrose, J. In *Adsorption of asphaltenes and water on reservoir rock minerals*, SPE Oilfield and Geothermal Chemistry Symposium, OnePetro: 1983.

47. González, G.; Moreira, M. B. C., Chapter 9 The Adsorption of Asphaltenes and Resins on Various Minerals. In *Developments in Petroleum Science*, Yen, T. F.; Chilingarian, G. V., Eds. Elsevier: 1994; Vol. 40, pp 207-231.

48. Saraji, S.; Goual, L.; Piri, M., Adsorption of Asphaltenes in Porous Media under Flow Conditions. *Energy & Fuels* **2010,** *24* (11), 6009-6017.

49. Chen, Q.; Gray, M. R.; Liu, Q., Irreversible Adsorption of Asphaltenes on Kaolinite: Influence of Dehydroxylation. *Energy & Fuels* **2017,** *31* (9), 9328-9336.

50. Adams, J. J., Asphaltene adsorption, a literature review. *Energy & Fuels* **2014,** *28* (5), 2831-2856.

51. Nikakhtari, H.; Vagi, L.; Choi, P.; Liu, Q.; Gray, M. R., Solvent screening for non-aqueous extraction of Alberta oil sands. *The Canadian Journal of Chemical Engineering* **2013,** *91* (6), 1153-1160.

52. Chen, Q.; Stricek, I.; Gray, M. R.; Liu, Q., Influence of hydrophobicity distribution of particle mixtures on emulsion stabilization. *Journal of colloid and interface science* **2017,** *491*, 179-189.

53. Pourmohammadbagher, A.; Shaw, J. M., Probing the Impact of Asphaltene Contamination on Kaolinite and Illite Clay Behaviors in Water and Organic Solvents: A Calorimetric Study. *Energy & Fuels* **2016,** *30* (8), 6561-6569.

54. Luo, L.; Nguyen, A. V., A review of principles and applications of magnetic flocculation to separate ultrafine magnetic particles. *Separation and Purification Technology* **2017,** *172*, 85-99.

CHAPTER 4 Removal of Fine Solids from Bitumen by Hetero-aggregation and Magnetic Separation Using Surface-modified Magnetite Nanoparticles: Role of Surface Modification*

4.1 Introduction

Owing to their distinctive characteristics (superparamagnetism, ease of manipulation, desired size, etc.), magnetic nanoparticles have been attracting significant attention and have found applications in diverse areas including soil/wastewater contamination treatment, probing and sensing, biomolecule isolation, and medical diagnostics [1-3]. In most cases, surface modification of the magnetic nanoparticles is crucial prior to their applications to ensure the adequacy of their properties in terms of wettability, specific adsorption properties, biocompatibility, etc. Each potential application of magnetic nanoparticles requires different surface properties, and the application objectives determine the modification type and strategy. For example, ferrofluids are widely used in machine element design [4], and excellent colloidal stability of the magnetic nanoparticles in the fluid system is required, which is usually realized by controlling the surface charge or steric repulsive force among the nanoparticles [5-6]. When applied in wastewater treatment, high adsorption capacity of magnetic nanoparticles is necessary and chelating ligands are normally used as functionalization agents to improve the particles' adsorption capacity to various contaminants through their multiple binding sites [7-8]. In drug delivery and tissue engineering, non-toxicity and biocompatibility are important factors to consider where the magnetic nanoparticles are used as carriers, which can be obtained through surface coating by specific polymers [9] or oxides (e.g. silica or alumina) [10].

* The main part of this chapter was published as: Liu X, Li J, Wang K, Tan X, Yeung A, Zeng H, Liu Q, 2024. Removal of fine solids from bitumen by hetero-aggregation and magnetic separation using surface-modified magnetite nanoparticles. Part II: role of surface modification. Separation and Purification Technology, Vol. 333, 125928.

Applications of magnetic nanoparticles in crude oil industry is a new research area over the last decade [11-12], and the potential applications include drilling fluid properties (stability or rheology) improvement [13-14], metal cations (Na^+, Mg^{2+} or Ca^{2+}) removal [12,15-16], oil product purification [17], and so on. The surface-modified magnetic nanoparticles have shown extraordinary advantages when used as adsorbent for impurities removal from crude oil or bitumen. For example, ethyl-cellulose-grafted magnetite (Fe_3O_4) nanoparticles exhibited a strong affinity to water droplets dispersed in bitumen and could remove more than 80% of water from an industrial bitumen froth through magnetic separation [18-19]. Amine-functionalized Fe_3O_4 nanoparticles [20] showed strong attachment with crude oil droplets in an oil-in-water emulsion, which is attributed to the electrostatic attraction between the positively charged surface of the amine-functionalized Fe_3O_4 nanoparticles and the negatively charged crude oil droplets, and the aggregation of the nanoparticles-oil droplets played a critical role in the efficient and accelerated oil droplets removal under magnetic field. In the work of Setoodeh et al. [21], it was observed that surface coating of Fe_3O_4 nanoparticles with polythiophene could increase the nanoparticles' adsorption capacity of asphaltene and thus could potentially be used in asphaltene removal from crude oil. In the previous chapter [22], we demonstrated a novel method of fine solids removal from non-aqueous extracted (NAE) bitumen by hetero-aggregation and magnetic separation using stearylamine acetate-modified magnetite nanoparticles (SAA-MNPs). It was shown that compared with bare magnetite nanoparticles (MNPs), the surface modification of MNPs with stearylamine acetate (SAA) could significantly strengthen their binding affinity with (organics-coated) fine solids, thus improving the capture and removal efficiency. It was also observed that cyclohexane-diluted bitumen could play a key role as a surface modifier for MNPs to enhance their ability to form hetero-aggregates

with suspended fine solids in NAE bitumen, i.e., after one cycle of use, the initially bare MNPs exhibited greatly improved capability to remove fine solids from NAE bitumen [22].

This work continues the research and aims, firstly, to further study and verify that the cyclohexane-diluted bitumen could function as a surface modifier for MNPs to improve their ability to capture NAE fine solids under an external magnetic field; secondly, to investigate how the surface modification of MNPs with SAA or bitumen components such as asphaltenes would influence their interaction with NAE fine solids. Asphaltene, the most polar component of bitumen, was used to modify the MNPs, and the NAE fine solids removal ability of the fabricated asphaltene-modified magnetite nanoparticles (Asp-MNPs) by using the proposed magnetic separation method was tested. The interfacial interactions between Fe_3O_4 surface and asphaltene surface, between SAA surface and asphaltene surface, and between asphaltene surface and asphaltene surface in cyclohexane were investigated through quartz crystal microbalance with dissipation monitoring (QCM-D) and atomic force microscopy (AFM) studies. In addition, the influences of the external magnetic field on the formation of hetero-aggregates were studied. Based on the above studies, the schematics of magnetic field-assisted hetero-aggregation between surface-modified MNPs and the NAE fine solids were proposed.

4.2 Materials and methods

4.2.1 Materials

All purchased chemicals were used as received. Ferrous chloride tetrahydrate ($FeCl_2 \cdot 4H_2O$, ≥99.0%), ferric chloride hexahydrate ($FeCl_3 \cdot 6H_2O$, ACS, 97.0%), and sodium citrate tribasic dihydrate (ACS, ≥99.0%) were purchased from Sigma-Aldrich. Ammonium hydroxide solution (ACS, 29.47 wt% NH_3), ethanol (90.0%), toluene (ACS, ≥99.5%), and cyclohexane (HPLC grade, ≥99.0%) were purchased from Fisher Scientific. Stearylamine acetate (SAA) was purchased from

Tokyo Chemical Industry Co., Ltd. The C7 asphaltene was extracted from Athabasca bitumen (provided by an oil sands company operating in northern Alberta) following the ASTM D6560-12 method [23]. The NAE bitumen sample was the same sample used in Chapter 3, with a fine solids content of 3600 ppm (0.36 wt%) [22]. The colloidal AFM probes (CP-qp-CONT-SiO) with a silica sphere (d = 6.62 μm) at the end of the cantilever were purchased from NanoAndMore USA. Milli Q water (resistance≥ 18.2MΩ·cm) was used throughout this study.

4.2.2 Preparation and characterization of Asp-MNPs

4.2.2.1 Preparation

The preparation of asphaltene-modified magnetic nanoparticles (Asp-MNPs) followed the common batch adsorption experiment procedure of asphaltene on solid sorbent [24-25] in a suitable organic solvent such as toluene. The sorbent MNPs were synthesized by co-precipitation method following the procedure described in Chapter 3 [22], section 3.2.2.1. Briefly, 2.13 g of $FeCl_2 \cdot 4H_2O$ and 5.79 g of $FeCl_3 \cdot 6H_2O$ were dissolved in 50 mL of distilled water that was previously purged with nitrogen gas. The temperature of the prepared solution was raised to and maintained at 75ºC. Afterwards, 25 mL of NH_4OH solution was introduced into the mixture under vigorous stirring. After 30 minutes, the resulting black precipitates (magnetite nanoparticles, MNPs) were collected by sedimentation under a magnetic field generated by two electromagnet poles, washed sequentially with water and ethanol, and re-dispersed in ethanol for use in this work. The asphaltene-in-toluene solution was prepared by dissolving a certain amount of asphaltene in toluene followed by 30 minutes ultrasonic treatment. The batch adsorption was conducted as follows: after thoroughly washing with toluene, bare MNPs were immediately added to the prepared 5 g/L asphaltene-toluene solution, then the MNPs-asphaltene-toluene mixture was shaken continuously by an orbital shaker (Corning® LSE™ Benchtop Shaking Incubator) at 25°C

for 24 hours. Afterwards, the asphaltene-coated MNP particles were separated by magnetic-field assisted sedimentation and washed with toluene several times to remove excess asphaltene, followed by 2 times of cyclohexane rinse. The product was re-dispersed in cyclohexane and labelled as Asp-MNPs for use in this work. During the preparation of Asp-MNPs, drying of the nanoparticles was avoided.

4.2.2.2 Characterization

The crystalline structure identification of the MNP samples was carried out with a Rigaku Ultima IV X-ray diffraction system with Cu Kα radiation (λ = 1.540 Å) source at 40 kV and 40 mA using the powder diffraction technique. The data was collected over the 2θ range of 20° to 70° at a scan speed of 2.00º/min and a step size of 0.02º. Data conversion was performed with JADE MDI 9.6 software and data interpretation with DIFFRAC.EVA software with the 2021 ICDD PDF 4+ database.

Surface modification of MNPs was verified by Fourier transform infrared (FTIR) spectroscopic measurements using a Bruker ALPHA FTIR spectrometer, which was equipped with a deuterated triglycine sulfate (DTGS) detector and a single-bounce diamond attenuated total reflectance (ATR) crystal. The measurements were carried out at room temperature in a wavelength range from 500 to 4000 cm^{-1}, the spectral resolution was set to 4 cm^{-1}, and 128 scans were taken per measurement. Dried powder samples were used directly for the measurements, and the pressure to press the powder sample onto the ATR crystal was controlled by the instrument's operating software. Processing of the FTIR data was performed using Bruker OPUS software.

The morphology of the prepared nanoparticles was observed using a transmission electron microscope (TEM, JEOL JEM-ARM200CF) operated at an accelerating voltage of 200 kV. A drop

of nanoparticle-cyclohexane solution (0.05 mg/mL) was placed on a carbon-coated copper grid for observation.

Magnetic property measurements of the prepared nanoparticles were performed on a superconducting quantum interference device (SQUID, MPMS®3, Quantum Design) at the University of Waterloo. For measurement, about 10 mg of powder samples were inserted in a gelatin capsule. The measurements were taken at room temperature within the magnetic field range from -2 to +2 Tesla.

4.2.3 Asp-MNPs for NAE fine solids removal

The NAE fine solids removal performance by Asp-MNPs was examined following a magnetic sedimentation + magnetic filtration separation process as described in the previous chapter [22]. First, 6 mL of Asp-MNPs-in-cyclohexane mixture with a concentration of 0.42 g/mL were added in a beaker with a well-mixed solution of 10 g NAE bitumen in 20 mL cyclohexane. After stirring for 30 minutes, the beaker was placed on top of the magnetic pole of a 3×4 L Outotec laboratory wet high-intensity magnetic separator (WHIMS), with a ~1 Tesla magnetic field generated to accelerate the sedimentation of magnetic nanoparticles. The supernatant was decanted, and the sediment (Asp-MNPs-fine solids hetero-aggregates) was washed twice with cyclohexane and then suspended in fresh cyclohexane for subsequent regeneration. The supernatants from the above decantation and washing were combined and passed through the WHIMS separation chamber, yielding a cleaned NAE bitumen product. The separation chamber was filled with steel wools to generate a high magnetic field gradient to increase the magnetic force acting on the magnetic particles. The "filter cake" retained on the steel wools was collected as solid waste. To regenerate the Asp-MNPs, the settled Asp-MNPs and fine solids hetero-aggregates were subjected to ultrasonic treatment and washed with cyclohexane, and reused for fine solids removal from NAE

bitumen in the next cycle. To determine the fine solids content in the cleaned bitumen product, the hot filtration method [23], or ashing method following the procedure described in ASTM D482-07 [26] was used.

4.2.4 Characterization of interfacial interactions

4.2.4.1 Surface preparation

All the surfaces for QCM-D and AFM studies were prepared by treating iron oxide QCM-D sensors (Fe_3O_4; QSX 326; Biolin Scientific, USA) with different solutions using dip-coating method. Prior to each treatment, the sensor surface was cleaned following the standard cleaning procedure (for QSX 326) provided by the vendor. Specifically, the iron oxide sensor was sonicated in 99% ethanol for 15 minutes, followed by Milli Q water rinsing and nitrogen gas blow-drying. For preparation of SAA surface, the cleaned iron oxide sensor was first immersed for 12 hours in 100 mL of sodium citrate aqueous solution (70 mg/mL) at 80ºC. Afterwards, the sensor was rinsed with Milli Q water, followed by submerging in 50 mL of SAA solution (12 mg/mL) for 12 hours at 80ºC. The sensor was subsequently rinsed with water and blow-dried using pure nitrogen gas. To obtain the asphaltene-coated surface, first a 0.5 mg/mL asphaltene-cyclohexane solution was prepared by diluting asphaltene in cyclohexane under ambient conditions. The solution was then sonicated for 15 minutes to disperse asphaltene aggregates in cyclohexane uniformly. To complete the surface coating, the cleaned iron oxide sensor was immersed in the asphaltene-cyclohexane solution for 1 hour at room temperature (RT), followed by rinsing with cyclohexane and blow-drying with nitrogen gas.

During each treatment step, the wettability of the sensor surface was examined by measuring the static water contact angle in air. The measurements were carried out by the sessile drop method and performed using an optical tensiometer (Attension, Biolin Scientific) at room temperature. A

water droplet with a volume of ~6 µL was deposited on the sensor surfaces through a syringe with a needle. The real-time results were obtained and analyzed by the OneAttension software. The measurement was repeated 3 times for each surface. The schematic surface preparation steps and the corresponding contact angles are shown in Figure 4.1.

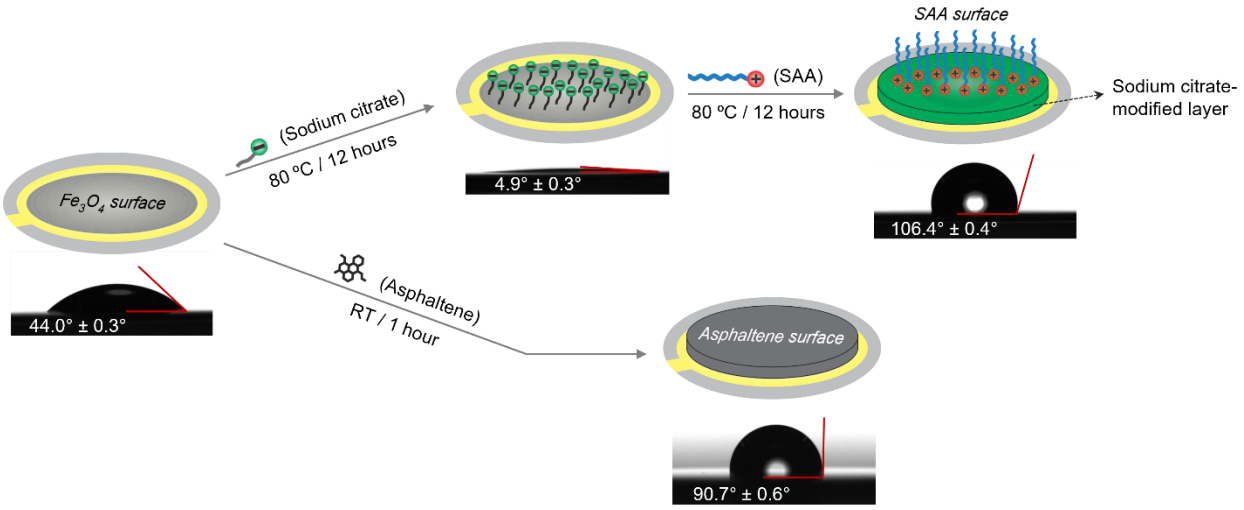

Figure 4.1 Schematic process for SAA surface or asphaltene surface preparation, on Fe_3O_4 QCM-D sensor substrate, and static water contact angle measurements for each surface. The water contact angle of iron oxide surface decreased from 44.0°±0.3° to 4.9°±0.3° after sodium citrate treatment indicating a more hydrophilic surface due to the exposure of -COO^- groups from sodium citrate; the contact angle increased from 4.9°±0.3° to 106.4°±0.4° indicating the successful treatment of sensor surface by SAA, and the hydrophobic surface shown was caused by the exposure of hydrocarbon chains from SAA at the sensor surface. Compared with the Fe_3O_4 surface, the prepared asphaltene surface showed an increased hydrophobicity with a water contact angle of 90.7±0.6°, which was consistent with that of the asphaltene surface reported in other studies [27-28].

4.2.4.2 QCM-D measurements

The adsorption of asphaltene on pristine or modified Fe_3O_4 surfaces was monitored by a Q-sense Quartz Crystal Microbalance with Dissipation (Biolin Scientific, USA) using sensors coated with iron oxide (Fe_3O_4; QSX 326; Biolin Scientific, USA). Prior to each measurement, the QSX 326 sensor surface was cleaned, and a stable baseline was established by pumping the background solution (cyclohexane) into the chamber. Asphaltene-cyclohexane solution with a concentration of 0.5 mg/mL or pure cyclohexane was allowed to flow through the sensor surface at 100 µL/min during the online monitoring. All the measurements were carried out at 25°C. For each sensor, the real-time frequency (f) and dissipation (D) at different overtone number ($n = 3, 5, 7, 9, 11$) were monitored. During the QCM-D measurements, the mass deposition on the sensor would induce a decrease in frequency (f) and an increase in dissipation (D), and vice versa.

4.2.4.3 AFM force measurements

The AFM force measurements were performed using the colloidal probe technique on an MFP-3D AFM system (Asylum Research, Santa Barbara, CA). The asphaltene probe was obtained by immersing an AFM silicon cantilever with a 6.62 µm diameter SiO_2 spherical tip in a 0.5 mg/mL asphaltene-cyclohexane solution for 30 min to allow asphaltene to adsorb on the silica surface, followed by thoroughly rinsing with cyclohexane and blow-drying with pure nitrogen. The cleaned pristine QCM-D iron oxide sensor surface, prepared SAA surface and asphaltene surface were used as substrates for AFM force measurements. A schematic illustration of the experimental setup is shown in Figure 4.2.

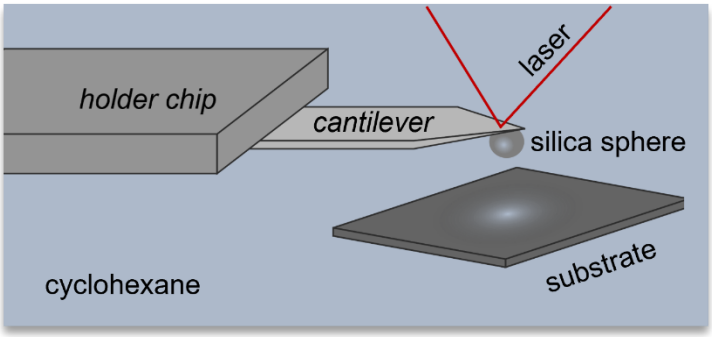

Figure 4.2 Schematic illustration of AFM force measurements.

4.2.5 Hetero-aggregation tests

Hetero-aggregation tests between Asp-MNPs nanoparticles and NAE fine solids in pure cyclohexane were performed under an external magnetic field. The NAE fine solids suspension was prepared from a cyclohexane-extracted gangue sample. The gangue sample was mixed with cyclohexane at a volume ratio of 1:1 and settled for 7 days. Afterwards, the supernatant was decanted and allowed to settle for another 2 days. The new supernatant was collected as NAE fine solids suspension and used in this work. To prepare the mixtures, about 20 mL fine solids-cyclohexane suspension with a solid concentration of about 1 mg/mL (about 1200 ppm) was sonicated for 10 minutes, afterwards about 1 mL of Asp-MNPs or MNPs in cyclohexane suspension with a concentration of 20 mg/mL was added and well-mixed in the suspension. The vials which contained the mixtures were placed next to a strong neodymium permanent magnet (N52; remanence: 1-1.3 Tesla; coercivity: 0.875–1.99 MA/m). Sedimentation tests of NAE fine solids in cyclohexane (without Asp-MNPs) were also conducted as blank tests without the magnet.

4.3 Results and discussion

4.3.1 Properties of Asp-MNPs

The crystallinity and phase purity of the as-prepared pristine and modified MNPs were characterized by X-ray diffraction (XRD) measurements. The XRD patterns of the synthesized nanoparticles are shown in Figure 4.3(a). For the XRD pattern of MNPs, the diffraction peaks at the 2θ angles of 30.2°, 35.5°, 43.2°, 53.6°, 57.2°, and 62.8° could be ascribed to the reflection from the (220), (311), (400), (422), (511), and (440) planes of the Fe_3O_4 (magnetite), respectively [29-30]. These peaks were consistent with the ICDD database of Fe_3O_4 (PDF # 85-1436) and also revealed that the nanoparticles consisted of a pristine Fe_3O_4 phase with a spinal structure. The identical set of characteristic peaks of Fe_3O_4 appeared in the pattern of Asp-MNPs, indicating the stability of the crystalline structure of Fe_3O_4 nanoparticles during the subsequent surface modification of the MNPs.

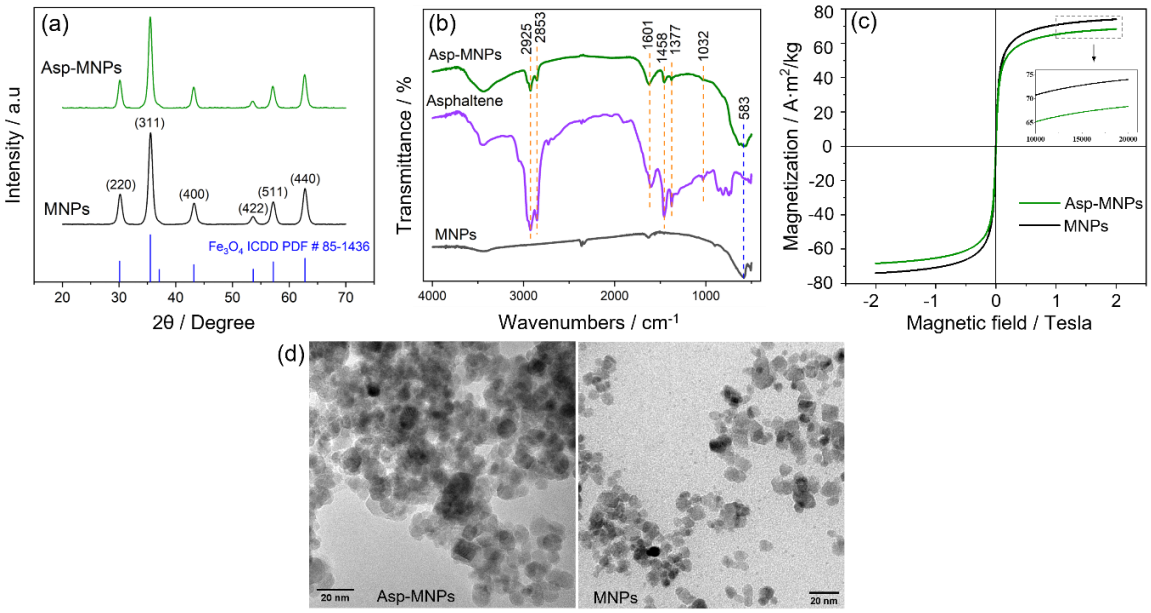

Figure 4.3 (a) XRD patterns, (b) FTIR spectra, (c) Magnetization curves, (d) TEM images of prepared magnetite nanoparticles.

The FTIR spectra of asphaltene and the prepared magnetite nanoparticles are presented in Figure 4.3(b). The spectra of both MNPs and Asp-MNPs samples exhibited a strong band at 583 cm^{-1}, corresponding to the characteristic stretching vibration of Fe-O bond from Fe_3O_4 [31]. Comparing the spectra of asphaltene and Asp-MNPs, the major characteristic peaks of asphaltene were also clearly observed in Asp-MNPs, which indicated the presence of asphaltene on Fe_3O_4 surface. Two adsorption peaks at 2925 cm^{-1} and 2853 cm^{-1} were respectively assigned to asymmetrical and symmetrical stretching of C-H from alkane chain ($-CH_2-$). Two peaks at 1458 cm^{-1} and 1377 cm^{-1} were respectively associated with the bending vibration of methyl groups ($-CH_3$) and methylene groups ($-CH_2-$). The adsorption peak at 1601 cm^{-1} could be assigned to the aromatic C=C stretching vibration. The peak at 1032 cm^{-1} corresponded to a sulfoxide functional group ($C_2S=O$) [32].

The magnetic behavior of magnetite nanoparticles is an important aspect of their properties and ensures their rapid separation from a complex matrix. A magnetometer was utilized to measure the magnetic hysteresis loops of MNPs and Asp-MNPs samples at room temperature. As shown in Figure 4.3(c), both curves showed nonlinear and reversible characteristics without hysteresis (naught remanence and zero coercivity), indicating the superparamagnetic behavior of both samples. The saturation magnetization for MNPs was around 74.0 $A \cdot m^2/kg$, which was consistent with earlier works [33-34]. The saturation magnetization of Asp-MNPs (68.4 $A \cdot m^2/kg$) was slightly lower than that of the pristine MNPs. This decrease of saturation magnetization per unit mass could be considered an indication that the asphaltene coating on the magnetite nanoparticle surface contributed as a nonmagnetic mass to the total sample weight. Generally, the magnetic susceptibility of the prepared magnetite nanoparticles would favor the separation and recovery of them from the solvent by simply applying an external magnetic field.

The TEM images of magnetite nanoparticles before and after asphaltene modification are shown in Figure 4.3(d). The pristine MNPs appeared to have a narrow size distribution with the sizes ranging from 6.5 to 10 nm in diameter. After asphaltene modification, the nanoparticles showed a similar morphology, which indicated a stable crystalline structure during the modification process.

4.3.2 NAE fine solids removal by Asp-MNPs

The performance of Asp-MNPs for fine solids removal in NAE bitumen was investigated. Figure 4.4 shows the removal efficiencies by magnetic separation using Asp-MNPs and MNPs. As demonstrated, the pristine MNPs were unable to remove fine solids from NAE bitumen, and by introducing Asp-MNPs in cyclohexane-diluted bitumen in the removal process, the fine solids content could be lowered from 3600 ppm to 570 ppm (84.2% removal). This fine-solids removal efficiency was consistent with the efficiency of fine solids removal by using recycled MNPs (78.8%). After one cycle of use, the NAE fine solids removal capability of Asp-MNPs remained the same, at an efficiency of 83.7%. The results illustrated that asphaltene was a potential modifier for MNPs to improve the NAE fine solids removal efficiency when using the proposed magnetic separation method.

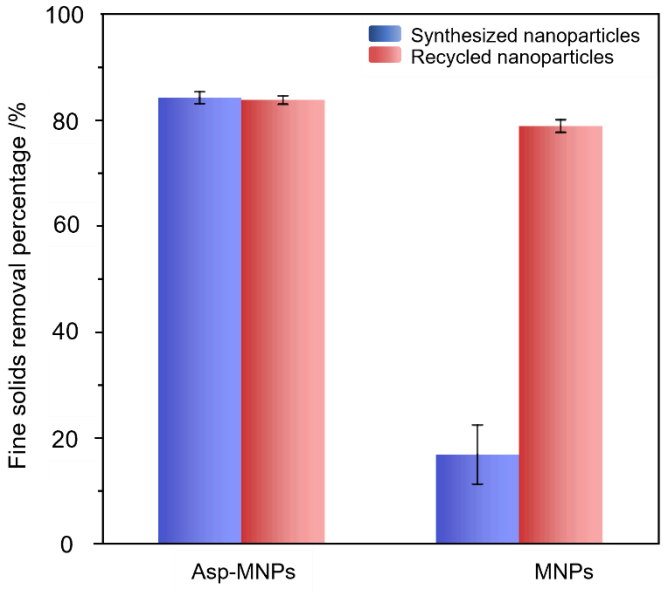

Figure 4.4 NAE fine solids removal efficiency by magnetic separation after the introduction of Asp-MNPs and MNPs. The weight ratio of cyclohexane to NAE bitumen was 2:1, and magnetic nanoparticles to NAE bitumen was 1:4. The magnetic separation was conducted under a magnetic field with a strength of 1 Tesla. The blue bars presented the initial cycle of fine solids removal, and the red bars indicated the fine solids removal by using recycled Asp-MNPs and MNPs from the initial solid removal cycle.

4.3.3 Interfacial interactions

4.3.3.1 Evaluation of asphaltene adsorption on different surfaces by QCM-D measurements

QCM-D measurements were designed and performed to evaluate the adsorption behavior of asphaltene on different surfaces including Fe_3O_4 surface, Fe_3O_4 surface coated with SAA (called "SAA surface"), and Fe_3O_4 surface coated by asphaltene (called "asphaltene surface"). The QCM-D experimental procedure was performed for chambers mounted with Fe_3O_4 sensor and SAA coated Fe_3O_4 sensor following the steps shown in Figure 4.5. As can be seen, for both surfaces, after obtaining the steady baseline (process I or I'), an immediate decrease in frequencies along

with an increase in dissipation were observed at T_A or T_A', suggesting the adsorption of asphaltene on both surfaces. Compared with SAA surface, the adsorption rate of asphaltene on Fe_3O_4 surface was much lower along the injection of asphaltene-cyclohexane solution, considering the relatively milder frequency and dissipation changes in process II compared to process II'. The adsorption equilibrium for SAA surface occurred 12 minutes after the initiation of asphaltene adsorption in process II'. Thoroughly rinsing the sensors was done in-situ in process III and process III'. An increase in frequencies accompanied by a decrease in dissipations took place for both sensors, but the shifts did not recover to the points where the adsorption was triggered, revealing the strong and irreversible adsorption of asphaltene on both surfaces.

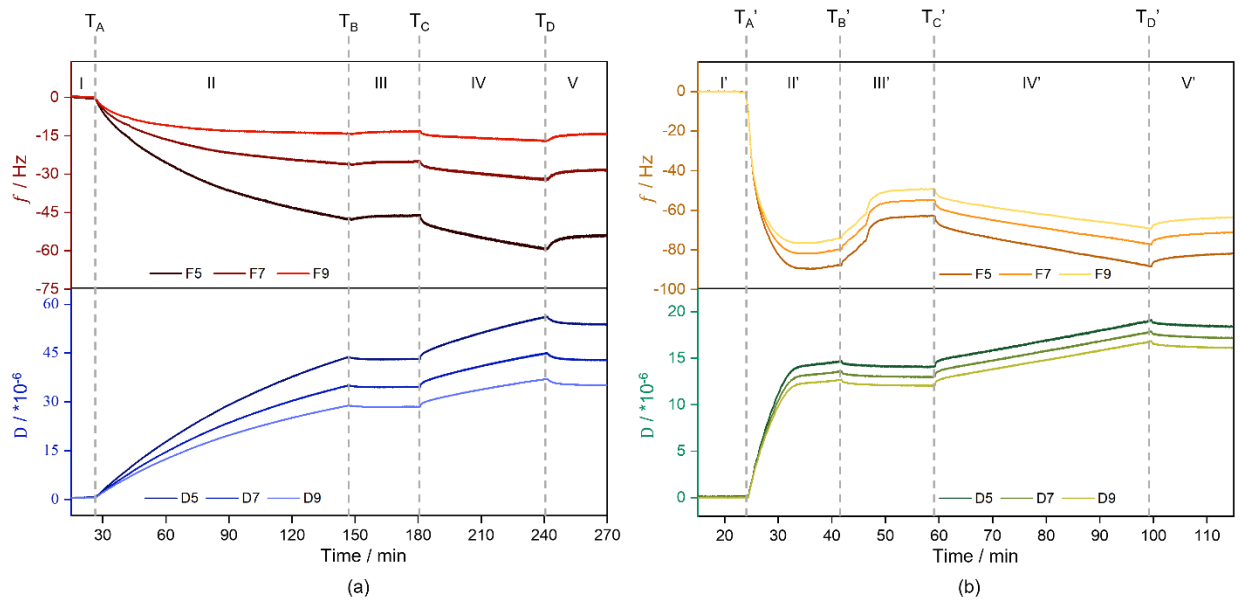

Figure 4.5 Shifts in frequency (f) and dissipation (D) (for overtone number $n = 3, 5, 7$) against time of (a) iron oxide (Fe_3O_4) surface and (b) SAA surface during asphaltene adsorption monitored by QCM-D. In process I (I'), cyclohexane was injected to obtain stable baseline. Asphaltene-cyclohexane solution (0.5 mg/mL) was introduced at T_A (T_A') to initiate asphaltene deposition. At the time of T_B (T_B'), the injected solution was substituted by cyclohexane for rinsing purposes. To

examine the second layer adsorption of asphaltene, cyclohexane was replaced with asphaltene-cyclohexane solution (0.5 mg/mL) at T_C (T_C'). At the time of T_D or T_D', asphaltene adsorption process was ended and the chambers were flowed with cyclohexane for washing. Flow rate of solvents was kept at 100 μL/min for both chambers during the online monitoring.

To study the asphaltene adsorption behavior on asphaltene-coated surfaces (i.e., asphaltene-adsorbed on SAA surface and asphaltene-adsorbed on Fe_3O_4 surface), asphaltene-cyclohexane solution was loaded again to both chambers to replace cyclohexane at the time of T_C or T_C'. It showed dropping tendencies for frequencies among processes IV and IV', which demonstrated that the second asphaltene layer could deposit on both the SAA-asphaltene surface and Fe_3O_4-asphaltene surface. Similar to process III or process III', in process V and process V', after introducing cyclohexane to substitute the asphaltene-cyclohexane solution, only partial desorption of asphaltenes were observed from the two surfaces, judging from the slight rise of frequencies and drop of dissipation.

4.3.3.2 Interfacial force measurements by AFM

The surface-modification of MNPs with SAA or asphaltene may significantly change their interfacial interactions with organically-coated NAE fine solids. Colloidal probe AFM technique was used to quantitatively measure the interfacial forces between a silica-asphaltene probe and Fe_3O_4 surface, SAA surface, and asphaltene surface, respectively. Figure 4.6(a) shows the typical force-distance curves measured between the probe and a flat Fe_3O_4 surface in cyclohexane. During the approach process, a weak attraction was detected when the separation distance was less than 13 nm, which was attributed to the van der Waals attraction between the probe and the surface. With further approaching of the asphaltene-coated silica probe, the interfacial force became repulsive due to the steric force arising from the interfacial asphaltene layer in cyclohexane, and the value

grew gradually after the probe came into contact with the Fe_3O_4 surface. During the retraction of the probe, a noticeable adhesion (0.15 nN) denoted by a distinct "jump-out" behavior was recorded, revealing that the probe was suddenly released from the Fe_3O_4 substrate.

Figure 4.6(b) shows the SAA-asphaltene interfacial force features in cyclohexane. Upon the approach of the probe, no noticeable repulsion was observed, and the force curve showed a "jump-in" behavior at the separation of less than 3 nm, which indicated that a relatively strong attraction pulled the probe into contact with the SAA surface. During the retraction of the probe, a "jump-out" behavior was also observed when the distance was close to ~4 nm, which implied a relatively strong adhesion (~0.85 nN) between the probe and the SAA surface. These two discontinuities suggested that SAA surface was able to physically bridge with asphaltene-coated silica probe.

The typical force-distance curves measured between an asphaltene-coated silica probe and an asphaltene surface in cyclohexane is presented in Figure 4.6(c). When the probe gradually approached the asphaltene surface in cyclohexane, an increasingly stronger repulsion was measured at the distance ≤ 40 nm. Cyclohexane was a good solvent for asphaltene and the steric repulsion between the extended aliphatic side chains predominated over the short-range attractive forces between asphaltene molecules, preventing the asphaltene-coated silica probe from attaching the asphaltene surface. The retraction curve also showed repulsive force between the probe and the asphaltene surface except for a weak attraction of approximately 0.15 nN. The bridging interaction was responsible for this measured attraction, which occurred due to the interdigitation of the confined asphaltenes between the two surfaces [35].

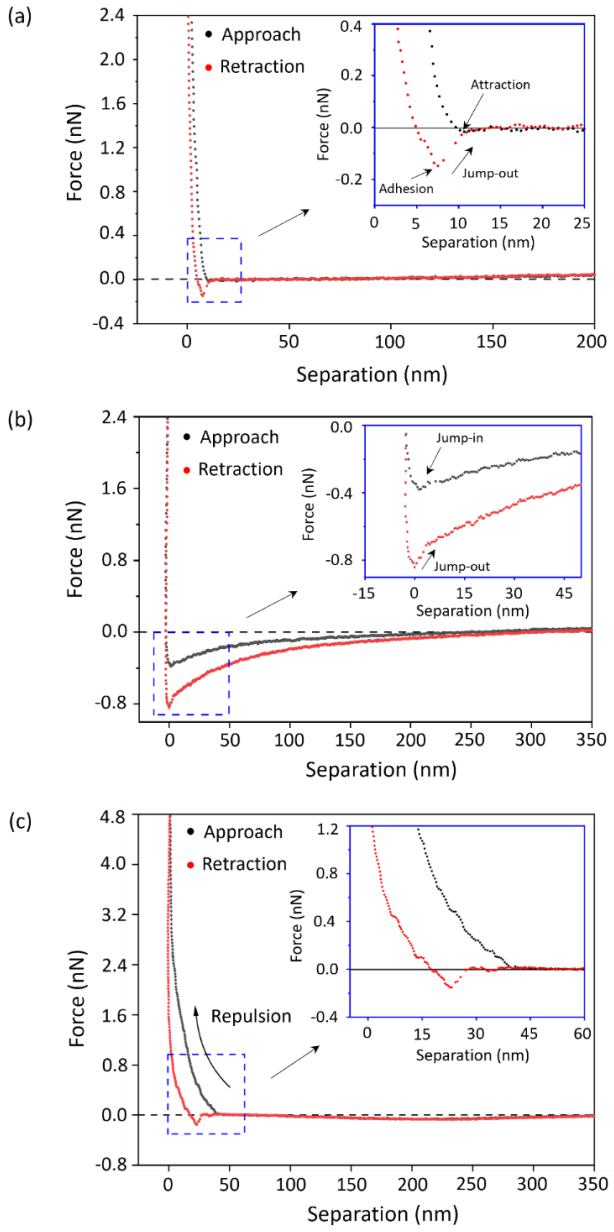

Figure 4.6 Force-distance curves for asphaltene-silica probe on (a) Fe_3O_4 surface, (b) SAA surface, and (c) asphaltene surface in cyclohexane by AFM measurements. The black and red circular symbols represented the measured data during the approach and retraction processes, respectively.

4.3.4 Hetero-aggregation between NAE fine solids and Asp-MNPs under external magnetic field

To learn NAE fine solids capture by Asp-MNPs, hetero-aggregation tests were performed and the images are shown in Figure 4.7. The clarity of the suspension in Figure 4.7(a) was largely enhanced in 4.5 minutes, and it was much higher than that of the NAE solids suspension in Figure 4.7(c), indicating the capture of NAE fine solids by Asp-MNPs and the formation of hetero-aggregates, which were removed by the magnetic-field assisted sedimentation. Upon subjecting the vials to the magnetic field for 0.5 minutes, it was noted that the vial in (b) in which un-modified magnetite MNPs were introduced exhibited higher transparency compared to the vial in (a). This was attributed to the higher degrees of dispersion of Asp-MNPs in cyclohexane in Figure 4.7(a) caused by the steric repulsion than in Figure 4.7(b). However, the vial in Figure 4.7(b) was more turbid than the vial in Figure 7(a) even after 10 minutes, and only slightly more clear than the vial in Figure 4.7(c) at 10 minutes, suggesting that only a small part of fine solids was captured by the un-modified MNPs and moved to the side of the vial in Figure 4.7(b).

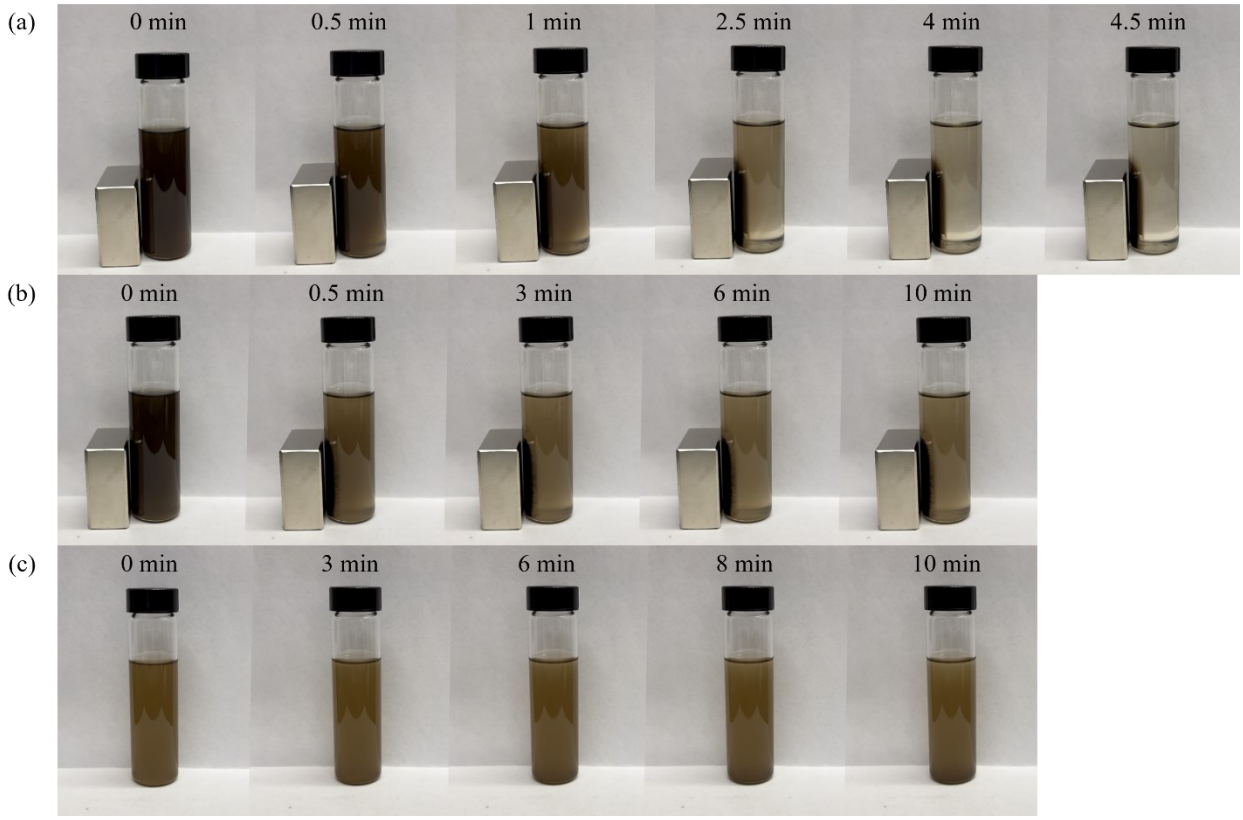

Figure 4.7 Images of hetero-aggregation between NAE fine solids and MNPs in cyclohexane. (a) mixture of Asp-MNPs and NAE fine solids in cyclohexane. (b) mixture of un-modified MNPs and NAE fine solids in cyclohexane. (c) NAE fine solids in cyclohexane. A strong magnet was placed next to the vials in (a) and (b) but not to the vial in (c). The sedimentation of NAE fine solids in cyclohexane is shown in (c) as blank test. The duration of solids suspensions for magnetic separation or sedimentation are also shown in the figure. The initial concentration of NAE fine solids in cyclohexane was 1 mg/mL.

4.3.5 Discussion

4.3.5.1 NAE fine solids capture and separation mechanisms

The polar Fe-O groups situated at the Fe_3O_4 surface could be considered as the active sites, and their binding configuration with functional groups from asphaltene may contribute to the adhesion

between the Fe_3O_4 and asphaltene [24,36]. However, due to the weak adhesion, the capture efficiency of NAE fine solids (covered by asphaltene) by the un-modified MNPs was low. The SAA modification enhanced the adhesion between the Fe_3O_4 and the asphaltene surfaces due to the bridging effect, enabling the formation of SAA-MNPs-NAE fine solids hetero-aggregates, improving the efficiency of fine solids removal from NAE bitumen from 16% to 89% (Chapter 3).

Another essential factor that facilitated the hetero-aggregation between MNPs and NAE fine solids was the applied magnetic field. Both the bare and surface-functionalized MNPs were magnetic, and the magnetic attractive force would affect the dispersion behavior of these particles, consequently influencing the motion or aggregation behavior of other colloidal particles in the surroundings. Two asphaltene-coated magnetic colloidal particles may show weak attraction due to the interdigitation and bridging of the asphaltene molecules when two asphaltene-coated magnetic particles were brought close by the external magnetic field. However, in general terms, in good solvents like cyclohexane, the asphaltene molecules tended to extend and swell, exhibiting a long-range steric repulsion among the swelled tails and loops. Apparently, the steric repulsion would not benefit hetero-aggregation between asphaltene-modified MNPs and the NAE fine solids. However, the hetero-aggregation tests and the NAE fine solids removal results showed that the asphaltene modification largely improved the NAE fine solids capture efficiency of the MNPs. The possible explanation was that under the magnetic field, Asp-MNPs would form aggregates due to their magnetic susceptibilities. This magnetic field-induced aggregation (magnetic aggregation) would strengthen the bridging among the Asp-MNPs nanoparticles, and the motion of the magnetic aggregates could trap or mop NAE fine solids, which were removed together with the Asp-MNPs. This sweeping effect may also exist in NAE fine solids capture by MNPs or SAA-MNPs. During the sweeping process, compared with bare MNPs, the surface grafts of SAA-MNPs

or Asp-MNPs would largely enhance the attachment of NAE fine solids with the formed aggregates through the bridging effect. Based on the above tests and analyses, the possible interaction schematics for SAA or asphaltene-modified magnetite nanoparticles to capture NAE fine solids under external magnetic field are proposed in Figure 4.8. When introducing SAA-MNPs to cyclohexane diluted bitumen, bridging effect occurred between SAA-MNPs and asphaltene-coated NAE fine solids before applying the magnetic field, and the external magnetic field would induce magnetic aggregation among the existing hetero-aggregates. The magnetic aggregates would create a sweeping effect to improve the capture of NAE fine solids (Fig. 4.8(a)). When Asp-MNPs were introduced, they were unlikely to aggregate with NAE fine solids due to steric repulsion. However, the applied magnetic field could induce the magnetic aggregation and bridging among the Asp-MNPs. The capture of NAE fine solids by Asp-MNPs was realized by the sweeping effect of the network-structured Asp-MNP magnetic aggregates with "asphaltene brushes" (Fig. 4.8(b)); In the case of bare MNPs (Fig. 4.8(c)), the external magnetic field could induce the aggregation of MNPs, and the sweeping effect contributed to their capture of NAE fine solids. However, without the surface asphaltene brushes, the NAE fine solids capture efficiency was much lower than Asp-MNPs.

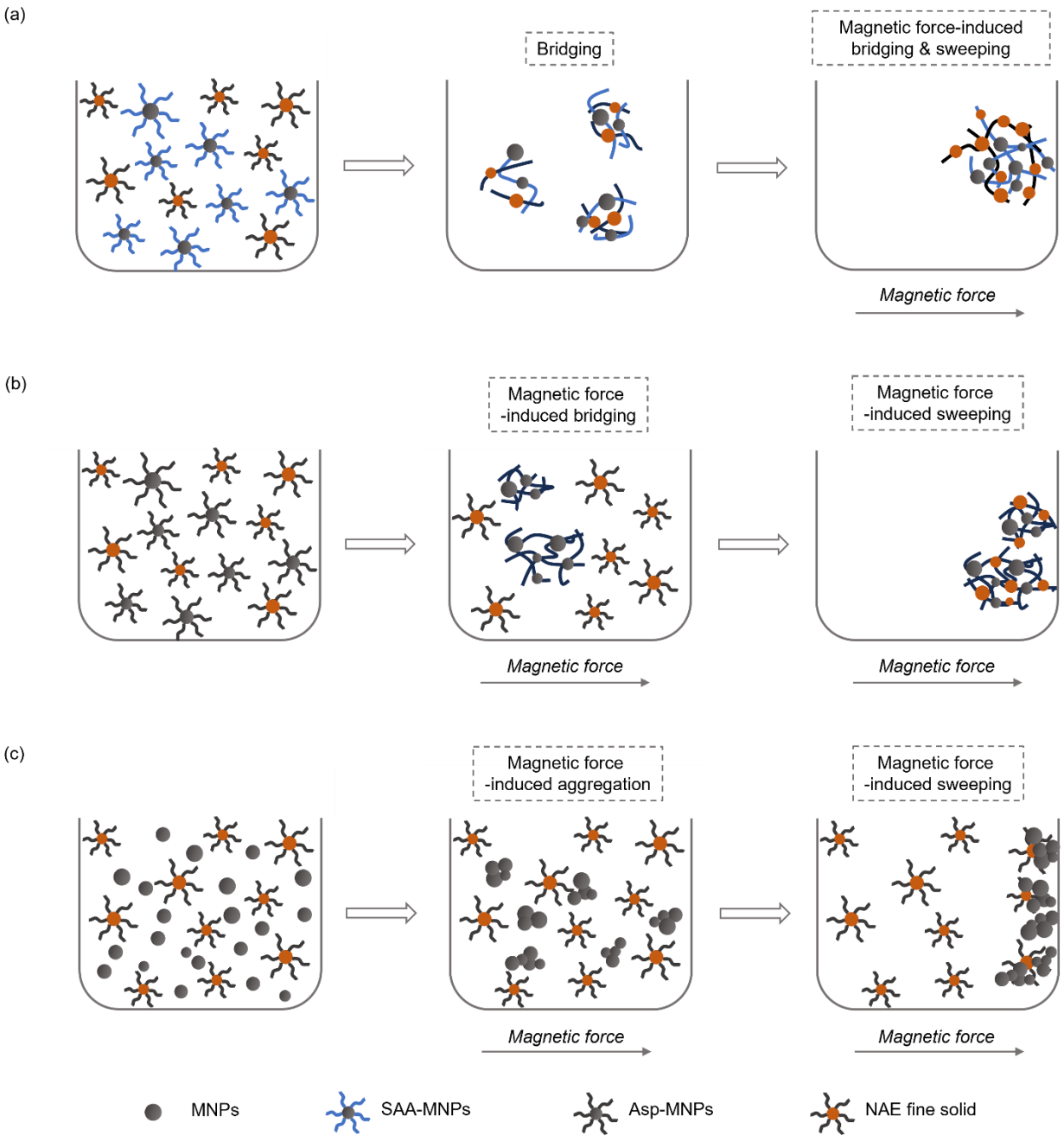

Figure 4.8 Proposed interaction schematics for capturing NAE fine solids in cyclohexane diluted bitumen under magnetic field by using (a) SAA-MNPs; (b) Asp-MNPs; (c) Bare MNPs.

4.3.5.2 Advantages of using surface-modified magnetite nanoparticles for NAE fine solids removal

Different strategies have been developed for NAE fine solids removal in the past decades. Comparatively, the proposed method in this work using surface-modified magnetite nanoparticles to capture and separate fine solids in a magnetic field had several advantages. Firstly, the removal efficiency was high. The SAA-modified and asphaltene-modified magnetite nanoparticles were able to decrease the fine solids content from the initial 0.36 wt % (3600 ppm) to 0.0389 wt% (389 ppm) and 0.057 wt% (570 ppm), respectively, i.e., 89% fine solids removal using SAA-modified MNPs and 84% fine solids removal using asphaltene-modified MNPs in a single stage. Using conventional solid-liquid separation methods such as gravitational sedimentation, centrifugation and membrane filtration following an NAE extraction, only relatively large solid particles could be removed, yielding a solids content of 0.5–15.0 wt% in NAE bitumen products [37-38]. Laboratory studies using water droplets or wetting surfactants during the NAE process, or ionic liquid-assisted solvent extraction could obtain cleaner NAE bitumen products but the fine solids contents were normally still much higher than 0.3 wt% [37,39]. Secondly, the solvent system used in this work was more compatible with commercial operation requirements. In contrast to the low solvent/bitumen ratio employed in the current study (2:1), all previous studies used high solvent/bitumen ratios, typically higher than 10, posing a challenge for alignment with commercial practices that generally require a solvent/bitumen ratio of 2:1 or less. Some NAE fine solids removal methods such as switchable hydrophilicity solvent extraction (SHSE) used high-cost and toxic solvents. Although the fine solids content in bitumen product from SHSE could be reduced to almost zero at high bitumen recovery, the solvents properties excluded the possibility of its application in commercial operations. Finally, magnetic separation made it much easier and more

effective to separate solvent-diluted-bitumen from the magnetic solid adsorbents. Separation of fine solids from the viscous solvent-diluted-bitumen at a low solvent/bitumen ratio of 2:1 using traditional methods such as gravity and centrifuge sedimentation or filtration was time-consuming and ineffective. The magnetite nanoparticles could be recycled and re-used without further surface treatment. During the fine solids removal process, the surfaces of the magnetite nanoparticles would have been modified by an asphaltene coating, and it was shown that the asphaltene coating made the magnetite nanoparticles more efficient in capturing and separating NAE fine solids. To realize the above advantages, further studies are required to optimize the process, such as the quantity of magnetite nanoparticles utilized, and the recycle of magnetite particles and steel wools, and so on.

4.4 Conclusions

In this work, the importance of surface modification of magnetite nanoparticles (MNPs) was demonstrated when using them to help remove fine solids from nonaqueous extracted (NAE) bitumen under an external magnetic field. The bare MNPs showed relatively low removal efficiency (16%). After surface functionalization with stearylamine acetate (SAA), the efficiency was improved to 89%, owing to the bridging effect between the SAA-MNPs and the asphaltene-coated fine solids in NAE bitumen. Coating the MNPs surfaces by asphaltene made the asphaltene-coated MNPs (Asp-MNPs) and the asphaltene-coated fine solids repel each other in cyclohexane-diluted NAE bitumen due to steric repulsion. However, with the asphaltene grafted on the MNPs surfaces, an applied external magnetic field could induce the bridging among the Asp-MNPs, thus realizing the NAE fine solids capture by a sweeping effect. The efficiency of fine solids removal from NAE bitumen by using Asp-MNPs and magnetic separation method was 84%, compared with 16% of the un-modified MNPs.

This work provided useful insights into the design and fabrication of surface-modified magnetite nanoparticles, and the mechanisms behind the hetero-aggregation process between these nanoparticles and the impurity solid particles when subjected to an external magnetic field.

4.5 References

1. Veiseh, O.; Gunn, J. W.; Zhang, M., Design and fabrication of magnetic nanoparticles for targeted drug delivery and imaging. *Advanced Drug Delivery Reviews* **2010,** *62* (3), 284-304.

2. Gloag, L.; Mehdipour, M.; Chen, D.; Tilley, R. D.; Gooding, J. J., Advances in the Application of Magnetic Nanoparticles for Sensing. *Advanced Materials* **2019,** *31* (48), e1904385.

3. Khan, F. S. A.; Mubarak, N. M.; Tan, Y. H.; Karri, R. R.; Khalid, M.; Walvekar, R.; Abdullah, E. C.; Mazari, S. A.; Nizamuddin, S., Magnetic nanoparticles incorporation into different substrates for dyes and heavy metals removal-A Review. *Environmental Science and Pollution Research* **2020,** *27* (35), 43526-43541.

4. Kole, M.; Khandekar, S., Engineering applications of ferrofluids: A review. *Journal of Magnetism and Magnetic Materials* **2021,** *537*, 168222.

5. Déry, J.-P.; Borra, E. F.; Ritcey, A. M., Ethylene Glycol Based Ferrofluid for the Fabrication of Magnetically Deformable Liquid Mirrors. *Chemistry of Materials* **2008,** *20* (20), 6420-6426.

6. Rodríguez-Arco, L.; López-López, M. T.; González-Caballero, F.; Durán, J. D. G., Steric repulsion as a way to achieve the required stability for the preparation of ionic liquid-based ferrofluids. *Journal of Colloid and Interface Science* **2011,** *357* (1), 252-254.

7. Wu, Q.; Cui, Y.; Li, Q.; Sun, J., Effective removal of heavy metals from industrial sludge with the aid of a biodegradable chelating ligand GLDA. *Journal of Hazardous Materials* **2015,** *283*, 748-754.

8. Wang, T.; Ai, S.; Zhou, Y.; Luo, Z.; Dai, C.; Yang, Y.; Zhang, J.; Huang, H.; Luo, S.; Luo, L., Adsorption of agricultural wastewater contaminated with antibiotics, pesticides and toxic metals by functionalized magnetic nanoparticles. *Journal of Environmental Chemical Engineering* **2018,** *6* (5), 6468-6478.

9. Gupta, A. K.; Gupta, M., Synthesis and surface engineering of iron oxide nanoparticles for biomedical applications. *Biomaterials* **2005,** *26* (18), 3995-4021.

10. Natarajan, S. K.; Selvaraj, S., Mesoporous silica nanoparticles: importance of surface modifications and its role in drug delivery. *RSC advances* **2014,** *4* (28), 14328-14334.

11. Zhou, K.; Zhou, X.; Liu, J.; Huang, Z., Application of magnetic nanoparticles in petroleum industry: A review. *Journal of Petroleum Science and Engineering* **2020,** *188*.

12. Yakasai, F.; Jaafar, M. Z.; Bandyopadhyay, S.; Agi, A.; Sidek, M. A., Application of iron oxide nanoparticles in oil recovery – A critical review of the properties, formulation, recent advances and prospects. *Journal of Petroleum Science and Engineering* **2022,** *208*.

13. Vryzas, Z.; Kelessidis, V. C.; Bowman, M. B.; Nalbantian, L.; Zaspalis, V.; Mahmoud, O.; Nasr-El-Din, H. A. In *Smart magnetic drilling fluid with in-situ rheological controllability*

using Fe_3O_4 nanoparticles, SPE Middle East Oil & Gas Show and Conference, OnePetro: **2017.**

14. Vipulanandan, C.; Mohammed, A.; Samuel, R. In *Smart bentonite drilling muds modified with iron oxide nanoparticles and characterized based on the electrical resistivity and rheological properties with varying magnetic field strengths and temperatures*, Offshore Technology Conference, OnePetro: **2017.**

15. Wanna, Y.; Chindaduang, A.; Tumcharern, G.; Phromyothin, D.; Porntheerapat, S.; Nukeaw, J.; Hofmann, H.; Pratontep, S., Efficiency of SPIONs functionalized with polyethylene glycol bis(amine) for heavy metal removal. *Journal of Magnetism and Magnetic Materials* **2016,** *414*, 32-37.

16. Prigiobbe, V.; Ko, S.; Wang, Q.; Huh, C.; Bryant, S. L.; Bennetzen, M. V. In *Magnetic Nanoparticles for Efficient Removal of Oilfield "Contaminants": Modeling of Magnetic Separation and Validation*, SPE International Symposium on Oilfield Chemistry, 2015.

17. Simonsen, G.; Strand, M.; Øye, G., Potential applications of magnetic nanoparticles within separation in the petroleum industry. *Journal of Petroleum Science and Engineering* **2018,** *165*, 488-495.

18. Peng, J.; Liu, Q.; Xu, Z.; Masliyah, J., Novel Magnetic Demulsifier for Water Removal from Diluted Bitumen Emulsion. *Energy & Fuels* **2012,** *26* (5), 2705-2710.

19. He, X.; Liu, Q.; Xu, Z., Cellulose-coated magnetic Janus nanoparticles for dewatering of crude oil emulsions. *Chemical Engineering Science* **2021,** *230*, 116215.

20. Ko, S.; Kim, E. S.; Park, S.; Daigle, H.; Milner, T. E.; Huh, C.; Bennetzen, M. V.; Geremia, G. A. In *Oil Droplet Removal from Produced Water Using Nanoparticles and Their Magnetic Separation*, SPE Annual Technical Conference and Exhibition, **2016**.

21. Setoodeh, N.; Darvishi, P.; Esmaeilzadeh, F., Adsorption of asphaltene from crude oil by applying polythiophene coating on Fe3O4 nanoparticles. *Journal of Dispersion Science and Technology* **2018,** *39* (4), 578-588.

22. Liu, X.; Wang, K.; Tan, X.; Zeng, H.; Liu, Q., Removal of fine solids from bitumen by hetero-aggregation and magnetic separation using surface-modified magnetite nanoparticles. Part 1: Proof of concept. *Separation and Purification Technology* **2022,** *300*.

23. ASTM, ASTM D6560-12, Standard Test Method for Determination of Asphaltenes (heptane insolubles) in Crude Petroleum and Petroleum Products. **2012**.

25. Adams, J. J., Asphaltene adsorption, a literature review. *Energy & Fuels* **2014,** *28* (5), 2831-2856.

25. Wang, S.; Liu, Q.; Tan, X.; Xu, C.; Gray, M. R., Adsorption of asphaltenes on kaolinite as an irreversible process. *Colloids and Surfaces A: Physicochemical and Engineering Aspects* **2016,** *504*, 280-286.

26. ASTM, ASTM D482-07, Standard Test Method for Ash from Petroleum Products. **2013**.

27. Wang, S.; Segin, N.; Wang, K.; Masliyah, J. H.; Xu, Z., Wettability Control Mechanism of Highly Contaminated Hydrophilic Silica/Alumina Surfaces by Ethyl Cellulose. *The Journal of Physical Chemistry C* **2011,** *115* (21), 10576-10587.

28. Wang, S.; Liu, Q.; Tan, X.; Xu, C.; Gray, M. R., Study of Asphaltene Adsorption on Kaolinite by X-ray Photoelectron Spectroscopy and Time-of-Flight Secondary Ion Mass Spectroscopy. *Energy & Fuels* **2013,** *27* (5), 2465-2473.

29. Daraei, P.; Madaeni, S. S.; Ghaemi, N.; Khadivi, M. A.; Astinchap, B.; Moradian, R., Fouling resistant mixed matrix polyethersulfone membranes blended with magnetic nanoparticles: Study of magnetic field induced casting. *Separation and Purification Technology* **2013,** *109*, 111-121.

30. Mahdavian, A. R.; Mirrahimi, M. A.-S., Efficient separation of heavy metal cations by anchoring polyacrylic acid on superparamagnetic magnetite nanoparticles through surface modification. *Chemical Engineering Journal* **2010,** *159* (1), 264-271.

31. Yang, K.; Peng, H.; Wen, Y.; Li, N., Re-examination of characteristic FTIR spectrum of secondary layer in bilayer oleic acid-coated Fe3O4 nanoparticles. *Applied Surface Science* **2010,** *256* (10), 3093-3097.

32. Pérez-Hernández, R.; Mendoza-Anaya, D.; Mondragón-Galicia, G.; Espinosa, M. E.; Rodríguez-Lugo, V.; Lozada, M.; Arenas-Alatorre, J., Microstructural study of asphaltene precipitated with methylene chloride and n-hexane☆. *Fuel* **2003,** *82* (8), 977-982.

33. Jun, Y.W.; Seo, J.W.; Cheon, J., Nanoscaling Laws of Magnetic Nanoparticles and Their Applicabilities in Biomedical Sciences. *Accounts of Chemical Research* **2008,** *41* (2), 179-189.

34. Shen, L.; Qiao, Y.; Guo, Y.; Meng, S.; Yang, G.; Wu, M.; Zhao, J., Facile co-precipitation synthesis of shape-controlled magnetite nanoparticles. *Ceramics International* **2014,** *40* (1, Part B), 1519-1524.

35. Natarajan, A.; Kuznicki, N.; Harbottle, D.; Masliyah, J.; Zeng, H.; & Xu, Z., Understanding mechanisms of asphaltene adsorption from organic solvent on mica. *Langmuir* **2014**, *30* (31), 9370-9377.

36. Liu, J.; Cui, X.; Huang, J.; Xie, L.; Tan, X.; Liu, Q.; Zeng, H., Understanding the stabilization mechanism of bitumen-coated fine solids in organic media from non-aqueous extraction of oil sands. *Fuel* **2019,** *242*, 255-264.

37. Lin, F.; Stoyanov, S.R.; Xu, Y., Recent advances in nonaqueous extraction of bitumen from mineable oil sands: a review. *Organic Process Research & Development* **2017,** *21* (4), 492-510.

38. Zhang, H.; Tan, X.; Liu, Q., Fine solids removal from non-aqueous extraction bitumen: A literature review. *Fuel* **2021,** *288*, 119727.

39. Painter, P.; Williams, P.; Lupinsky, A., Recovery of bitumen from Utah tar sands using ionic liquids. *Energy & Fuels* **2010,** *24* (9), 5081-5088.

CHAPTER 5 Surface-modified Core-Shell Fe_3O_4@SiO_2 Magnetic Beads for RNA Extraction and Detection of SARS-CoV-2 Virus

5.1 Introduction

The extraction of nucleic acids is a crucial prerequisite for any detection and diagnosis that involves nucleic acid testing. This is particularly essential for early disease diagnoses such as cancers or tumors [1-2], the rapid and accurate detection of contagious viral infections such as H7N9 or SARS (severe acute respiratory syndrome) [3-5], on-site environmental monitoring, and ensuring food safety [6-8]. Therefore, achieving rapid and efficient extraction of high-quality nucleic acids is critical to guarantee the accuracy and reliability of the final test results. Conventional nucleic acid extraction methods are time-consuming, inefficient, and expensive [9]. Surface modified magnetic particles, or magnetic beads, have been proven to be a powerful tool for nucleic acid extraction. By combining magnetic properties with specific ligands on the functionalized magnetic beads, it is possible to separate and purify nucleic acids with exceptional efficiency and specificity. In fact, the method of nucleic acid extraction using magnetic beads has become the mainstream of modern molecular biology [10]. Many commercial nucleic acid extraction kits have been developed based on magnetic beads coupled with suitable buffer systems.

Since the appearance of SARS-CoV-2 (COVID-19) coronavirus in 2019, it rapidly spread and evolved into a global pandemic. Magnetic bead-based extraction of SARS-CoV-2 viral RNA has been extensively utilized as an upstream process for reverse transcription-polymerase chain reaction (RT-PCR) tests, which is regarded as the gold standard for rapid diagnosis of SARS-CoV-2 for patients. Studies have also shown that wastewater surveillance of SARS-CoV-2 could provide an early indication of appearance or increased COVID-19 infection in a community [11-12]. However, the pandemic outbreak has led to shortages of various materials and supplies,

particularly in diagnostic and treatment resources for SARS-CoV-2 due to disruptions in manufacturing, transportation, and supply chains caused by lockdown measures, and rapidly increasing demands. As a result, laboratories and research facilities have faced challenges in acquiring essential materials required for rapid SARS-CoV-2 diagnosis and surveillance, which consequently impacted the early detection and management of the pandemic. This issue has been particularly pronounced in Canada, where the supply of SARS-CoV-2 viral RNA extraction kits has relied heavily on foreign suppliers such as Thermo Fisher Scientific Inc. (USA), PerkinElmer Chemagen Technologie GmbH. (Germany), and Promega Corp. (USA). Thus, there has been an urgent need to establish Canadian-based access to magnetic-based reagents for sample preparation and viral RNA extraction.

In the present study, three magnetic beads including Fe_3O_4@SiO_2, Fe_3O_4@SiO_2-NH_2, and Fe_3O_4@SiO_2-COOH, along with the associated buffers were developed, and the protocol established here aimed at extracting SARS-CoV-2 viral RNA. Wastewater sample containing SARS-CoV-2 virus collected from a wastewater plant in Alberta was used for the studies. The human coronavirus strain 229E (hCoV-229E) was spiked into the wastewater sample as a surrogate to study the RNA extraction abilities of the magnetic beads and to optimize the extraction process. Subsequently, the SARS-CoV-2 RNA extraction performances by using the developed magnetic beads and protocols were investigated and compared with that of a commonly used nucleic acid extraction kit (based on magnetic beads method) through RT-PCR assays.

5.2 Materials and methods

5.2.1 Materials and samples

Ferric chloride hexahydrate ($FeCl_3 \cdot 6H_2O$), ferrous chloride tetrahydrate ($FeCl_2 \cdot 4H_2O$), tetraethyl orthosilicate (TEOS), 3-(2-aminoethylamino) propyl trimethoxysilane (AEAPTMS), guanidinium

thiocyanate, sodium citrate tribasic dihydrate, dithiothreitol, and anhydrous isopropanol were purchased from Sigma Aldrich. Ammonium hydroxide, ethanol, urea, UltraPure™ DNase/RNase-free distilled water, and Taqman Fast Virus One-Step RT-PCR Master Mix were purchased from Fisher Scientific. N-[(3-Trimethoxysilyl) propyl] ethylenediamine triacetic acid trisodium salt (TMS-EDTA) was purchased from Oakwood Product Inc. hCoV-229E strain was purchased from ATCC (VR-740, propagated in human fibro blast cell line MRC-5).

For the wastewater sample collection, five hundred milliliters of post-grit raw influent wastewater samples were subsampled from the daily 24-hour composite samples from a wastewater treatment plant located in Alberta, Canada for a period of two weeks in May 2020. Samples were frozen at -20°C upon collection and shipped to the lab every week. Once received, the sample was either immediately processed, or stored at -20°C if not processed within 72 hours. The wastewater sample was processed directly without heat inactivation. The human coronavirus strain 229E (hCoV-229E) spiked samples were tested as surrogates to study the RNA extraction ability of the magnetic beads and to optimize the extraction process. To prepare the samples, 100 µL of cultured hCoV-229E (4.8×10^5 IU/mL) was spiked into either 1 mL of RNase-free water or 100 mL of the wastewater sample.

The wastewater samples (spiked or not spiked with hCoV-229E) needed to be concentrated to increase the viral RNA concentration. First, the pH of the sample was adjusted to 9.6–10 using 5 N NaOH, followed by centrifugation at 4500 g for 10 min to remove solids. The supernatant was collected, and the pH was adjusted to neutral (7–7.5) using 1.2 N HCl. The supernatant was then transferred into a Centricon Plus-70 centrifugal ultrafilter cup (30-kDa MWCO, Millipore) and centrifuged at 3000 g for 10 minutes using a refrigerated centrifuge (Allegra X-15R, Beckman Coulter), following the procedure described in [13]. The filtrate was discarded, and the same

procedure was repeated until all the 100 mL supernatant was filtered. The filtrate collection cup was then removed and replaced with a concentration cup. The entire device was inverted carefully and centrifuged at 800 g for 2 min. The concentrated sample was collected from the concentration cup and adjusted to a final volume of 1 mL with PBS. The concentrated sample was stored at −70°C until later use.

5.2.2 Preparation of surface-modified magnetic beads

5.2.2.1 Synthesis of magnetite core

The synthesis of magnetite nanoparticles followed the co-precipitation route using urea to induce precipitation. Briefly, 11.7 g of $FeCl_3 \cdot 6H_2O$ and 4.3 g of $FeCl_2 \cdot 4H_2O$ were dissolved in 100 mL of distilled water and degassed with high purity nitrogen for 20 min to remove oxygen in the solution. 33.7 g of urea was dissolved in 50 mL of deoxygenated distilled water. Then, the iron chloride solution and the urea solution were transferred into a 250 mL round-bottom flask with reflux condenser and vigorously mixed under constant mechanical stirring. Subsequently, the temperature was raised and maintained at 90-95ºC for 24 hours. A slowly and gradually altered color of the reaction system was observed from orange to black, indicating the formation of co-precipitated magnetite (Fe_3O_4). The resulting black precipitates were collected with a magnet and dispersed in ethanol after rinsing several times with distilled water and ethanol.

5.2.2.2 Preparation of Fe_3O_4@SiO_2 core-shell magnetic beads

SiO_2 shells were encapsulated on the surface of synthesized Fe_3O_4 nanoparticles by the Stöber approach with modification [14]. In a typical process, 150 mL of 75 wt% ethanol aqueous solution containing 5 g Fe_3O_4 nanoparticles was transferred into a 250 mL round-bottom flask, followed by the addition of a pre-determined amount of concentrated ammonia under vigorous stirring.

After 15 minutes of mixing, tetraethyl orthosilicate (TEOS) was added dropwise through a peristaltic pump at a flow rate of 0.5-1.0 mL/min at room temperature. To achieve a uniform and thorough encapsulation of SiO_2, the molar ratio of TEOS to Fe_3O_4 was optimized as 8:1. Afterwards, the reaction system was kept at 50ºC for 6 hours to further promote the hydrolysis of TEOS and the continuing growth of the SiO_2 shell. Finally, the precipitates turned from the initial blackish color to brownish, showing the successful encapsulation of SiO_2 shell. The product was separated from the solution by magnetic-field assisted sedimentation and rinsed with distilled water and ethanol several times, respectively.

5.2.2.3 Preparation of amine- and carboxyl- modified Fe_3O_4@SiO_2 magnetic beads

Two types of functional groups, i.e., amine groups and carboxyl groups, were grafted on the core-shell Fe_3O_4@SiO_2 magnetic beads through surface condensation by different silane coupling agents, following common procedure for silane coupling on silica surface [15-16] but with significant modifications such as solvent type, solvent/water ratio, and temperature, etc. The preparation of Fe_3O_4@SiO_2 core-shell magnetic beads and subsequent modifications are shown in Figure 5.1.

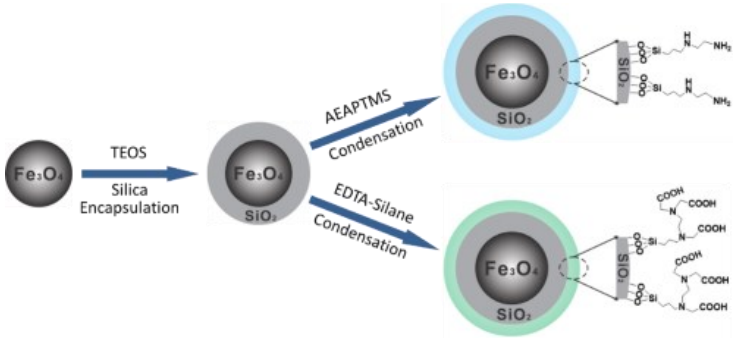

Figure 5.1 Schematic illustration of the Fe_3O_4@SiO_2 magnetic beads synthesis and their subsequent modifications.

For amine modification, typically, 1 g of Fe_3O_4@SiO_2 beads were dispersed in 150 mL of 95 vol% ethanol aqueous solution with vigorous stirring. 10 mL of 3-(2-aminoethylamino) propyl trimethoxysilane (AEAPTMS) were then added dropwise into the suspension. The mixture was continuously refluxed for 24 hours at 110ºC to enhance the covalent bonding of the amino groups to the silica shell. The final beads products were collected with a magnet and rinsed several times with ethanol and water. The final product was designated as Fe_3O_4@SiO_2-NH_2 and dispersed in nuclease-free water for late usage.

The carboxyl modification of the Fe_3O_4@SiO_2 beads surfaces was achieved through surface condensation by EDTA-silane coupling agent. Specifically, a suspension of 1 g Fe_3O_4@SiO_2 beads in 150 mL ethanol aqueous solution (40 vol%) was prepared. 10 mL of N-[(3-trimethoxysilyl) propyl] ethylenediamine triacetic acid trisodium salt (TMS-EDTA) was added dropwise into the suspension under vigorous and continuous stirring. Afterwards, the mixture was continuously refluxed for 24 h at 110ºC. The final product, Fe_3O_4@SiO_2-COOH, was collected with a magnet and dispersed into nuclease-free water after rinsing several times with ethanol and water.

5.2.3 Characterization of prepared magnetic beads

The crystalline structure identification of the powder samples was carried out with a Rigaku Ultima IV X-ray diffraction system with Co Kα radiation (λ = 1.790 Å) source at 38 kV and 38 mA. For the measurements, the samples were loaded into 2 mm deep alumina wells and the data was collected over the 2θ range of 10° to 90° at a scan speed of 2.00º/min and a step size of 0.02º. Data conversion was done with JADE MDI 9.6 software and data interpretation was done using DIFFRAC.EVA software with the 2021 ICDD PDF 4+ and PDF 4+/Organics databases.

Surface modification of nanoparticles was confirmed by Fourier transform infrared (FTIR) spectroscopy using a Bruker ALPHA FT-IR spectrometer. Dried powder samples were used

directly for the measurements using the DRIFTS sampling module. The measurements were carried out at room temperature in a wavelength range from 500 to 4000 cm^{-1}, employing a spectral resolution of 4 cm^{-1} and conducting 128 scans for each measurement. The FTIR data was processed using Bruker OPUS software.

The particle size distribution was estimated using a Malvern Mastersizer 3000 particle size analyzer with Hydro LV wet sample dispersion unit. The prepared magnetic beads in water with a concentration of 10 mg/mL were added dropwise into the dispenser to adjust the laser obscuration to 5%-12%. The measurements were carried out at room temperature and particle size distribution results were the average of five consecutive measurements. For each sample, the particle sizes at 10% (Dn_{10}), 50% (Dn_{50}), and 90% (Dn_{90}) of the number distribution were calculated using the Mastersizer 3000 software.

Magnetic properties were characterized with a Quantum Design MPMS®3 SQUID magnetometer at 300 K within the applied magnetic field range of -2 to 2 Tesla.

5.2.4 RNA extraction using prepared magnetic beads

All three types of magnetic beads were washed thoroughly with RNase-free water, and dispersed in RNase-free water at a concentration of 30 mg/mL for the extraction. The buffer system of RNA extraction contained the following ingredients: lysis/binding buffer (2 M guanidinium thiocyanate, 20 mM sodium citrate, 25 mM dithiothreitol); wash buffer 1 (75 vol% ethanol); wash buffer 2 (RNase-free water), and elution buffer (RNase-free water). To perform the RNA extraction, first, 200 µL of lysis/binding buffer, 200 µL of sample, and 8 µL of glycogen (1 mg/mL) were well mixed in a deep-well plate and incubated for 10 min at room temperature. Then the magnetic beads (40 µL or 80 µL) along with 200 µL isopropanol were added, and the resulting mixture was well mixed and incubated for another 5 min at room temperature. Subsequently, the deep-well plate

was placed on a magnet plate and let stand for about 3 min. Afterwards, the liquid was removed, and the magnetic beads were washed with 75 vol% ethanol twice and RNase-free water twice. Finally, 50 μL of RNase-free water was added to elute the RNA. After a 5-minute incubation, the mixture was placed on the magnet plate, and the supernatant was collected for the RT-PCR tests.

5.2.5 RT-PCR analysis for detecting hCoV-229E and SARS-CoV-2

RT-PCR is widely used in genetic testing and has been recognized as the gold standard for SARS-CoV-2 diagnosis. In RT-PCR, RNA is first converted into its complementary DNA sequence by reverse transcriptase, to synthesize a second strand with DNA polymerase, and finally to generate a double stranded complementary DNA molecule. Then multiple cycles of heating and cooling are performed, facilitating the amplification of the target DNA segment through denaturation, annealing, and extension of DNA sequences in each cycle [17]. If the target is present in the sample, then each cycle of amplification results in a doubling of the amount of target present. The amplified DNA products are detected using fluorescent dyes for quantification of the initial amount of RNA present in the sample. The Ct (cycle threshold) is defined as the number of cycles required for the fluorescent signal to cross the threshold. A lower Ct value indicated a higher initial concentration of the target nucleic acid in the sample, while a higher Ct value suggested a lower initial concentration.

The RT-PCR analysis in this study was carried out using an ABI 7500Fast PCR instrument. For hCoV-229E detection, the RT-PCR system included 5 μL of RNA template, 2.5 μL of 4 × Taqman Fast Virus One-Step RT-PCR Master Mix, 400 nM each of forward and reverse primer along with 200 nM probe in a total volume of 10 μL. Thermal cycling included 50℃ for 5 minutes for reverse transcription reaction, 95℃ for 20 seconds for enzyme activation, and 45 cycles of 95℃ for 3 seconds and 60℃ for 30 seconds for PCR amplification. A threshold of 0.05 was set for data

analysis. The RT-PCR reactions for SARS-CoV-2 N1 and N2 genes detection were identical to those for hCoV-229E, except using 800 nM of the primers for SARS-CoV-2 rather than 400 nM. All the experiments were performed in triplicate and the reported Ct values represent the mean of three test results. Sequences of primers and probes for hCoV-229E, SARS-CoV-2 N1, and SARS-CoV-2 N2 genes are summarized in Table 5.1.

Table 5.1 Primer and probe sequences of target genes for hCoV-229E and SARS-CoV-2.

Target		Sequence (5'-3')
hCoV-229E [18]	Forward primer	TTCCGACGTGCTCGAACTTT
	Reverse primer	CCAACACGGTTGTGACAGTGA
	Probe	FAM-TCCTGAGGTCAATGCA-MGB
N1 gene (2019-nCoV CDC)	Forward primer	GACCCCAAAATCAGCGAAAT
	Reverse primer	TCTGGTTACTGCCAGTTGAATCTG
	Probe	FAM-ACCCCGCATTACGTTTGGTGG ACC-BHQ1
N2 gene (2019-nCoV CDC)	Forward primer	TTACAAACATTGGCCGCAAA
	Reverse primer	GCGCGACATTCCGAAGAA
	Probe	FAM-ACAATTTGCCCCCAGCGCTTC AG-BHQ1

5.3 Results and discussion

5.3.1 Properties of prepared magnetic beads

The crystalline structures of the magnetic nanoparticles were identified with powder X-ray diffraction (XRD) and the XRD pattern is shown in Figure 5.2. For pristine Fe_3O_4, the results are in good agreement with the XRD pattern of Fe_3O_4 nanoparticles reported previously [19]. The characteristic diffraction peaks with 2θ at 21.4°, 35.2°, 41.5°, 50.7°, 63.4°, 67.7°, 74.7° and 89.1° respectively, referring to (111), (220), (311), (400), (422), (511), (440) and (533) facets, were

observed, indicative of a cubic spinel structure of the magnetite nanocrystal clusters [19]. The identical set of characteristic peaks were also clearly observed for Fe_3O_4@SiO_2, Fe_3O_4@SiO_2-NH_2, and Fe_3O_4@SiO_2-COOH, demonstrating the stability of the crystalline phase of Fe_3O_4 nanoparticles during the silica encapsulation and subsequent surface functionalization. Moreover, a broad peak with 2θ around 23° appeared after silica encapsulation, indicating the formation of amorphous silica [20].

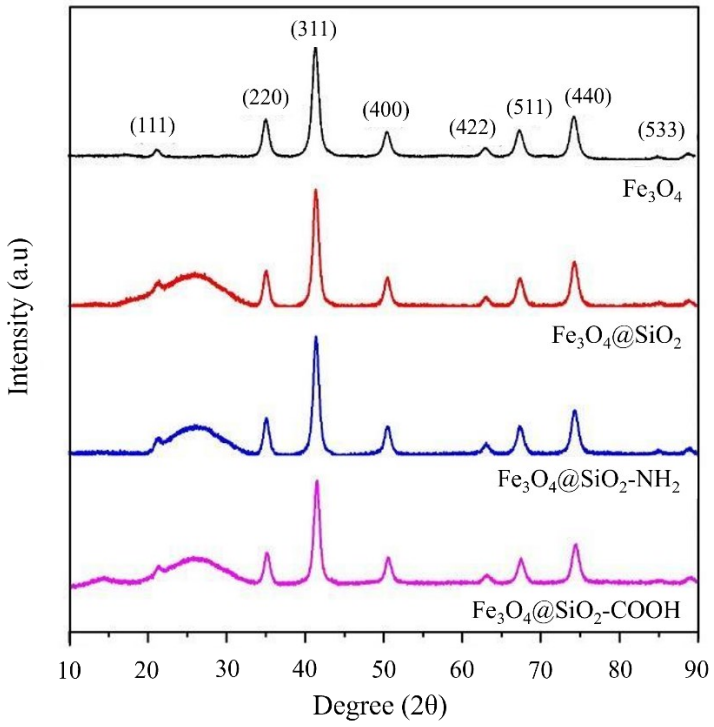

Figure 5.2 XRD patterns of prepared samples.

The FTIR spectra of Fe_3O_4, Fe_3O_4@SiO_2, Fe_3O_4@SiO_2-NH_2 and Fe_3O_4@SiO_2-COOH nanoparticles are compared in Figure 5.3. For all four nanoparticles prepared, an absorption peak at 571 cm^{-1} was observed, corresponding to the characteristic Fe–O vibration from the magnetite phase [21]. This further verified the stability of Fe_3O_4. After the silica encapsulation, Fe_3O_4@SiO_2 showed bands at 1095 cm^{-1}, 946 cm^{-1} and 796 cm^{-1}, corresponding to the stretching vibration of

Si-O-Si, Si-OH and Si-O-Fe respectively [22-23], which reflected the coating of silica on the magnetite surface. As shown in the spectrum of Fe_3O_4@SiO_2-NH_2, successful amino functionalization of the silica layer on Fe_3O_4@SiO_2 was evidenced by the peak at 1459 cm^{-1}, attributed to the bending vibration of N-H in the primary amino group. The peaks at 2983 cm^{-1} and 2857 cm^{-1} were associated with the C-H stretching vibration of the alkane chain in the amino silane [24]. The broad peak at 3400 cm^{-1} could be attributed to the O–H and N–H stretching bands [25]. The weak peaks at 1728 cm^{-1} and 1647 cm^{-1} shown in the Fe_3O_4@SiO_2-COOH spectrum represent the C=O stretch and asymmetric COO^- stretch, respectively, indicating successful condensation between COOH-silane and silica layer [26]. The broad band observed at around 3400 cm^{-1} in the spectrum of Fe_3O_4@SiO_2-COOH could be assigned to the stretching vibration of O–H of the carboxylic group and OH groups on the surface [27].

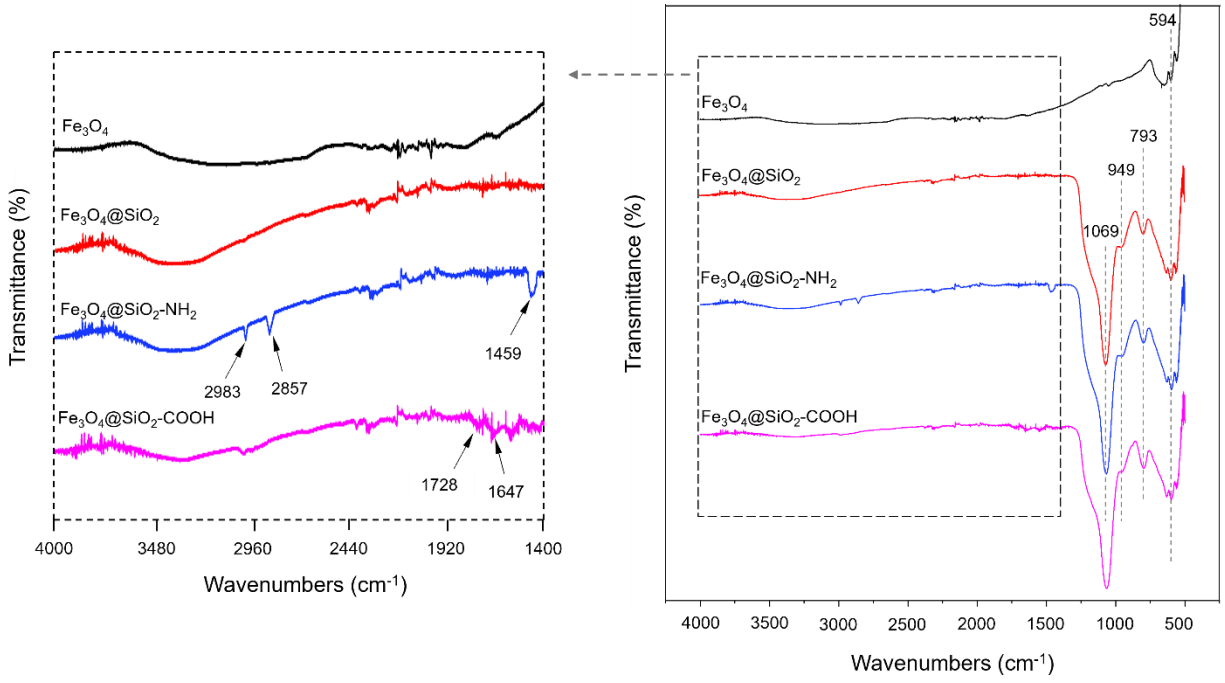

Figure 5.3 FTIR spectra of prepared magnetic beads.

The magnetization curves of the prepared magnetic beads are compared in Figure 5.4. There was no obvious hysteresis in the magnetization for the four tested magnetic beads. Neither coercivity nor remanence was observed, suggesting that all nanoparticles obtain the peculiarity of superparamagnetism. The saturation magnetization values were measured to be 73 $A \cdot m^2/kg$ for Fe_3O_4, 26 $A \cdot m^2/kg$ for $Fe_3O_4@SiO_2$, 25 $A \cdot m^2/kg$ for $Fe_3O_4@SiO_2$-NH_2 and 26 $A \cdot m^2/kg$ for $Fe_3O_4@SiO_2$-COOH. Although the saturation magnetization decreased after the silica encapsulation on the surface of the Fe_3O_4 core, the magnetic beads could be highly effectively captured and separated from the suspension using a magnetic field.

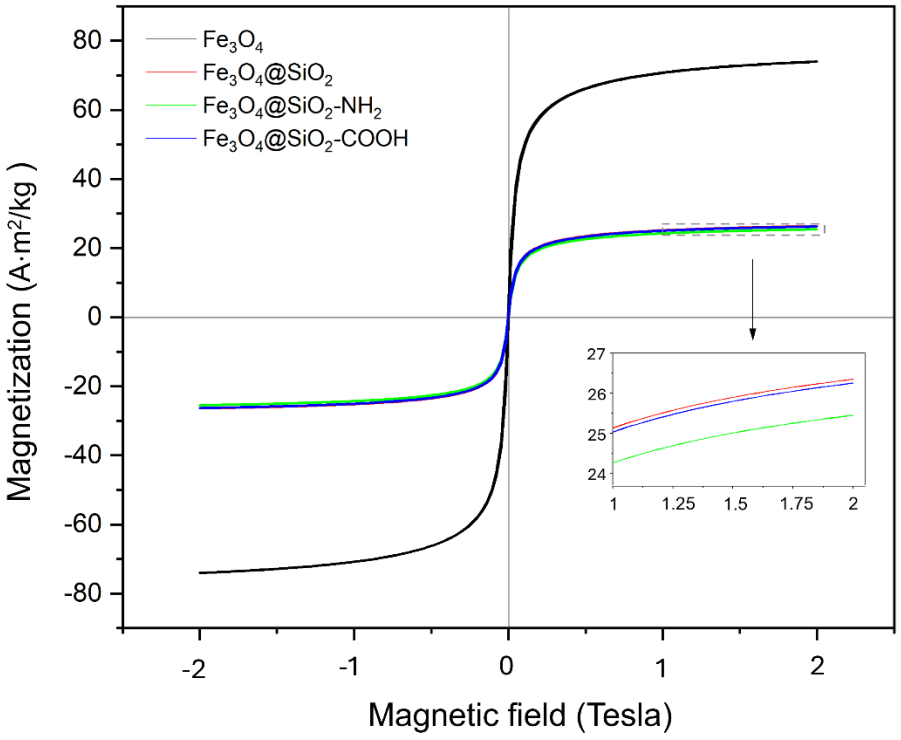

Figure 5.4 Magnetization curves of prepared samples.

The DLS particle size distributions of the prepared samples are illustrated in Figure 5.5 and compared with the distribution of magnetic beads from a commercial nucleic acid extraction kit (which was also employed for RNA extractions in this study). All the four samples exhibited a

similar size range, with median sizes measuring 0.89 µm for Fe_3O_4@SiO_2, 0.77 µm for Fe_3O_4@SiO_2-NH_2, 0.92 µm for Fe_3O_4@SiO_2-COOH, and 0.79 µm for the commercial magnetic beads.

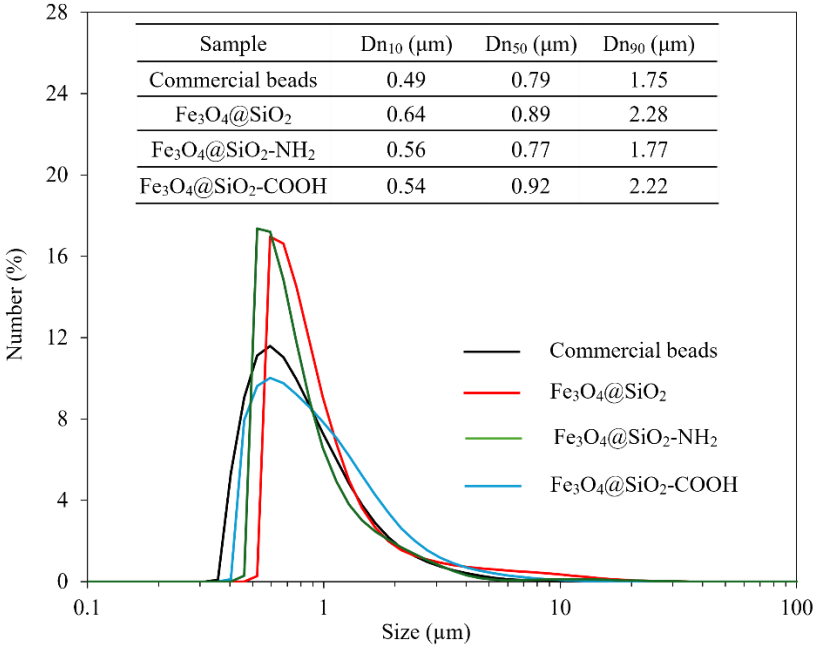

Figure 5.5 Particle size distribution of prepared samples.

5.3.2 RT-PCR amplification results

The prepared magnetic beads, i.e., Fe_3O_4@SiO_2, Fe_3O_4@SiO_2-NH_2, and Fe_3O_4@SiO_2-COOH, were used for the extraction of hCoV-229E viral RNA from the prepared hCoV-229E-spiked RNase-free water sample and hCoV-229E-spiked wastewater sample, respectively. A widely used commercial nucleic acid extraction kit based on the magnetic beads method was also employed for the same extractions following the manufacturer's instructions. RT-PCR amplification results for hCoV-229E from the elutes were compared to evaluate the extraction performances. Two different volumes of the magnetic beads, i.e., 40 µL and 80 µL (30 mg/mL), were added in a single extraction to examine the effect of magnetic beads quantity used in the extraction process. As

shown in Figure 5.6 (a), when extracting hCoV-229E viral RNA from hCoV-229E-spiked RNase-free water sample, for both magnetic beads input amounts, the Fe_3O_4@SiO_2 and Fe_3O_4@SiO_2-COOH have shown comparable extraction performances with the commercial kit, indicated by the very close Ct values from the RT-PCR amplifications. However, the Fe_3O_4@SiO_2-NH_2 showed much lower extraction abilities, judging by the notably higher Ct values for Fe_3O_4@SiO_2-NH_2 (35.7 for 40 µL input magnetic beads and 35.6 for 80 µL input magnetic beads) compared to the Ct value for the commercial kit (23.4). When the input magnetic beads amount was increased from 40 µL to 80 µL, there were minimal changes in the performances of all three types of magnetic beads for hCoV-229E RNA extraction from hCoV-229E-spiked RNase-free water samples, with the Ct values changing from 23.5 to 23.6, 35.7 to 35.6, and 23.3 to 23.6 for Fe_3O_4@SiO_2, Fe_3O_4@SiO_2-NH_2, and Fe_3O_4@SiO_2-COOH, respectively. However, when extracting hCoV-229E RNA from hCoV-229E-spiked wastewater samples using each type of magnetic beads (as illustrated in Figure 5.6 (b)), a larger difference in Ct values was observed between the extractions conducted with 40 µL and 80 µL of added magnetic beads. For each type of magnetic beads, the increase of magnetic beads amounts from 40 µL to 80 µL resulted in a higher Ct value, indicating a decrease in extraction efficiency. Particularly for Fe_3O_4@SiO_2-COOH, the Ct value for extraction with 80 µL magnetic beads was increased by 1.0 compared to the extraction with 40 µL magnetic beads added. In other words, the concentration of hCoV-229E in the eluate extracted with 40 µL of magnetic Fe_3O_4@SiO_2-COOH was twice that in the eluate extracted with 80 µL of the beads. This increase in Ct values could possibly be attributed to the increased binding of non-target molecules on magnetic beads due to a higher magnetic beads amount. Compared with Fe_3O_4@SiO_2 and Fe_3O_4@SiO_2-NH_2, Fe_3O_4@SiO_2-COOH showed a higher extraction ability of hCoV-229E RNA from the hCoV-229E-spiked wastewater sample. For instance, for the extraction

with 40 µL input of magnetic beads, the Ct value was 24.3 for the Fe_3O_4@SiO_2-COOH compared with 25.7 and 27.9 for Fe_3O_4@SiO_2 and Fe_3O_4@SiO_2-NH_2, respectively. This Ct value was lower than that obtained by using the commercial kit for the extraction, indicating a higher extraction efficiency of hCoV-229E from the hCoV-229E-spiked wastewater sample by using Fe_3O_4@SiO_2-COOH than using the commercial kit.

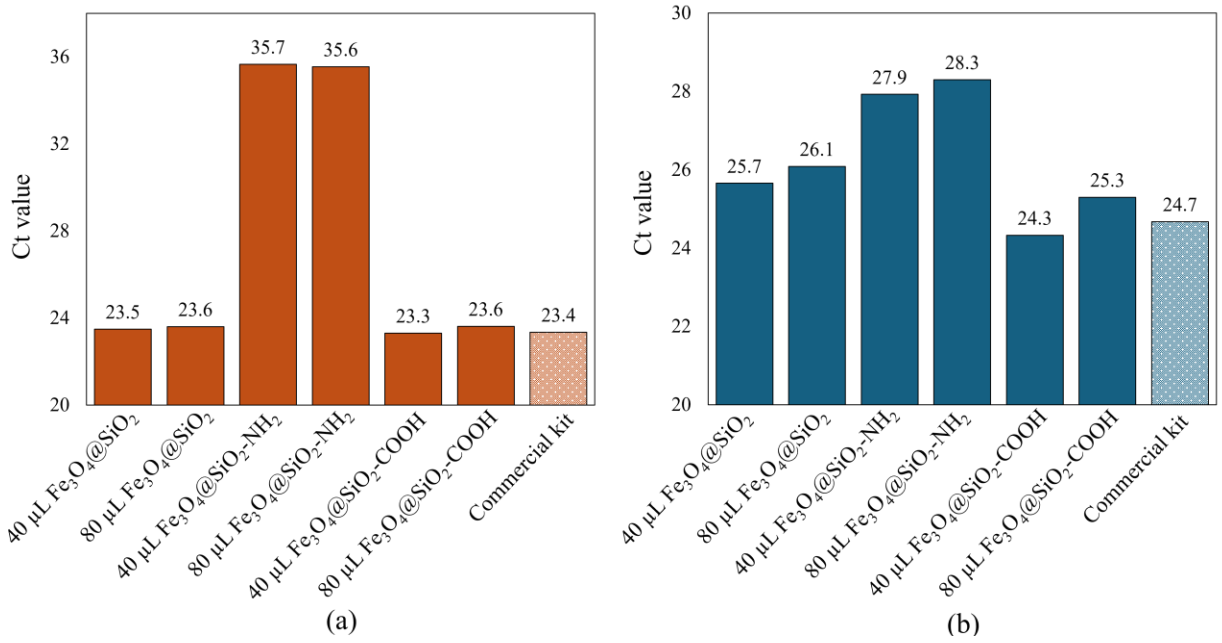

Figure 5.6 RT-PCR amplification results for hCoV-229E. (a) RT-PCR templates extracted from hCoV-229E-spiked RNase-free water samples using prepared magnetic beads; (b) RT-PCR templates extracted from hCoV-229E-spiked wastewater samples using prepared magnetic beads.

Fe_3O_4@SiO_2, Fe_3O_4@SiO_2-NH_2, and Fe_3O_4@SiO_2-COOH were employed for SARS-CoV-2 viral RNA extraction from the concentrated wastewater sample. For each extraction, the input magnetic beads amount was 40 µL. The extraction performances were evaluated by conducting RT-PCR amplifications targeting both the SARS-CoV-2 N1 and N2 genes using elutes obtained from the extraction process, and the results were compared with the extraction performance of the same commercial kit used above. As illustrated in Figure 5.7, for SARS-CoV-2 N1 gene detection, the

Ct value of 29.5 for elute extracted by Fe_3O_4@SiO_2-COOH was the lowest among the Ct values for elutes extracted by the three beads samples, compared with the values of 29.9 and 34.3 for Fe_3O_4@SiO_2 and Fe_3O_4@SiO_2-NH_2, respectively. For SARS-CoV-2 N2 gene detection, the Ct value for the sample extracted with Fe_3O_4@SiO_2 (30.0) was nearly the same as that for the sample extracted with Fe_3O_4@SiO_2-COOH (30.1), but much lower than the Ct value for the sample extracted with Fe_3O_4@SiO_2-NH_2 (34.6). The amplification results for SARS-CoV-2 N1 gene detection and SARS-CoV-2 N2 detection were consistent with each other. It was also found that the Ct values for extracted samples from Fe_3O_4@SiO_2 and Fe_3O_4@SiO_2-COOH were comparable to the Ct values obtained by the commercial kit, for both the SARS-CoV-2 N1 gene and SARS-CoV-2 N2 gene detection. For instance, for Fe_3O_4@SiO_2-COOH, the Ct values were 29.5 and 30.1 for SARS-CoV-2 N1 gene and N2 gene, respectively, compared to 29.3 and 29.8 for the commercial kit. The results showed that Fe_3O_4@SiO_2, Fe_3O_4@SiO_2-COOH and commercial beads exhibited comparable extraction abilities of SARS-CoV-2 viral RNA from the concentrated wastewater sample. The Fe_3O_4@SiO_2-NH_2 beads, however, demonstrated much lower extraction ability for SARS-CoV-2 viral RNA from the same sample.

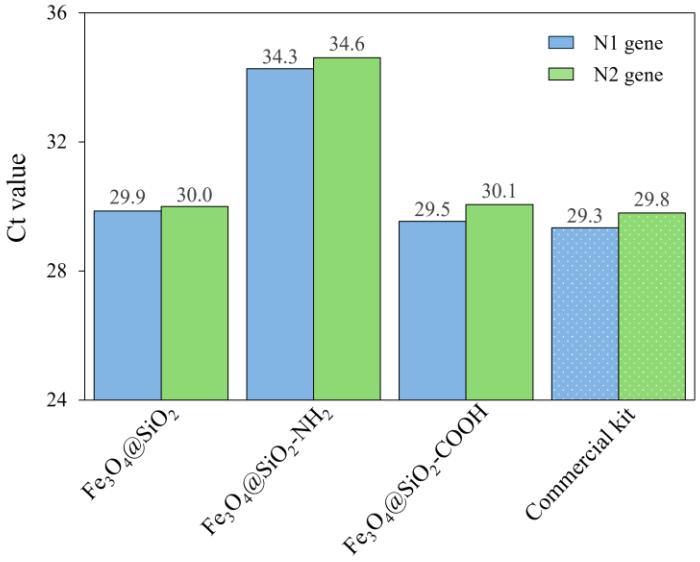

Figure 5.7 RT-PCR amplification results for SARS-CoV-2 N1 and N2 genes. RT-PCR templates were extracted from concentrated wastewater samples using the prepared magnetic beads.

5.4 Conclusions

In this work, three core-shell magnetic beads i.e., Fe_3O_4@SiO_2, Fe_3O_4@SiO_2-NH_2, and Fe_3O_4@SiO_2-COOH, along with the associated buffers were developed for the SARS-CoV-2 RNA extraction from wastewater. By using the developed protocol, both Fe_3O_4@SiO_2 and Fe_3O_4@SiO_2-COOH demonstrated high hCoV-229E extraction efficiency from hCoV-229E-spiked wastewater samples, with Fe_3O_4@SiO_2-COOH exhibiting superior extraction efficiency over a commercial kit. Additionally, following the developed protocol, Fe_3O_4@SiO_2 and Fe_3O_4@SiO_2-COOH showed comparable abilities as the commercial kit in extracting SARS-CoV-2 viral RNA from wastewater. However, Fe_3O_4@SiO_2-NH_2 showed significantly lower efficiency for hCoV-229E or SARS-CoV-2 viral RNA extraction from the same sample.

The developed Fe_3O_4@SiO_2 and Fe_3O_4@SiO_2-COOH magnetic beads, as well as the buffer system and the extraction protocol have shown significant potential in SARS-CoV-2 RNA extraction. This

presented a valuable tool in public health surveillance of COVID-19 and could offer support in case of shortages of commercial nucleic acid extraction kits in Canada.

5.5 References

1. Bonin, S.; Stanta, G., Nucleic acid extraction methods from fixed and paraffin-embedded tissues in cancer diagnostics. *Expert Review of Molecular Diagnostics* **2013,** *13* (3), 271-282.

2. Nana-Sinkam, S.P.; Croce, C.M., Clinical applications for microRNAs in cancer. *Clinical Pharmacology & Therapeutics* **2013,** *93* (1), 98-104.

3. Lau, L.T.; Fung, Y.W.W.; Yu, A.C.H., Detection of animal viruses using nucleic acid sequence-based amplification (NASBA). *Developments in Biologicals* **2006,** *126*, 7.

4. Yu, C.Y.; Chan, K.G.; Yean, C.Y.; Ang, G.Y., Nucleic acid-based diagnostic tests for the detection SARS-CoV-2: an update. *Diagnostics* **2021,** *11* (1), 53.

5. Courtney, S.J.; Stromberg, Z.R.; Kubicek-Sutherland, J.Z., Nucleic acid-based sensing techniques for diagnostics and surveillance of influenza. *Biosensors* **2021,** *11* (2), 47.

6. Carew, M.E.; Pettigrove, V.J.; Metzeling, L.; Hoffmann, A.A., Environmental monitoring using next generation sequencing: rapid identification of macroinvertebrate bioindicator species. *Frontiers in Zoology* **2013,** *10*, 1-15.

7. Ahmed, W.; Angel, N.; Edson, J.; Bibby, K.; Bivins, A.; O'Brien, J.W.; Choi, P.M.; Kitajima, M.; Simpson, S.L.; Li, J.; Tscharke, B., First confirmed detection of SARS-CoV-2 in untreated wastewater in Australia: a proof of concept for the wastewater surveillance of COVID-19 in the community. *Science of the Total Environment* **2020,** *728*, 138764.

8. Ceuppens, S.; Li, D.; Uyttendaele, M.; Renault, P.; Ross, P.; Ranst, M.V.; Cocolin, L.; Donaghy, J., Molecular methods in food safety microbiology: interpretation and implications of nucleic acid detection. *Comprehensive Reviews in Food Science and Food Safety* **2014,** *13* (4), 551-577.

9. Shin, J.H., Nucleic acid extraction and enrichment. *Advanced Techniques in Diagnostic Microbiology: Volume 1: Techniques* **2018,** 273-292.

10. Tang, C.; He, Z.; Liu, H.; Xu, Y.; Huang, H.; Yang, G.; Xiao, Z.; Li, S.; Liu, H.; Deng, Y.; Chen, Z., Application of magnetic nanoparticles in nucleic acid detection. *Journal of Nanobiotechnology* **2020,** *18* (1), 1-19.

11. Ahmed, W.; Angel, N.; Edson, J.; Bibby, K.; Bivins, A.; O'Brien, J.W.; Choi, P.M.; Kitajima, M.; Simpson, S.L.; Li, J.; Tscharke, B., First confirmed detection of SARS-CoV-2 in untreated wastewater in Australia: a proof of concept for the wastewater surveillance of COVID-19 in the community. *Science of the Total Environment* **2020,** *728*, 138764.

12. Weidhaas, J.; Aanderud, Z.T.; Roper, D.K.; VanDerslice, J.; Gaddis, E.B.; Ostermiller, J.; Hoffman, K.; Jamal, R.; Heck, P.; Zhang, Y.; Torgersen, K., Correlation of SARS-CoV-2 RNA in wastewater with COVID-19 disease burden in sewersheds. *Science of The Total Environment* **2021,** *775*, 145790.

13. Qiu, Y.; Lee, B.E.; Ruecker, N.J.; Neumann, N.; Ashbolt, N.; Pang, X., A one-step centrifugal ultrafiltration method to concentrate enteric viruses from wastewater. *Journal of Virological Methods* **2016,** *237*, 50-153.

14. Stöber, W.; Fink, A.; Bohn, E., Controlled growth of monodisperse silica spheres in the micron size range. *Journal of Colloid and Interface Science* **1968,** *26* (1), 62-69.

15. Fang, G.; Chen, H.; Zhang, Y.; Chen, A., Immobilization of pectinase onto Fe_3O_4@ SiO_2–NH_2 and its activity and stability. *International Journal of Biological Macromolecules* **2016,** *88*, 189-195.

16. Liu, Y.; Lou, Z.; Sun, Y.; Zhou, X.; Baig, S.A.; Xu, X., Influence of complexing agent on the removal of Pb (II) from aqueous solutions by modified mesoporous SiO_2. *Microporous and Mesoporous Materials* **2017,** *246*, 1-13.

17. Bachman, J., Reverse-transcription PCR (rt-PCR). *Methods in Enzymology* **2013,** *530*, 67-74.

18. Vijgen, L.; Keyaerts, E.; Moes, E.; Maes, P.; Duson, G.; Van Ranst, M.; Development of one-step, real-time, quantitative reverse transcriptase PCR assays for absolute quantitation of human coronaviruses OC43 and 229E. *Journal of Clinical Microbiology* **2005,** *43* (11), 5452–5456.

19. Yang, Z.; Qian, K.; Lv, J.; Yan, W.; Liu, J.; Ai, J.; Zhang, Y.; Guo, T.; Zhou, X.; Xu, S.; Guo, Z., Encapsulation of Fe3O4 nanoparticles into N, S co-doped graphene sheets with greatly enhanced electrochemical performance. *Scientific Reports* **2016,** *6* (1), 27957.

20. Kurnaz Yetim, N.; Kurşun Baysak, F.; Koç, M.M.; Nartop, D., Characterization of magnetic Fe_3O_4@SiO_2 nanoparticles with fluorescent properties for potential multipurpose imaging and theranostic applications. *Journal of Materials Science: Materials in Electronics* **2020,** *31* (20), 18278-18288.

21. Ruparelia, N.; Soni, U.; Desai, R. P.; Ray, A., Silica anchored colloidal suspension of magnetite nanorods. *Journal of Solid State Chemistry* **2020,** *290*, 121574.

22. Xie, X.; Chen, L.; Pan, X.; Wang, S., Synthesis of magnetic molecularly imprinted polymers by reversible addition fragmentation chain transfer strategy and its application in the Sudan dyes residue analysis. *Journal of Chromatography A* **2015,** *1405*, 32-39.

23. Doelsch, E.; Stone, W.E.; Petit, S.; Masion, A.; Rose, J.; Bottero, J.Y.; Nahon, D., Speciation and crystal chemistry of Fe (III) chloride hydrolyzed in the presence of SiO_4 ligands. 2. Characterization of Si−Fe aggregates by FTIR and ^{29}Si solid-state NMR. *Langmuir* **2001,** *17* (5), 1399-1405.

24. Sarker, M.Z.; Rahman, M.M.; Minami, H.; Suzuki, T.; Ahmad, H., Amine functional silica–supported bimetallic Cu-Ni nanocatalyst and investigation of some typical reductions of aromatic nitro-substituents. *Colloid and Polymer Science* **2022,** 1-18.

25. Hou, S.; Li, X.; Wang, H.; Wang, M.; Zhang, Y.; Chi, Y.; Zhao, Z., Synthesis of core–shell structured magnetic mesoporous silica microspheres with accessible carboxyl functionalized surfaces and radially oriented large mesopores as adsorbents for the removal of heavy metal ions. *RSC Advances* **2017,** *7* (82), 51993-52000.

26. Lounasvuori, M.M.; Rosillo-Lopez, M.; Salzmann, C.G.; Caruana, D.J.; Holt, K.B., The influence of acidic edge groups on the electrochemical performance of graphene nanoflakes. *Journal of Electroanalytical Chemistry* **2015,** *753*, 28-34.

27. Kheilkordi, Z.; Mohammadi Ziarani, G.; Mohajer, F.; Badiei, A.; Varma, R.S., Synthesis and Application of Novel Nanomagnetic Catalyst Fe3O4@ SiO2@ Pr–Gu–Cr–COOH in the Green Multi-component Synthesis of 1-(Benzothiazolylamino) methyl-2-naphthol. *Journal of Inorganic and Organometallic Polymers and Materials* **2023,** *33* (4), 1028-1036.

CHAPTER 6 Conclusions and Future Work

6.1 Summary and conclusions

Surface-modified magnetic nanoparticles (MNPs) have demonstrated excellent performance in the selective adsorption of metal ions, organic components, biomolecules, etc., while their magnetic core facilitates rapid separation under an external magnetic field, making them a promising solution for challenging and demanding separation problems. This thesis research investigated the potential and significance of employing surface-modified MNPs in two specific domains: (1) the removal of fine mineral solids from non-aqueous extracted (NAE) bitumen, and (2) the extraction and purification of nucleic acids from biomatrix. The research hypothesis was that the specific modification of MNPs enhanced their affinity to the targets, i.e., NAE fine solids or viral RNA, thereby facilitating the hetero-aggregation between the MNPs and the targets. Subsequently, the formed aggregates could be isolated via magnetic separation to obtain the purified products.

In the oil sands industry, relatively high fine solids content, on the order of 300 ppm (0.03 wt%), in produced bitumen is one of the hurdles preventing NAE process from being used in commercial operations. Different strategies have been investigated to separate fine solids from NAE bitumen, yet they all suffer from severe handicaps such as the inability to meet the refinery's requirement with respect to fine solid content, the high costs/toxicity associated with the solvents utilized, and high solvent-to-bitumen ratio of 10:1 or higher that does not comply with industry practices which require the ratio to be 2:1 or less. The method of using surface-modified MNPs for NAE fine solids capture followed by magnetic separation was investigated in this work. Stearylamine acetate-modified MNPs (SAA-MNPs) were synthesized, characterized, and their performance in separating fine mineral solids from NAE bitumen was quantitatively evaluated and compared with un-modified MNPs. The feasibility of employing asphaltene, a component of bitumen, as a

modifier for MNPs in the proposed separation process was also examined. Furthermore, the impact of surface modification on the MNPs in their interactions with NAE fine solids was investigated. The main conclusions of this portion of the work were as follows:

- Scanning electron microscope images and hetero-aggregation test results showed that when mixing the prepared SAA-MNPs with cyclohexane-diluted bitumen, hetero-aggregation occurred between the modified MNPs and the NAE fine solids. Through a subsequent magnetic field-assisted sedimentation and filtration process, the fine solids could be effectively removed. At a solvent (cyclohexane) to NAE bitumen weight ratio of 2:1, and magnetic nanoparticles to NAE bitumen weight ratio of 1:4, the fine solids content in the NAE bitumen was reduced from 3600 ppm to 389 ppm (89% removal) using the SAA-MNPs. With no surface modification, the MNPs were only able to reduce the fine solid content to 3000 ppm (16% removal).
- Cyclohexane-diluted bitumen could modify MNPs to improve their fine solids capture and removal abilities, enabling the re-use of the MNPs. With asphaltene modification, Asp-MNPs reduced the fine solids content in NAE bitumen from 3600 ppm to 570 ppm (84% removal). Regeneration studies showed that after one cycle of use, the surfaces of the MNPs underwent modification by bitumen components (presumably asphaltene), significantly improving their fine-solids-removal capacity and lowering fine solid content to 763 ppm (79% removal). The recycled SAA-MNPs and Asp-MNPs lowered the fine solids content to 417 ppm (88% removal) and 587 ppm (84% removal), respectively.
- Surface modification of MNPs played a crucial role in their application for removing fine solids from NAE bitumen through the hetero-aggregation and magnetic separation method. The SAA modification enhanced the adhesion between the Fe_3O_4 and the (asphaltene-

coated) NAE fine solids due to the bridging effect, enabling the formation of hetero-aggregates between SAA-MNPs and NAE fine solids, and improving the efficiency of fine solids removal.

- Despite the steric repulsion between Asp-MNPs and asphaltene-coated NAE fine solids, an applied magnetic field enabled the formation of network-structured aggregates of Asp-MNPs. This facilitated the capture of NAE fine solids through a sweeping effect of these network-structured Asp-MNP aggregates with extending "asphaltene brushes". Without surface modification by asphaltene, the adhesion between bare MNPs and NAE fine solids was weak, and the magnetic field-induced MNP aggregates were not in network structure. Consequently, their efficiency in capturing and removing NAE fine solids was significantly lower compared to MNPs modified with SAA or asphaltene.

Magnetic bead-based extraction of SARS-CoV-2 viral RNA has been utilized as an upstream process for reverse transcription polymerase chain reaction (RT-PCR) tests for early detection and rapid diagnosis of SARS-CoV-2 during the pandemic. However, the rapid pandemic outbreak has led to a severe shortage of the magnetic beads-based nucleic acid extraction kit, impacting its surveillance and management. In this study, surface-modified MNPs and associated buffers were developed for the extraction of SARS-CoV-2 viral RNA. A wastewater sample containing the SARS-CoV-2 virus collected from a wastewater plant in Alberta was used for the extraction studies. Firstly, the human coronavirus strain 229E (hCoV-229E) was spiked into the wastewater sample as a surrogate to assess the RNA extraction capabilities of the magnetic beads and to optimize the extraction process. Subsequently, the efficiency of SARS-CoV-2 RNA extraction using the developed magnetic beads, buffer system, and

protocol was evaluated and compared with that of a commercial magnetic beads nucleic acid extraction kit through RT-PCR analysis. The main conclusion of this portion of work was:

- By using the developed protocol, both the core-shell Fe_3O_4@SiO_2 and Fe_3O_4@SiO_2-COOH demonstrated high hCoV-229E extraction efficiency from hCoV-229E-spiked wastewater samples, with Fe_3O_4@SiO_2-COOH exhibiting superior extraction efficiency over the commercial kit. Additionally, following the developed protocol, the core-shell Fe_3O_4@SiO_2 and Fe_3O_4@SiO_2-COOH showed comparable abilities as the commercial kit in extracting SARS-CoV-2 viral RNA from wastewater. On the other hand, the amine-functionalized core-shell Fe_3O_4@SiO_2-NH_2 showed significantly lower efficiency for hCoV-229E or SARS-CoV-2 viral RNA extraction from the same sample.

6.2 Original contributions

(1) For the first time, a novel strategy using surface-modified magnetic nanoparticles (MNPs) to remove fine solids from non-aqueous extracted (NAE) bitumen products through hetero-aggregation and magnetic separation was formulated. The effectiveness of the strategy has been demonstrated using stearylamine acetate-modified magnetite nanoparticles (SAA-MNPs) for fine solids capture and removal from an NAE bitumen sample. The results showed that a high efficiency of 89% removal in a single stage has been achieved. It was further showed that asphaltene coating, inevitable when the MNPs were submerged in solvent-diluted bitumen, enhanced Asp-MNP's fine solids capture and removal abilities, therefore indicating that asphaltene coating on the MNPs was not a detriment but an advantage because the MNPs could be reused. This was confirmed in the MNP regeneration and reuse studies. Furthermore, to the best of the author's knowledge, this was the only work that could achieve 89% fine solid removal efficiency in a single stage at a cyclohexane/bitumen ratio of 2:1. All reported work in the open literature had

to resort to much higher cyclohexane/bitumen ratios (typically exceeding 10) which were impractical for commercial applications. At the low solvent/bitumen ratio of 2:1, all the reported processes ceased to function.

(2) New mechanisms of how magnetic sorbents captured and removed target species under an external magnetic field was discovered. It was shown that the capture and removal of NAE fine solids by modified MNPs was based on two separate mechanisms: (a) the increased adhesion between modified MNPs and NAE fine solids through bridging effect made available by the introduced functional groups, such as stearylamine, (b) the formation of magnetic aggregates by an applied magnetic field, which captured NAE fine solids only when an adsorption layer was present on the MNP surface acting as polymer brushes. Either or both of the two mechanisms could contribute to the capture of NAE fine solids by the surface-modified MNPs. In this context, the SAA-MNPs functioned with both mechanisms, while the Asp-MNPs functioned only through the second mechanism. In fact, coating the MNPs by asphaltene created a repulsive force to NAE fine solids (which were also coated by asphaltene). However, the adsorbed asphaltene acted as polymer brushes, so that the magnetic field induced magnetic aggregates of the Asp-MNPs could capture NAE fine solids. The bare MNPs could not capture the fine solids although they also formed magnetic aggregates. The study provided insights into the significant advantages of magnetic sorbents in separation processes, i.e., even when there is no affinity between the magnetic sorbents and the target species, the magnetic sorbents could still remove the target provided that the magnetic sorbents have surface polymer brushes and that an external magnetic field is applied. This is a phenomenon that would not be possible with non-magnetic sorbents.

(3) An effective SARS-CoV-2 RNA extraction kit based on magnetic beads method, including core-shell magnetic beads Fe_3O_4@SiO_2 and Fe_3O_4@SiO_2-COOH, buffer system, and extraction

protocol was developed. The study presented a valuable tool that could be used in the public health system for early detection, diagnosis, and surveillance, and could offer domestic support to make up for the shortages of commercial RNA extraction kits. The study also provided insights into the design and development of magnetic beads intended for nucleic acid extraction.

6.3 Recommendations for future work

(1) Although the proposed method for fine solids removal has been demonstrated to be effective, further studies are required to optimize the separation process. Firstly, parameters such as the quantity of the surface-modified magnetite nanoparticles, the recycle steps of the magnetic nanoparticles, and the steel wools can be optimized to lower the cost or simplify the process. Besides, NAE bitumen samples with different initial fine solids concentrations can be tested to further evaluate the proposed method. Secondly, further study could be focused on achieving the goal of removing fine solids to less than 300 ppm in NAE bitumen, which is the refinery requirement for the fine solids content in NAE bitumen products. This may be achieved by multiple stages of separation.

(2) Interactions between nucleic acids and different surfaces can be studied to understand the affinity of different beads (Fe_3O_4@SiO_2, Fe_3O_4@SiO_2-COOH, and Fe_3O_4@SiO_2-NH_2) to nucleic acids, and to learn the underlying mechanisms of nucleic acid extraction by using the prepared magnetic beads.

(3) To further evaluate the extraction performance of the developed magnetic beads-based nucleic acid extraction kit (with Fe_3O_4@SiO_2 or Fe_3O_4@SiO_2-COOH magnetic beads) for SARS-CoV-2 RNA extraction, and to assess the feasibility of using the developed kit in early detection and

surveillance of public health systems. Samples obtained from patients diagnosed with SARS-CoV-2 may be utilized for the extraction.

(4) Magnetic sorbents in other advanced separation and purification applications can be explored, such as lithium extraction from brines, base metal, and rare earth metal recovery and separation.

Bibliography

Qu, X.; Alvarez, P.J.; Li, Q., Applications of nanotechnology in water and wastewater treatment. *Water Research* **2013,** *47* (12), 3931-3946.

Wang, T.; Ai, S.; Zhou, Y.; Luo, Z.; Dai, C.; Yang, Y.; Zhang, J.; Huang, H.; Luo, S.; Luo, L., Adsorption of agricultural wastewater contaminated with antibiotics, pesticides and toxic metals by functionalized magnetic nanoparticles. *Journal of Environmental Chemical Engineering* **2018,** *6* (5), 6468-6478.

Meadus, F.W.; Bassaw, B.P.; Sparks, B.D., Solvent extraction of Athabasca oil-sand in a rotating mill Part 2. Solids—liquid separation and bitumen quality. *Fuel Processing Technology* **1982,** *6* (3), 289-300.

Nikakhtari, H.; Wolf, S.; Choi, P.; Liu, Q.; Gray, M.R., Migration of fine solids into product bitumen from solvent extraction of Alberta oilsands. *Energy & Fuels* **2014,** *28* (5), 2925-2932.

Wang, S.; Liu, Q.; Tan, X.; Xu, C.; Gray, M.R., Study of asphaltene adsorption on kaolinite by X-ray photoelectron spectroscopy and time-of-flight secondary ion mass spectroscopy. *Energy & Fuels* **2013,** *27* (5), 2465-2473.

Pal, K.; Nogueira Branco, L. d. P.; Heintz, A.; Choi, P.; Liu, Q.; Seidl, P. R.; Gray, M. R., Performance of solvent mixtures for non-aqueous extraction of Alberta oil sands. *Energy & Fuels* **2015,** *29* (4), 2261-2267.

Lin, F.; Stoyanov, S.R.; Xu, Y., Recent advances in nonaqueous extraction of bitumen from mineable oil sands: a review. *Organic Process Research & Development* **2017,** *21* (4), 492-510.

Peng, J.; Liu, Q.; Xu, Z.; Masliyah, J., Novel Magnetic demulsifier for water removal from diluted bitumen emulsion. *Energy & Fuels* **2012,** *26* (5), 2705-2710.

He, X.; Liu, Q.; Xu, Z., Cellulose-coated magnetic Janus nanoparticles for dewatering of crude oil emulsions. *Chemical Engineering Science* **2021,** *230*, 116215.

Ko, S.; Kim, E. S.; Park, S.; Daigle, H.; Milner, T. E.; Huh, C.; Bennetzen, M. V.; Geremia, G. A. In oil droplet removal from produced water using nanoparticles and their magnetic separation, *SPE Annual Technical Conference and Exhibition* **2016.**

Setoodeh, N.; Darvishi, P.; Esmaeilzadeh, F., Adsorption of asphaltene from crude oil by applying polythiophene coating on Fe_3O_4 nanoparticles. *Journal of Dispersion Science and Technology* **2018,** *39* (4), 578-588.

Moeer, G.D.; Roach, K.A.; Green, W.H.; Alan Hatton, T.; Laibinis, P.E., High-gradient magnetic separation of coated magnetic nanoparticles. *AIChE Journal* **2004,** *50* (11), 2835-2848.

Gómez-Pastora, J.; Bringas, E.; Ortiz, I., Recent progress and future challenges on the use of high performance magnetic nano-adsorbents in environmental applications. *Chemical Engineering Journal* **2014,** *256*, 187-204.

Hejazian, M.; Li, W.; Nguyen, N.T., Lab on a chip for continuous-flow magnetic cell separation. *Lab on a Chip* **2015,** *15* (4), 959-970.

Yildiz, I., Applications of magnetic nanoparticles in biomedical separation and purification. *Nanotechnology Reviews* **2016,** *5* (3), 331-340.

Tang, C.; He, Z.; Liu, H.; Xu, Y.; Huang, H.; Yang, G.; Xiao, Z.; Li, S.; Liu, H.; Deng, Y; Chen, Z., Application of magnetic nanoparticles in nucleic acid detection. *Journal of Nanobiotechnology* **2020,** *18* (1), 1-19.

Berensmeier, S., Magnetic particles for the separation and purification of nucleic acids. *Applied Microbiology and Biotechnology* **2006,** *73*, 495-504.

World Health Organization Report. https://covid19.who.int/ Accessed on 20th September 2023.

Peralta, M.E.; Ocampo, S.; Funes, I.G.; Onaga Medina, F.; Parolo, M.E.; Carlos, L., Nanomaterials with tailored magnetic properties as adsorbents of organic pollutants from wastewaters. *Inorganics* **2020,** *8* (4), 24.

Nikakhtari, H.; Wolf, S.; Choi, P.; Liu, Q.; Gray, M.R., Migration of fine solids into product bitumen from solvent extraction of Alberta oilsands. *Energy & Fuels* **2014,** *28* (5), 2925-2932.

Tarleton, E., The role of field-assisted techniques in solid/liquid separation. *Filtration & Separation* **1992**, *29* (3), 246-238.

Czarnecka, E.; Gillott, J.E., Formation and characterization of clay complexes with bitumen from Athabasca oil sand. *Clays and Clay Minerals* **1980,** *28*, 197-203.

Wang, S.; Liu, Q.; Tan, X.; Xu, C.; Gray, M.R., Study of asphaltene adsorption on kaolinite by X-ray photoelectron spectroscopy and time-of-flight secondary ion mass spectroscopy. *Energy & Fuels* **2013,** *27* (5), 2465-2473.

Osacky, M.; Geramian, M.; Ivey, D.G.; Liu, Q.; Etsell, T.H., Influence of nonswelling clay minerals (illite, kaolinite, and chlorite) on nonaqueous solvent extraction of bitumen. *Energy & Fuels* **2015,** *29* (7), 4150-4159.

Bensebaa, F.; Kotlyar, L.S.; Sparks, B.D.; Chung, K.H., Organic coated solids in Athabasca bitumen: Characterization and process implications. *The Canadian Journal of Chemical Engineering* **2000,** *78* (4), 610-616.

Lin, F.; He, L.; Primkulov, B.; Xu, Z., Dewetting dynamics of a solid microsphere by emulsion drops. *The Journal of Physical Chemistry C* **2014,** *118* (25), 13552-13562.

Hannisdal, A.; Ese, M.H.; Hemmingsen, P.V.; Sjöblom, J., Particle-stabilized emulsions: Effect of heavy crude oil components pre-adsorbed onto stabilizing solids. *Colloids and Surfaces A: Physicochemical and Engineering Aspects* **2006,** *276* (1-3), 45-58.

Dubey, S.T.; Waxman, M.L., Asphaltene adsorption and desorption from mineral surfaces. *SPE Reservoir Engineering* **1991,** *6* (03), 389-395.

González, G.; Moreira, M.B., The wettability of mineral surfaces containing adsorbed asphaltene. *Colloids and Surfaces* **1991,** *58* (3), 293-302.

Nalwaya, V.; Tantayakom, V.; Piumsomboon, P.; Fogler, S., Studies on asphaltenes through analysis of polar fractions. *Industrial & Engineering Chemistry Research* **1999,** *38* (3), 964-972.

Carbognani, L., Effects of iron compounds on the retention of oil polar hydrocarbons over solid sorbents. *Petroleum Science and Technology* **2000,** *18* (3-4), 335-360.

Alvarez-Ramirez, F.; Garcia-Cruz, I.; Tavizon, G.; Martinez-Magadan, J.M., Docking of an asphaltene molecular model on a Fe_2O_3 surface, an ab initio simulated annealing. *Petroleum Science and Technology* **2004,** *22* (7-8), 915-926.

Madge, D.N.; Garner, W.N., Theory of asphaltene precipitation in a hydrocarbon cyclone. *Minerals Engineering* **2007,** *20* (4), 387-394.

Farnand, J.R.; Meadus, F.W.; Sparks, B.D., Removal of intractable fine solids from bitumen solutions obtained by solvent extraction of oil sands. *Fuel Processing Technology* **1985,** *10* (2), 131-144.

Lin, F.; Stoyanov, S.R.; Xu, Y., Recent advances in nonaqueous extraction of bitumen from mineable oil sands: a review. *Organic Process Research & Development* **2017,** *21* (4), 492-510.

Graham, R.J.; Helstrom, J.J.; Mehlberg, R.L., 1987. A solvent extraction process for tar sand. *Eastern Oil Shale Symposium* **1987**, 93–99.

Dixon, D.V.; Stoyanov, S.R.; Xu, Y.; Zeng, H.; Soares, J.B., Challenges in developing polymer flocculants to improve bitumen quality in non-aqueous extraction processes: an experimental study. *Petroleum Science* **2020,** *17*, 811-821.

Ngnie, G.; Baitan, D.; Dedzo, G.K.; Detellier, C., Sedimentation of fine particles of kaolinite and polymer-coated kaolinite in cyclohexane: Implications for fines removal from extracted bitumen in non-aqueous processes. *Fuel* **2018,** *234*, 218-224.

Alquist, H.E.; Ammerman, A.M., Phillips Petroleum Co, Process for extracting bitumen from tar sands. **1980,** *U.S. Patent 4,229,281.*

Liu, J.; Cui, X.; Santander, C.; Tan, X.; Liu, Q.; Zeng, H., Destabilization of fine solids suspended in oil media through wettability modification and water-assisted agglomeration. *Fuel* **2019,** *254,* 115623.

Zhang, H.; Tan, X.; Wang, K.; Liu, Q., Electrodeposition of bitumen-, asphaltene-, or maltene-coated kaolinite from cyclohexane suspensions. *Fuel* ***2022,*** *311*, 122582.

Cullinane, J.T.; Minhas, B.S., ExxonMobil Upstream Research Co, Electrostatic filtration of fine solids from bitumen. **2017,** *U.S. Patent 9,752,079.*

Sparks, B.D.; Meadus, F.W.; Hoefele, E.O., Canadian Patents and Development Ltd, Solvent extraction spherical agglomeration of oil sands. **1988,** *U.S. Patent 4,719,008.*

Sui, H.; Xu, L.; Li, X.; He, L., Understanding the roles of switchable-hydrophilicity tertiary amines in recovering heavy hydrocarbons from oil sands. *Chemical Engineering Journal* **2016,** *290*, 312-318.

Holland, A.; Wechsler, D.; Patel, A.; Molloy, B.M.; Boyd, A.R.; Jessop, P.G., Separation of bitumen from oil sands using a switchable hydrophilicity solvent. *Canadian Journal of Chemistry* **2012,** *90* (10), 805-810.

Plechkova, N.V.; Seddon, K.R., Applications of ionic liquids in the chemical industry. *Chemical Society Reviews* **2008,** *37* (1), 123-150.

Joshi, V.A. and Kundu, D., 2021. Ionic liquid promoted extraction of bitumen from oil sand: A review. *Journal of Petroleum Science and Engineering*, *199*, p.108232.

Painter, P.; Williams, P.; Mannebach, E., Recovery of bitumen from oil or tar sands using ionic liquids. *Energy & Fuels* **2010,** *24* (2), 1094-1098.

Hou, J.; Lin, S.; Zhang, M., Ionic-liquid-enhanced solvent extraction mechanism: A novel concept. *Journal of Environmental Chemical Engineering* **2022,** *10* (3), 107899.

Liu, J.; Xu, Z.; Masliyah, J., Studies on bitumen− silica interaction in aqueous solutions by atomic force microscopy. *Langmuir* **2003,** *19* (9), 3911-3920.

Pulati, N.; Lupinsky, A.; Miller, B.; Painter, P., Extraction of bitumen from oil sands using deep eutectic ionic liquid analogues. *Energy & Fuels* **2015,** *29* (8), 4927-4935.

Price, C.W.; Leslie, D.C.; Landers, J.P., Nucleic acid extraction techniques and application to the microchip. *Lab on a Chip* **2009,** *9* (17), 2484-2494.

McKiernan, H.E.; Danielson, P.B., Molecular diagnostic applications in forensic science. *Molecular Diagnostics* **2017,** 371-394. Academic Press.

Tan, S.C.; Yiap, B.C., DNA, RNA, and protein extraction: the past and the present. *BioMed Research International* **2009.**

Sobieralski, C.A.; Stanley, D.M., DNA Extraction Strategies for amplified fragment length polymorphism analysis. *Journal of Forensic Science* ***1994.*** 1254-1269.

Chomczynski, P.; Sacchi, N., Single-step method of RNA isolation by acid guanidinium thiocyanate-phenol-chloroform extraction. *Analytical Biochemistry*, **1987,** *162* (1), 156-159.

Chomczynski, P.; Sacchi, N., The single-step method of RNA isolation by acid guanidinium thiocyanate–phenol–chloroform extraction: twenty-something years on. *Nature Protocols* **2006,** *1* (2), 581-585.

Köchl, S.; Niederstätter, H.; Parson, W., DNA extraction and quantitation of forensic samples using the phenol-chloroform method and real-time PCR. *Forensic DNA Typing Protocols* **2005,** 13-29.

Maaroufi, Y.; Ahariz, N., Husson, M.; Crokaert, F., Comparison of different methods of isolation of DNA of commonly encountered Candida species and its quantitation by using a real-time PCR-based assay. *Journal of Clinical Microbiology* **2004,** *42* (7), 3159-3163.

Shin, J.H., Nucleic acid extraction techniques. *Advanced Techniques in Diagnostic Microbiology* **2013,** 209-225.

Ali, N.; Rampazzo, R.D.C.P.; Costa, A.D.T.; Krieger, M.A., Current nucleic acid extraction methods and their implications to point-of-care diagnostics. *BioMed Research International* **2017.**

Wink, M. ed., An introduction to molecular biotechnology: fundamentals, methods and applications. *John Wiley & Sons* **2020.**

Marko, M.A.; Chipperfield, R.; Birnboim, H.C., A procedure for the large-scale isolation of highly purified plasmid DNA using alkaline extraction and binding to glass powder. *Analytical Biochemistry* **1982,** *121* (2), 382-387.

Shi, R.; Lewis, R.S.; Panthee, D.R., Filter paper-based spin column method for cost-efficient DNA or RNA purification. *PLOS One* **2018,** *13* (12), e0203011.

Mirna Lorena, S.; Cynthia, P.C.; Maria Isabela, A.R.; Pamela, V.M.; Gabriela, R.H.; Jorge, B.; Mariano, G., Nucleic Acids Isolation for Molecular Diagnostics: Present and Future of the Silica-based DNA/RNA Purification Technologies. *Separation & Purification Reviews* **2023,** *52* (3), 193-204.

Gautam, A., Spin Column-Based Isolation of Nucleic Acid. *DNA and RNA Isolation Techniques for Non-Experts* **2022,** 47-53 Cham: Springer International Publishing.

Éva Mészáros, Spin column extraction, May 27, 2021. https://www.integra-biosciences.com/france/en/blog/article/comparison-rna-and-dna-extraction-methods Accessed on 14th November 2023.

Olsvik, O.; Popovic, T.; Skjerve, E.; Cudjoe, K.S.; Hornes, E.; Ugelstad, J.; Uhlén, M., Magnetic separation techniques in diagnostic microbiology. *Clinical microbiology reviews* **1994,** *7* (1), 43-54.

Stormer, M.; Kleesiek, K.; Dreier, J., High-volume extraction of nucleic acids by magnetic bead technology for ultrasensitive detection of bacteria in blood components. *Clinical chemistry* **2007,** *53* (1), 104-110.

Tang, C.; He, Z.; Liu, H.; Xu, Y.; Huang, H.; Yang, G.; Xiao, Z.; Li, S.; Liu, H.; Deng, Y.; Chen, Z., Application of magnetic nanoparticles in nucleic acid detection. *Journal of Nanobiotechnology* **2020,** *18* (1), 1-19.

Chen, Y.; Liu, Y.; Shi, Y.; Ping, J.; Wu, J.; Chen, H., Magnetic particles for integrated nucleic acid purification, amplification and detection without pipetting. *TrAC Trends in Analytical Chemistry* **2020,** *127*, 115912.

Berensmeier, S., Magnetic particles for the separation and purification of nucleic acids. *Applied Microbiology and Biotechnology* **2006,** *73*, 495-504.

Fang, X.; Willis, R.C.; Burrell, A.; Evans, K.; Hoang, Q.; Xu, W.; Bounpheng, M., Automation of nucleic acid isolation on KingFisher magnetic particle processors. *JALA: Journal of the Association for Laboratory Automation* **2007,** *12* (4), 195-201.

Rittich, B.; Španová, A., SPE and purification of DNA using magnetic particles. *Journal of Separation Science* **2013,** *36* (15), 2472-2485.

Melzak, K.A.; Sherwood, C.S.; Turner, R.F.; Haynes, C.A., Driving forces for DNA adsorption to silica in perchlorate solutions. *Journal of Colloid and Interface Science* **1996,** *181* (2), 635-644.

Lakshmi, R.; Baskar, V.; Ranga, U., Extraction of superior-quality plasmid DNA by a combination of modified alkaline lysis and silica matrix. *Analytical Biochemistry* **1999,** *272* (1), 109-112.

Li, X.; Zhang, J.; Gu, H., Adsorption and desorption behaviors of DNA with magnetic mesoporous silica nanoparticles. *Langmuir* **2011,** *27* (10), 6099-6106.

Luhmer, M.; d'Espinose, J.B.; Hommel, H.; Legrand, A.P., High-resolution ^{29}Si solid-state NMR study of silicon functionality distribution on the surface of silicas. *Magnetic Resonance Imaging* **1996,** *14* (7-8), 911-913.

Braga, P.R.; Costa, A.A.; de Macedo, J.L.; Ghesti, G.F.; de Souza, M.P.; Dias, J.A.; Dias, S.C., Liquid phase calorimetric-adsorption analysis of Si-MCM-41: Evidence of strong hydrogen-bonding sites. *Microporous and Mesoporous Materials* **2011,** *139* (1-3), 74-80.

Rosenholm, J.M. and Lindén, M., Towards establishing structure–activity relationships for mesoporous silica in drug delivery applications. *Journal of Controlled Release* **2008,** *128* (2), 157-164.

Trachtová, Š.; Kaman, O.; Španová, A.; Veverka, P.; Pollert, E.; Rittich, B., Silica-coated $La_{0.75}Sr_{0.25}MnO_3$ nanoparticles for magnetically driven DNA isolation. *Journal of Separation Science* **2011,** *34* (21), 3077-3082.

Prodělalová, J.; Rittich, B.; Španová, A.; Petrová, K.; Beneš, M.J., Isolation of genomic DNA using magnetic cobalt ferrite and silica particles. *Journal of Chromatography a* **2004,** *1056* (1-2), 43-48.

Yue, H.; Shin, J.M.; Tegafaw, T.; Han, H.S.; Chae, K.S.; Chang, Y.; Lee, G.H., Magnetic separation of nucleic acids from various biological samples using silica-coated iron oxide nanobeads. *Journal of Nanoparticle Research* **2020,** *22*, 1-12.

Wang, J.; Ali, Z.; Si, J.; Wang, N.; He, N.; Li, Z., Simultaneous extraction of DNA and RNA from hepatocellular carcinoma (Hep G2) based on silica-coated magnetic nanoparticles. *Journal of Nanoscience and Nanotechnology* **2017,** *17* (1), 802-806.

Algar, W.R.; Krull, U.J., Adsorption and hybridization of oligonucleotides on mercaptoacetic acid-capped CdSe/ZnS quantum dots and quantum dot-oligonucleotide conjugates. *Langmuir* **2006,** *22* (26), 11346-11352.

Liang, G.; Zhang, P.; Li, H.; Zhang, Z.; Chen, H.; Zhang, S.; Kong, J., An efficient strategy for unmodified nucleotide-mediated dispersion of magnetic nanoparticles, leading to a highly sensitive MRI-based mercury ion assay. *Analytica Chimica Acta* **2012,** *726*, 73-78.

DeAngelis, M.M.; Wang, D.G.; Hawkins, T.L., Solid-phase reversible immobilization for the isolation of PCR products. *Nucleic Acids Research* **1995,** *23* (22), 4742.

Skowronski, E.W.; Armstrong, N.; Andersen, G.; Macht, M.; McCready, P.M., Magnetic, microplate-format plasmid isolation protocol for high-yield, sequencing-grade DNA. *Biotechniques* **2000,** *29* (4), 786-792.

Španová, A.; Rittich, B.; Štyriak, I.; Štyriaková, I.; Horák, D., Isolation of polymerase chain reaction-ready bacterial DNA from Lake Baikal sediments by carboxyl-functionalised magnetic polymer microspheres. *Journal of Chromatography A* **2006,** *1130* (1), 115-121.

Horák, D.; Rittich, B.; Španová, A., Carboxyl-functionalized magnetic microparticle carrier for isolation and identification of DNA in dairy products. *Journal of Magnetism and Magnetic Materials* **2007,** *311* (1), 249-254.

Messina, R., Holm, C.; Kremer, K., Like-charge colloid-polyelectrolyte complexation. *The Journal of Chemical Physics* **2002,** *117* (6), 2947-2960.

Jiang, H.; Han, X.; Li, Z.; Chen, X.; Hou, Y.; Gai, L.; Li, D.; Lu, X.; Fu, T., Superparamagnetic core–shell structured microspheres carrying carboxyl groups as adsorbents for purification of genomic DNA. *Colloids and surfaces a: physicochemical and engineering aspects* **2012,** *401*, 74-80.

Chen, Y.; Liu, Y.; Shi, Y.; Ping, J.; Wu, J.; Chen, H., Magnetic particles for integrated nucleic acid purification, amplification and detection without pipetting. *TrAC Trends in Analytical Chemistry* **2020,** *127*, 115912.

Kleideiter, G.; Nordmeier, E., Poly (ethylene glycol)-induced DNA condensation in aqueous/methanol containing low-molecular-weight electrolyte solutions I. Theoretical considerations. *Polymer* **1999,** *40* (14), 4013-4023.

Vasilevskaya, V.V.; Khokhlov, A.R.; Matsuzawa, Y.; Yoshikawa, K., Collapse of single DNA molecule in poly (ethylene glycol) solutions. *The Journal of chemical physics* **1995,** *102* (16), 6595-6602.

Kahánková, J.; Španová, A.; Pantůček, R.; Horák, D.; Doškař, J.; Rittich, B., Extraction of PCR-ready DNA from Staphylococcus aureus bacteriophages using carboxyl functionalized magnetic nonporous microspheres. *Journal of Chromatography B* **2009,** *877* (7), 599-602.

Sarkar, T.R.; Irudayaraj, J., Carboxyl-coated magnetic nanoparticles for mRNA isolation and extraction of supercoiled plasmid DNA. *Analytical Biochemistry* **2008,** *379* (1), 130-132.

Lipfert, J.; Doniach, S.; Das, R.; Herschlag, D., Understanding nucleic acid–ion interactions. *Annual Review of Biochemistry* **2014,** *83*, 813-841.

He, X.; Huo, H.; Wang, K.; Tan, W.; Gong, P.; Ge, J., Plasmid DNA isolation using amino-silica coated magnetic nanoparticles (ASMNPs). *Talanta* **2007,** *73* (4), 764-769.

Bai, Y.; Cui, Y.; Paoli, G.C.; Shi, C.; Wang, D.; Zhou, M.; Zhang, L.; Shi, X., Synthesis of amino-rich silica-coated magnetic nanoparticles for the efficient capture of DNA for PCR. *Colloids and Surfaces B: Biointerfaces* **2016,** *145*, 257-266.

Lin, F.; Stoyanov, S. R.; Xu, Y., Recent Advances in Non-aqueous Extraction of Bitumen from Mineable Oil Sands: A Review. *Organic Process Research & Development* **2017,** *21* (4), 492-510.

Zhang, H.; Tan, X.; Liu, Q., Fine solids removal from non-aqueous extraction bitumen: A literature review. *Fuel* **2021,** *288*.

Pal, K.; Nogueira Branco, L. d. P.; Heintz, A.; Choi, P.; Liu, Q.; Seidl, P. R.; Gray, M. R., Performance of Solvent Mixtures for Non-aqueous Extraction of Alberta Oil Sands. *Energy & Fuels* **2015,** *29* (4), 2261-2267.

Hooshiar, A.; Uhlik, P.; Ivey, D. G.; Liu, Q.; Etsell, T. H., Clay minerals in non-aqueous extraction of bitumen from Alberta oil sands: Part 2. Characterization of clay minerals. *Fuel processing technology* **2012,** *96*, 183-194.

Nikakhtari, H.; Wolf, S.; Choi, P.; Liu, Q.; Gray, M. R., Migration of Fine Solids into Product Bitumen from Solvent Extraction of Alberta Oilsands. *Energy & Fuels* **2014,** *28* (5), 2925-2932.

Wu, J.; Dabros, T., Process for Solvent Extraction of Bitumen from Oil Sand. *Energy & Fuels* **2012,** *26* (2), 1002-1008.

Hooshiar, A.; Uhlik, P.; Liu, Q.; Etsell, T. H.; Ivey, D. G., Clay minerals in non-aqueous extraction of bitumen from Alberta oil sands. *Fuel Processing Technology* **2012,** *94* (1), 80-85.

Farnand, J. R.; F. W. Meadus;d B. D. Sparks., Removal of intractable fine solids from bitumen solutions obtained by solvent extraction of oil sands. *Fuel processing technology* **1985**, 10, 131-144.

Graham, R.; Helstrom, J.; Mehlberg, R., A Solvent Extraction Process for Tar Sand. *Eastern Oil Shale Symposium* **1987**, 93-99.

Painter, P.; Williams, P.; Lupinsky, A., Recovery of bitumen from Utah tar sands using ionic liquids. *Energy & Fuels* **2010,** *24* (9), 5081-5088.

Pulati, N.; Lupinsky, A.; Miller, B.; Painter, P., Extraction of bitumen from oil sands using deep eutectic ionic liquid analogues. *Energy & Fuels* **2015,** *29* (8), 4927-4935.

Sparks, B. D.; Meadus, F. W.; Hoefele, E. O., Canadian Patents and Development Ltd, Solvent extraction spherical agglomeration of oil sands. **1988,** *U.S. Patent 4,719,008.*

Zhang, H.; Tan, X.; Wang, K.; Liu, Q., Electrodeposition of bitumen-, asphaltene-, or maltene-coated kaolinite from cclohexane suspensions. *Fuel* **2022,** *311*, 122582.

Fritsche, G. R.; Bujas, R. S.; Caprioglio, G. C., General Atomics Corp, Electrostatic separator using a bead bed. **1994,** *U.S. Patent 5,308,586.*

Cullinane, J. T.; Minhas, B. S., ExxonMobil Upstream Research Co, Electrostatic filtration of fine solids from bitumen. **2017,** *U.S. Patent 9,752,079.*

Liu, J.; Cui, X.; Santander, C.; Tan, X.; Liu, Q.; Zeng, H., Destabilization of fine solids suspended in oil media through wettability modification and water-assisted agglomeration. *Fuel* **2019,** *254*.

HollandAmy; WechslerDominik; PatelAnjali; M., M.; R., B.; G., J., Separation of bitumen from oil sands using a switchable hydrophilicity solvent. *Canadian Journal of Chemistry* **2012,** *90* (10), 805-810.

Jessop, P. G.; Heldebrant, D. J.; Li, X.; Eckert, C. A.; Liotta, C. L., Reversible nonpolar-to-polar solvent. *Nature* **2005,** *436* (7054), 1102-1102.

Simonsen, G.; Strand, M.; Øye, G., Potential applications of magnetic nanoparticles within separation in the petroleum industry. *Journal of Petroleum Science and Engineering* **2018,** *165*, 488-495.

Xu, P.; Zeng, G. M.; Huang, D. L.; Feng, C. L.; Hu, S.; Zhao, M. H.; Lai, C.; Wei, Z.; Huang, C.; Xie, G. X.; Liu, Z. F., Use of iron oxide nanomaterials in wastewater treatment: a review. *Sci Total Environ* **2012,** *424*, 1-10.

Pan, Y.; Du, X.; Zhao, F.; Xu, B., Magnetic nanoparticles for the manipulation of proteins and cells. *Chem Soc Rev* **2012,** *41* (7), 2912-42.

Wierucka, M.; Biziuk, M., Application of magnetic nanoparticles for magnetic solid-phase extraction in preparing biological, environmental and food samples. *TrAC Trends in Analytical Chemistry* **2014,** *59*, 50-58.

You, N.; Wang, X.-F.; Li, J.-Y.; Fan, H.-T.; Shen, H.; Zhang, Q., Synergistic removal of arsanilic acid using adsorption and magnetic separation technique based on Fe_3O_4@ graphene nanocomposite. *Journal of Industrial and Engineering Chemistry* **2019,** *70*, 346-354.

Yue, T.; Niu, Z.; Tao, H.; He, X.; Sun, W.; Hu, Y.; Xu, Z., Green Recycling of Goethite and Gypsum Residues in Hydrometallurgy with α-Fe_3O_4 and γ-Fe_2O_3 Nanoparticles: Application, Characterization, and DFT Calculation. *ACS Sustainable Chemistry & Engineering* **2019**, 7 (7), 6821-6829.

Yue, T.; Xu, Z.; Hu, Y.; Han, H.; Sun, W., Magnetic Separation and Recycling of Goethite and Calcium Sulfate in Zinc Hydrometallurgy in the Presence of Maghemite Fine Particles. *ACS Sustainable Chemistry & Engineering* **2018**, 6 (2), 1532-1538.

Yildiz, I., Applications of magnetic nanoparticles in biomedical separation and purification. *Nanotechnology Reviews* **2016,** *5* (3), 331-340.

Gupta, A. K.; Gupta, M., Synthesis and surface engineering of iron oxide nanoparticles for biomedical applications. *Biomaterials* **2005,** *26* (18), 3995-4021.

Peng, J.; Liu, Q.; Xu, Z.; Masliyah, J., Novel Magnetic Demulsifier for Water Removal from Diluted Bitumen Emulsion. *Energy & Fuels* **2012,** *26* (5), 2705-2710.

Ali, N.; Zhang, B.; Zhang, H.; Zaman, W.; Li, X.; Li, W.; Zhang, Q., Interfacially active and magnetically responsive composite nanoparticles with raspberry like structure; synthesis and its applications for heavy crude oil/water separation. *Colloids and Surfaces A: Physicochemical and Engineering Aspects* **2015,** *472*, 38-49.

Nikakhtari, H.; Vagi, L.; Choi, P.; Liu, Q.; Gray. MR., Solvent screening for a non-aqueous extraction of Alberta oil sands process. *Canadian Journal of Chemical Engineering* **2012,** *91* (6), 1153-1160.

Wu, W.; He, Q.; Jiang, C., Magnetic iron oxide nanoparticles: synthesis and surface functionalization strategies. *Nanoscale research letters* **2008,** *3* (11), 397-415.

ASTM, ASTM D4807-05, Standard Test Method for Sediment in Crude Oil by Membrane Filtration. **2017**.

ASTM, ASTM D482-07, Standard Test Method for Ash from Petroleum Products. **2013**.

Adhikari, M.; Echeverria, E.; Risica, G.; McIlroy, D. N.; Nippe, M.; Vasquez, Y., Synthesis of Magnetite Nanorods from the Reduction of Iron Oxy-Hydroxide with Hydrazine. *ACS omega* **2020,** *5* (35), 22440-22448.

Singh, D.; Gautam, R. K.; Kumar, R.; Shukla, B. K.; Shankar, V.; Krishna, V., Citric acid coated magnetic nanoparticles: Synthesis, characterization and application in removal of Cd(II) ions from aqueous solution. *Journal of Water Process Engineering* **2014,** *4*, 233-241.

Ruparelia, N.; Soni, U.; Desai, R. P.; Ray, A., Silica anchored colloidal suspension of magnetite nanorods. *Journal of Solid State Chemistry* **2020,** *290*, 121574.

Hong, R.; Zhang, S.; Di, G.; Li, H.; Zheng, Y.; Ding, J.; Wei, D., Preparation, characterization, and application of Fe3O4/ZnO core/shell magnetic nanoparticles. *Materials Research Bulletin* **2008,** *43* (8-9), 2457-2468.

Lawrie, G.; Keen, I.; Drew, B.; Chandler-Temple, A.; Rintoul, L.; Fredericks, P.; Grøndahl, L., Interactions between alginate and chitosan biopolymers characterized using FTIR and XPS. *Biomacromolecules* **2007,** *8* (8), 2533-2541.

Zaitsev, V. S.; Filimonov, D. S.; Presnyakov, I. A.; Gambino, R. J.; Chu, B., Physical and chemical properties of magnetite and magnetite-polymer nanoparticles and their colloidal dispersions. *Journal of Colloid and Interface Science* **1999,** *212* (1), 49-57.

Fang, M.; Ström, V.; Olsson, R. T.; Belova, L.; Rao, K. V., Particle size and magnetic properties dependence on growth temperature for rapid mixed co-precipitated magnetite nanoparticles. *Nanotechnology* **2012,** *23* (14), 145601.

Radoń, A.; Drygała, A.; Hawełek, Ł.; Łukowiec, D., Structure and optical properties of Fe3O4 nanoparticles synthesized by co-precipitation method with different organic modifiers. *Materials Characterization* **2017,** *131*, 148-156.

Ma, M.; Zhang, Y.; Yu, W.; Shen, H.-y.; Zhang, H.-q.; Gu, N., Preparation and characterization of magnetite nanoparticles coated by amino silane. *Colloids and Surfaces A: Physicochemical and Engineering Aspects* **2003,** *212* (2), 219-226.

Jin, Y.; Liu, W.; Liu, Q.; Yeung, A., Aggregation of silica particles in non-aqueous media. *Fuel* **2011,** *90* (8), 2592-2597.

Dongbao, F.; Woods, J. R.; Kung, J.; Kingston, D. M.; Kotlyar, L. S.; Sparks, B. D.; Mercier, P. H. J.; McCracken, T.; Ng, S., Residual Organic Matter Associated with Toluene-Extracted Oil

Sands Solids and Its Potential Role in Bitumen Recovery via Adsorption onto Clay Minerals. *Energy & Fuels* **2010,** *24* (4), 2249-2256.

Couillard, M.; Mercier, P. H. J., Analytical Electron Microscopy of Carbon-Rich Mineral Aggregates in Solvent-Diluted Bitumen Products from Mined Alberta Oil Sands. *Energy & Fuels* **2016,** *30* (7), 5513-5524.

Collins, S.; Melrose, J. In *Adsorption of asphaltenes and water on reservoir rock minerals*, SPE Oilfield and Geothermal Chemistry Symposium, OnePetro: 1983.

González, G.; Moreira, M. B. C., Chapter 9 The Adsorption of Asphaltenes and Resins on Various Minerals. In *Developments in Petroleum Science*, Yen, T. F.; Chilingarian, G. V., Eds. Elsevier: 1994; Vol. 40, pp 207-231.

Saraji, S.; Goual, L.; Piri, M., Adsorption of Asphaltenes in Porous Media under Flow Conditions. *Energy & Fuels* **2010,** *24* (11), 6009-6017.

Chen, Q.; Gray, M. R.; Liu, Q., Irreversible Adsorption of Asphaltenes on Kaolinite: Influence of Dehydroxylation. *Energy & Fuels* **2017,** *31* (9), 9328-9336.

Adams, J. J., Asphaltene adsorption, a literature review. *Energy & Fuels* **2014,** *28* (5), 2831-2856.

Nikakhtari, H.; Vagi, L.; Choi, P.; Liu, Q.; Gray, M. R., Solvent screening for non-aqueous extraction of Alberta oil sands. *The Canadian Journal of Chemical Engineering* **2013,** *91* (6), 1153-1160.

Chen, Q.; Stricek, I.; Gray, M. R.; Liu, Q., Influence of hydrophobicity distribution of particle mixtures on emulsion stabilization. *Journal of colloid and interface science* **2017,** *491*, 179-189.

Pourmohammadbagher, A.; Shaw, J. M., Probing the Impact of Asphaltene Contamination on Kaolinite and Illite Clay Behaviors in Water and Organic Solvents: A Calorimetric Study. *Energy & Fuels* **2016,** *30* (8), 6561-6569.

Luo, L.; Nguyen, A. V., A review of principles and applications of magnetic flocculation to separate ultrafine magnetic particles. *Separation and Purification Technology* **2017,** *172*, 85-99.

Veiseh, O.; Gunn, J. W.; Zhang, M., Design and fabrication of magnetic nanoparticles for targeted drug delivery and imaging. *Advanced Drug Delivery Reviews* **2010,** *62* (3), 284-304.

Gloag, L.; Mehdipour, M.; Chen, D.; Tilley, R. D.; Gooding, J. J., Advances in the Application of Magnetic Nanoparticles for Sensing. *Advanced Materials* **2019,** *31* (48), e1904385.

Khan, F. S. A.; Mubarak, N. M.; Tan, Y. H.; Karri, R. R.; Khalid, M.; Walvekar, R.; Abdullah, E. C.; Mazari, S. A.; Nizamuddin, S., Magnetic nanoparticles incorporation into different substrates for dyes and heavy metals removal-A Review. *Environmental Science and Pollution Research* **2020,** *27* (35), 43526-43541.

Kole, M.; Khandekar, S., Engineering applications of ferrofluids: A review. *Journal of Magnetism and Magnetic Materials* **2021,** *537*, 168222.

Déry, J.-P.; Borra, E. F.; Ritcey, A. M., Ethylene Glycol Based Ferrofluid for the Fabrication of Magnetically Deformable Liquid Mirrors. *Chemistry of Materials* **2008,** *20* (20), 6420-6426.

Rodríguez-Arco, L.; López-López, M. T.; González-Caballero, F.; Durán, J. D. G., Steric repulsion as a way to achieve the required stability for the preparation of ionic liquid-based ferrofluids. *Journal of Colloid and Interface Science* **2011,** *357* (1), 252-254.

Wu, Q.; Cui, Y.; Li, Q.; Sun, J., Effective removal of heavy metals from industrial sludge with the aid of a biodegradable chelating ligand GLDA. *Journal of Hazardous Materials* **2015,** *283*, 748-754.

Wang, T.; Ai, S.; Zhou, Y.; Luo, Z.; Dai, C.; Yang, Y.; Zhang, J.; Huang, H.; Luo, S.; Luo, L., Adsorption of agricultural wastewater contaminated with antibiotics, pesticides and toxic metals by functionalized magnetic nanoparticles. *Journal of Environmental Chemical Engineering* **2018,** *6* (5), 6468-6478.

Gupta, A. K.; Gupta, M., Synthesis and surface engineering of iron oxide nanoparticles for biomedical applications. *Biomaterials* **2005,** *26* (18), 3995-4021.

Natarajan, S. K.; Selvaraj, S., Mesoporous silica nanoparticles: importance of surface modifications and its role in drug delivery. *RSC advances* **2014,** *4* (28), 14328-14334.

Zhou, K.; Zhou, X.; Liu, J.; Huang, Z., Application of magnetic nanoparticles in petroleum industry: A review. *Journal of Petroleum Science and Engineering* **2020,** *188*.

Yakasai, F.; Jaafar, M. Z.; Bandyopadhyay, S.; Agi, A.; Sidek, M. A., Application of iron oxide nanoparticles in oil recovery – A critical review of the properties, formulation, recent advances and prospects. *Journal of Petroleum Science and Engineering* **2022,** *208*.

Vryzas, Z.; Kelessidis, V. C.; Bowman, M. B.; Nalbantian, L.; Zaspalis, V.; Mahmoud, O.; Nasr-El-Din, H. A. In *Smart magnetic drilling fluid with in-situ rheological controllability using Fe_3O_4 nanoparticles*, SPE Middle East Oil & Gas Show and Conference, OnePetro: **2017.**

Vipulanandan, C.; Mohammed, A.; Samuel, R. In *Smart bentonite drilling muds modified with iron oxide nanoparticles and characterized based on the electrical resistivity and rheological*

properties with varying magnetic field strengths and temperatures, Offshore Technology Conference, OnePetro: **2017.**

Wanna, Y.; Chindaduang, A.; Tumcharern, G.; Phromyothin, D.; Porntheerapat, S.; Nukeaw, J.; Hofmann, H.; Pratontep, S., Efficiency of SPIONs functionalized with polyethylene glycol bis(amine) for heavy metal removal. *Journal of Magnetism and Magnetic Materials* **2016,** *414*, 32-37.

Prigiobbe, V.; Ko, S.; Wang, Q.; Huh, C.; Bryant, S. L.; Bennetzen, M. V. In *Magnetic Nanoparticles for Efficient Removal of Oilfield "Contaminants": Modeling of Magnetic Separation and Validation*, SPE International Symposium on Oilfield Chemistry, 2015.

Simonsen, G.; Strand, M.; Øye, G., Potential applications of magnetic nanoparticles within separation in the petroleum industry. *Journal of Petroleum Science and Engineering* **2018,** *165*, 488-495.

Peng, J.; Liu, Q.; Xu, Z.; Masliyah, J., Novel Magnetic Demulsifier for Water Removal from Diluted Bitumen Emulsion. *Energy & Fuels* **2012,** *26* (5), 2705-2710.

He, X.; Liu, Q.; Xu, Z., Cellulose-coated magnetic Janus nanoparticles for dewatering of crude oil emulsions. *Chemical Engineering Science* **2021,** *230*, 116215.

Ko, S.; Kim, E. S.; Park, S.; Daigle, H.; Milner, T. E.; Huh, C.; Bennetzen, M. V.; Geremia, G. A. In *Oil Droplet Removal from Produced Water Using Nanoparticles and Their Magnetic Separation*, SPE Annual Technical Conference and Exhibition, 2016.

Setoodeh, N.; Darvishi, P.; Esmaeilzadeh, F., Adsorption of asphaltene from crude oil by applying polythiophene coating on Fe3O4 nanoparticles. *Journal of Dispersion Science and Technology* **2018,** *39* (4), 578-588.

Liu, X.; Wang, K.; Tan, X.; Zeng, H.; Liu, Q., Removal of fine solids from bitumen by hetero-aggregation and magnetic separation using surface-modified magnetite nanoparticles. Part 1: Proof of concept. *Separation and Purification Technology* **2022,** *300*.

ASTM, ASTM D6560-12, Standard Test Method for Determination of Asphaltenes (heptane insolubles) in Crude Petroleum and Petroleum Products. **2012**.

Adams, J. J., Asphaltene adsorption, a literature review. *Energy & Fuels* **2014,** *28* (5), 2831-2856.

Wang, S.; Liu, Q.; Tan, X.; Xu, C.; Gray, M. R., Adsorption of asphaltenes on kaolinite as an irreversible process. *Colloids and Surfaces A: Physicochemical and Engineering Aspects* **2016,** *504*, 280-286.

ASTM, ASTM D482-07, Standard Test Method for Ash from Petroleum Products. **2013**.

Wang, S.; Segin, N.; Wang, K.; Masliyah, J. H.; Xu, Z., Wettability Control Mechanism of Highly Contaminated Hydrophilic Silica/Alumina Surfaces by Ethyl Cellulose. *The Journal of Physical Chemistry C* **2011,** *115* (21), 10576-10587.

Wang, S.; Liu, Q.; Tan, X.; Xu, C.; Gray, M. R., Study of Asphaltene Adsorption on Kaolinite by X-ray Photoelectron Spectroscopy and Time-of-Flight Secondary Ion Mass Spectroscopy. *Energy & Fuels* **2013,** *27* (5), 2465-2473.

Daraei, P.; Madaeni, S. S.; Ghaemi, N.; Khadivi, M. A.; Astinchap, B.; Moradian, R., Fouling resistant mixed matrix polyethersulfone membranes blended with magnetic nanoparticles: Study of magnetic field induced casting. *Separation and Purification Technology* **2013,** *109*, 111-121.

Mahdavian, A. R.; Mirrahimi, M. A.-S., Efficient separation of heavy metal cations by anchoring polyacrylic acid on superparamagnetic magnetite nanoparticles through surface modification. *Chemical Engineering Journal* **2010,** *159* (1), 264-271.

Yang, K.; Peng, H.; Wen, Y.; Li, N., Re-examination of characteristic FTIR spectrum of secondary layer in bilayer oleic acid-coated Fe3O4 nanoparticles. *Applied Surface Science* **2010,** *256* (10), 3093-3097.

Pérez-Hernández, R.; Mendoza-Anaya, D.; Mondragón-Galicia, G.; Espinosa, M. E.; Rodríguez-Lugo, V.; Lozada, M.; Arenas-Alatorre, J., Microstructural study of asphaltene precipitated with methylene chloride and n-hexane☆. *Fuel* **2003,** *82* (8), 977-982.

Jun, Y.W.; Seo, J.W.; Cheon, J., Nanoscaling Laws of Magnetic Nanoparticles and Their Applicabilities in Biomedical Sciences. *Accounts of Chemical Research* **2008,** *41* (2), 179-189.

Shen, L.; Qiao, Y.; Guo, Y.; Meng, S.; Yang, G.; Wu, M.; Zhao, J., Facile co-precipitation synthesis of shape-controlled magnetite nanoparticles. *Ceramics International* **2014,** *40* (1, Part B), 1519-1524.

Natarajan, A.; Kuznicki, N.; Harbottle, D.; Masliyah, J.; Zeng, H.; & Xu, Z., Understanding mechanisms of asphaltene adsorption from organic solvent on mica. *Langmuir* **2014**, *30* (31), 9370-9377.

Liu, J.; Cui, X.; Huang, J.; Xie, L.; Tan, X.; Liu, Q.; Zeng, H., Understanding the stabilization mechanism of bitumen-coated fine solids in organic media from non-aqueous extraction of oil sands. *Fuel* **2019,** *242*, 255-264.

Lin, F.; Stoyanov, S.R.; Xu, Y., Recent advances in nonaqueous extraction of bitumen from mineable oil sands: a review. *Organic Process Research & Development* **2017,** *21* (4), 492-510.

Zhang, H.; Tan, X.; Liu, Q., Fine solids removal from non-aqueous extraction bitumen: A literature review. *Fuel* **2021,** *288*, 119727.

Painter, P.; Williams, P.; Lupinsky, A., Recovery of bitumen from Utah tar sands using ionic liquids. *Energy & Fuels* **2010,** *24* (9), 5081-5088.

Bonin, S.; Stanta, G., Nucleic acid extraction methods from fixed and paraffin-embedded tissues in cancer diagnostics. *Expert Review of Molecular Diagnostics* **2013,** *13* (3), 271-282.

Nana-Sinkam, S.P.; Croce, C.M., Clinical applications for microRNAs in cancer. *Clinical Pharmacology & Therapeutics* **2013,** *93* (1), 98-104.

Lau, L.T.; Fung, Y.W.W.; Yu, A.C.H., Detection of animal viruses using nucleic acid sequence-based amplification (NASBA). *Developments in Biologicals* **2006,** *126*, 7.

Yu, C.Y.; Chan, K.G.; Yean, C.Y.; Ang, G.Y., Nucleic acid-based diagnostic tests for the detection SARS-CoV-2: an update. *Diagnostics* **2021,** *11* (1), 53.

Courtney, S.J.; Stromberg, Z.R.; Kubicek-Sutherland, J.Z., Nucleic acid-based sensing techniques for diagnostics and surveillance of influenza. *Biosensors* **2021,** *11* (2), 47.

Carew, M.E.; Pettigrove, V.J.; Metzeling, L.; Hoffmann, A.A., Environmental monitoring using next generation sequencing: rapid identification of macroinvertebrate bioindicator species. *Frontiers in Zoology* **2013,** *10*, 1-15.

Ahmed, W.; Angel, N.; Edson, J.; Bibby, K.; Bivins, A.; O'Brien, J.W.; Choi, P.M.; Kitajima, M.; Simpson, S.L.; Li, J.; Tscharke, B., First confirmed detection of SARS-CoV-2 in untreated wastewater in Australia: a proof of concept for the wastewater surveillance of COVID-19 in the community. *Science of the Total Environment* **2020,** *728*, 138764.

Ceuppens, S.; Li, D.; Uyttendaele, M.; Renault, P.; Ross, P.; Ranst, M.V.; Cocolin, L.; Donaghy, J., Molecular methods in food safety microbiology: interpretation and implications of nucleic acid detection. *Comprehensive Reviews in Food Science and Food Safety* **2014,** *13* (4), 551-577.

Shin, J.H., Nucleic acid extraction and enrichment. *Advanced Techniques in Diagnostic Microbiology: Volume 1: Techniques* **2018,** 273-292.

Tang, C.; He, Z.; Liu, H.; Xu, Y.; Huang, H.; Yang, G.; Xiao, Z.; Li, S.; Liu, H.; Deng, Y.; Chen, Z., Application of magnetic nanoparticles in nucleic acid detection. *Journal of Nanobiotechnology* **2020,** *18* (1), 1-19.

Ahmed, W.; Angel, N.; Edson, J.; Bibby, K.; Bivins, A.; O'Brien, J.W.; Choi, P.M.; Kitajima, M.; Simpson, S.L.; Li, J.; Tscharke, B., First confirmed detection of SARS-CoV-2 in untreated wastewater in Australia: a proof of concept for the wastewater surveillance of COVID-19 in the community. *Science of the Total Environment* **2020,** *728*, 138764.

Weidhaas, J.; Aanderud, Z.T.; Roper, D.K.; VanDerslice, J.; Gaddis, E.B.; Ostermiller, J.; Hoffman, K.; Jamal, R.; Heck, P.; Zhang, Y.; Torgersen, K., Correlation of SARS-CoV-2 RNA in wastewater with COVID-19 disease burden in sewersheds. *Science of The Total Environment* **2021,** *775*, 145790.

Qiu, Y.; Lee, B.E.; Ruecker, N.J.; Neumann, N.; Ashbolt, N.; Pang, X., A one-step centrifugal ultrafiltration method to concentrate enteric viruses from wastewater. *Journal of Virological Methods* **2016,** *237*, 50-153.

Stöber, W.; Fink, A.; Bohn, E., Controlled growth of monodisperse silica spheres in the micron size range. *Journal of Colloid and Interface Science* **1968,** *26* (1), 62-69.

Fang, G.; Chen, H.; Zhang, Y.; Chen, A., Immobilization of pectinase onto Fe_3O_4@ SiO_2–NH_2 and its activity and stability. *International Journal of Biological Macromolecules* **2016,** *88*, 189-195.

Liu, Y.; Lou, Z.; Sun, Y.; Zhou, X.; Baig, S.A.; Xu, X., Influence of complexing agent on the removal of Pb (II) from aqueous solutions by modified mesoporous SiO_2. *Microporous and Mesoporous Materials* **2017,** *246*, 1-13.

Bachman, J., Reverse-transcription PCR (rt-PCR). *Methods in Enzymology* **2013,** *530*, 67-74.

Vijgen, L.; Keyaerts, E.; Moes, E.; Maes, P.; Duson, G.; Van Ranst, M.; Development of one-step, real-time, quantitative reverse transcriptase PCR assays for absolute quantitation of human coronaviruses OC43 and 229E. *Journal of Clinical Microbiology* **2005,** *43* (11), 5452–5456.

Yang, Z.; Qian, K.; Lv, J.; Yan, W.; Liu, J.; Ai, J.; Zhang, Y.; Guo, T.; Zhou, X.; Xu, S.; Guo, Z., Encapsulation of Fe3O4 nanoparticles into N, S co-doped graphene sheets with greatly enhanced electrochemical performance. *Scientific Reports* **2016,** *6* (1), 27957.

Kurnaz Yetim, N.; Kurşun Baysak, F.; Koç, M.M.; Nartop, D., Characterization of magnetic Fe_3O_4@SiO_2 nanoparticles with fluorescent properties for potential multipurpose imaging and theranostic applications. *Journal of Materials Science: Materials in Electronics* **2020,** *31* (20), 18278-18288.

Ruparelia, N.; Soni, U.; Desai, R. P.; Ray, A., Silica anchored colloidal suspension of magnetite nanorods. *Journal of Solid State Chemistry* **2020,** *290*, 121574.

Xie, X.; Chen, L.; Pan, X.; Wang, S., Synthesis of magnetic molecularly imprinted polymers by reversible addition fragmentation chain transfer strategy and its application in the Sudan dyes residue analysis. *Journal of Chromatography A* **2015,** *1405*, 32-39.

Doelsch, E.; Stone, W.E.; Petit, S.; Masion, A.; Rose, J.; Bottero, J.Y.; Nahon, D., Speciation and crystal chemistry of Fe (III) chloride hydrolyzed in the presence of SiO_4 ligands. 2.

Characterization of Si−Fe aggregates by FTIR and ^{29}Si solid-state NMR. *Langmuir* **2001,** *17* (5), 1399-1405.

Sarker, M.Z.; Rahman, M.M.; Minami, H.; Suzuki, T.; Ahmad, H., Amine functional silica–supported bimetallic Cu-Ni nanocatalyst and investigation of some typical reductions of aromatic nitro-substituents. *Colloid and Polymer Science* **2022,** 1-18.

Hou, S.; Li, X.; Wang, H.; Wang, M.; Zhang, Y.; Chi, Y.; Zhao, Z., Synthesis of core–shell structured magnetic mesoporous silica microspheres with accessible carboxyl functionalized surfaces and radially oriented large mesopores as adsorbents for the removal of heavy metal ions. *RSC Advances* **2017,** *7* (82), 51993-52000.

Lounasvuori, M.M.; Rosillo-Lopez, M.; Salzmann, C.G.; Caruana, D.J.; Holt, K.B., The influence of acidic edge groups on the electrochemical performance of graphene nanoflakes. *Journal of Electroanalytical Chemistry* **2015,** *753*, 28-34.

Kheilkordi, Z.; Mohammadi Ziarani, G.; Mohajer, F.; Badiei, A.; Varma, R.S., Synthesis and Application of Novel Nanomagnetic Catalyst Fe3O4@ SiO2@ Pr–Gu–Cr–COOH in the Green Multi-component Synthesis of 1-(Benzothiazolylamino) methyl-2-naphthol. *Journal of Inorganic and Organometallic Polymers and Materials* **2023,** *33* (4), 1028-1036.